TOMOGRAPHIC SITE CHARACTERIZATION

USING CPT, ERT, & GPR

Final Report

July 1999

Award Number DE-AR21-96MC33077

Principal Authors:

Rexford M. Morey

Susanne M. Conklin

Stephen P. Farrington, P.E.

James D. Shinn II, P.E.

For:

U.S. Dept. of Energy

Office of Fossil Energy

Morgantown Energy Technology Center

Morgantown, West Virginia

COR: Karen Cohen

By:

Applied Research Associates, Inc.

120-A Waterman Road

South Royalton, VT 05068

SUMMARY

The U.S. Department of Energy (DOE) is responsible for the cleanup of inactive DOE sites and for bringing DOE sites and facilities into compliance with federal, state, and local laws and regulations. The DOE's Office of Environmental Management (EM) needs advanced technologies that can make environmental restoration and waste management operations more efficient and less costly. These techniques are required to better characterize the physical, hydrogeological, and chemical properties of the subsurface while minimizing and optimizing the use of boreholes and monitoring wells. Today the cone penetrometer technique (CPT) is demonstrating the value of a minimally invasive deployment system for site characterization.

Applied Research Associates, Inc. is developing to new sensor packages for site characterization and monitoring. The two new methods are:

- Electrical Resistivity Tomography (ERT); and
- Ground Penetrating Radar (GPR) Tomography.

These sensor systems are now integrated with the CPT. The results of this program now make it possible to install ERT and GPR units by CPT methods and thereby reduce installation costs and total costs for ERT and GPR surveys. These two techniques can complement each other in regions of low resistivity where ERT is more effective and regions of high resistivity where GPR is more effective.

The results show that CPT-installed GeoWells can be used for both ERT and GPR borehole tomographic subsurface imaging. These two imaging techniques can be used for environmental site characterization and monitoring have numerous and diverse applications within site cleanup and waste management operations.

TABLE OF CONTENTS

List of Figures

List of Tables

SECTION 1.
INTRODUCTION

The U.S. Department of Energy (DOE) is responsible for the cleanup of inactive DOE sites and for bringing DOE sites and facilities into compliance with federal, state, and local laws and regulations. The DOE's Office of Environmental Management needs advanced technologies that can make environmental restoration and waste management operations more efficient and less costly. Significant savings in both time and money can be realized with better site characterization and monitoring techniques. These techniques are required to better characterize the physical, hydrogeological, and chemical properties of the subsurface while minimizing and optimizing the use of boreholes and monitoring wells. Today the cone penetrometer technique (CPT) is demonstrating the value of a minimally invasive deployment system for site characterization.

ARA's CPT uses a variety of sensors for measuring soil properties, such as pore pressure, resistivity, temperature, pH, and seismic wave speed. Studies have shown that ARA's CPT site investigations at hazardous waste sites are very cost effective when compared to standard drilling methods [1,2]. In its continuing effort to support cost-effective environmental restoration, ARA proposed the development of two new sensor packages for site characterization and monitoring:

- Electrical Resistivity Tomography (ERT); and
- Ground Penetrating Radar (GPR) Tomography.

The CPT has proven to be an efficient and cost effective method for accessing the subsurface without drilling. ERT and GPR have proven to be useful techniques for imaging subsurface structures and processes. Past use of ERT and GPR has required the installation of system components via drilled boreholes. The purpose of this project is to make possible the installation of ERT and GPR units by cone penetrometers, reducing installation costs and thereby total costs for ERT and GPR surveys.

The ERT technique uses quasi-DC methods where conduction currents are greater than displacement currents. For most soils the resistivity ranges from 10 to 10^5 ohm-meters and the

dielectric constant, which is dictated by the water content, from 4 (dry) to 40 (saturated). In low resistivity conditions, the displacement current (or dielectric effect) is insignificant for frequencies less than 100 kHz. GPR methods, on the other hand, use frequencies from 10 to 1000 MHz where the response is controlled by water content as well as conductivity and where the depth of penetration is limited by attenuation due to low resistivity (high conductivity). Thus, ERT is more effective in *low* resistivity environments and GPR is more effective in *high* resistivity conditions.

Combining the two methods, through an intelligent data fusion process, in a single site characterization survey will greatly enhance the available information about the subsurface conditions at the site.

SECTION 2.

PURPOSE

This project addresses a range of DOE problems which fall into two categories: site characterization and monitoring. Technologies used for these purposes have numerous and diverse applications within site clean-up and waste-management operations. DOE has identified a need for sensors, sensor deployment means, and sensor data processing, including sensor data fusion methodologies for:

- Detection and monitoring of contaminants in soils, groundwater, and process effluents;
- Expediting site characterization; and
- Geological and hydrogeological characterization and monitoring of the subsurface environment.

Our project specifically addresses each of these needs:

1. Sensors: ERT and GPR Tomography
2. Sensor Deployment: CPT
3. Sensor Data Processing: Tomographic Imaging
4. Sensor Data Fusion: ERT and GPR

There are numerous specific applications where cost-effective underground imaging is very important:

1. Delineating the continuity of soil layers between penetrometer holes;
2. Locating and mapping sand and clay lenses between penetrometer holes;
3. Mapping DNAPL plumes;
4. Defining spatial and temporal behavior of a steam flood for dynamic stripping;
5. Detecting leaks under tanks at the DOE's Hanford, WA, site;
6. Monitoring the efficiency of air sparging;
7. Monitoring an ohmic heating thermal front; and
8. Characterization of burial trenches and pits, including boundaries and contents.

SECTION 3.
BACKGROUND

This project's goal is to successfully integrate three existing technologies into a successful, cost efficient sensor unit and deployment method. The following describes these three technologies.

A. CONE PENETROMETER TECHNOLOGY

The Cone Penetrometer Test was originally developed in the Netherlands in the early 1930's for geotechnical site investigations. The original cones involved mechanical measurements of the penetration resistance on a conical tip. A friction sleeve was added in 1965 [3]. Electronic measurements were added in 1948 and improved in 1971 [Ref. 4]. Pore pressure probes were introduced in 1975 [5,6], originally as independent probes, but were soon added to the cone penetrometer instrumentation. These features are illustrated on the CPT probe shown in Figure 3.1. It contains the primary geotechnical sensors for tip stress, sleeve friction, pore pressure along with an inclinometer to measure the tilt of the probe, and resistivity as discussed later. This type of cone is used widely in Europe for geotechnical investigations. Its acceptance in the United States has been rather limited for geotechnical studies; however, the significant advantages it provides for environmental work are leading to much wider acceptance by the environmental site characterization community. This is due largely to the development of new sensors which allow detection of chemical pollutants *in situ.*

Major components of the modern cone penetrometer system are the instrumented probe, the instrumentation conditioning and recording system, the hydraulic push system, and the vehicle on which the system is mounted. Enclosure in a van body allows all weather operation. The common configuration provides the reaction mass for a hydraulic push force of about 20 tons (18,000 kgs). Standardization for the geotechnical applications of the cone penetration test was established by the American Society of Testing and Materials in 1986. This standard allows for a probe diameter of 1.44 or 1.75 inches (3.658 cm or 4.445 cm). The most common for standard work is the 1.44-inch probe.

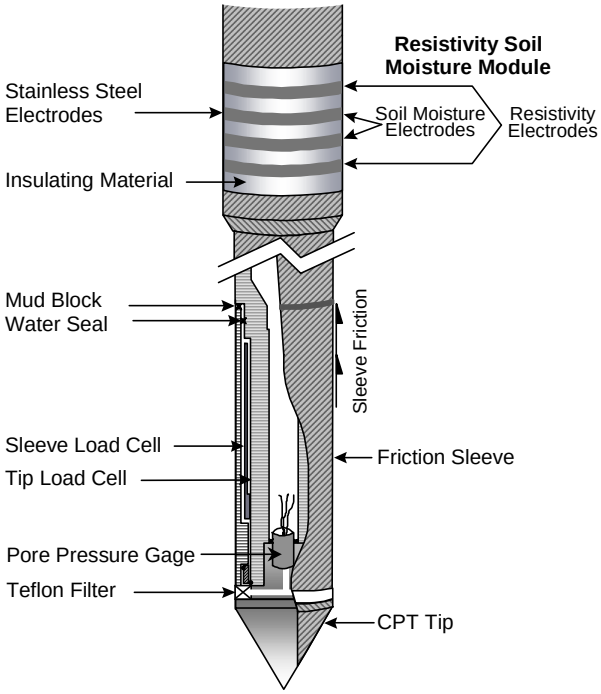

Figure 3.1. Schematic of ARA's cone penetrometer probe.

Recent environmental work has led to the requirement to push deeper than possible with the 20 ton configuration. This has been accomplished by increasing the reaction weight to 30-35 tons (27,000 -32,000 kgs) and using the larger 1.75-inch probe and rod. This increases the rod buckling resistance at the higher loads. The maximum depth of penetration possible varies greatly with soil type. In soft damp soil, the 20 ton systems have penetrated 300 feet (91.5 m); but in gravely soils, such as the DOE's Hanford Site in southwestern Washington, these systems met refusal at 10-20 feet (3-6 m). A 30-ton system using the larger diameter rods has reached depths of approximately 150 feet (46 m) in these same gravely soils [Ref. 7].

Using the cone penetrometer for environmental site characterization represents a new application of the technology. Significant advantages of the CPT include: eliminating drilling wastes and the need for treatment and disposal of drill spoils as hazardous material; providing continuous data on the subsurface stratigraphy in real time; identifying thin layers of significantly different hydraulic conductivity; eliminating the possibility of the crew being exposed to the potentially hazardous material; reducing the possibility of cross contamination (by grouting the

hole as the probe is withdrawn), and faster results when compared to conventional drilling and sampling.

In addition to being an excellent platform for making continuous measurements of contaminant information with depth, the CPT is also useful for pushing monitoring sensors into the subsurface and for taking gas, water, or soil samples for environmental testing.

1. CPT Hardware

ARA designs and manufactures CPT equipment for its own use and sale to others. Since 1982, we have pushed a combined total of over 200,000 feet and record depths of nearly 300 feet. Push depth is a function of reaction weight (e.g. the push weight of the truck), the resistance or friction of the soil, and any impenetrable obstruction (i.e. a large boulder).

Figure 3.2 shows a CPT truck in operation. Four-point leveling hydraulics lift the truck off the ground and provide a horizontal platform for insuring vertical penetration into the ground. The operator stands next to the hydraulic CPT push system. Figure 3.3 illustrates the major components of the CPT hydraulic push system. Twin main hydraulic cylinders can apply 75,000 pounds of force. This is enough force to lift the CPT truck off the ground, hence the limiting factors become the weight or effective mass of the truck and the strength of the CPT rods. Numerous hydraulic, mechanical, and electronic safety devices have been incorporated into the basic design of the CPT push system which meet or exceed industry standards.

Figure 3.2. Open frame CPT truck.

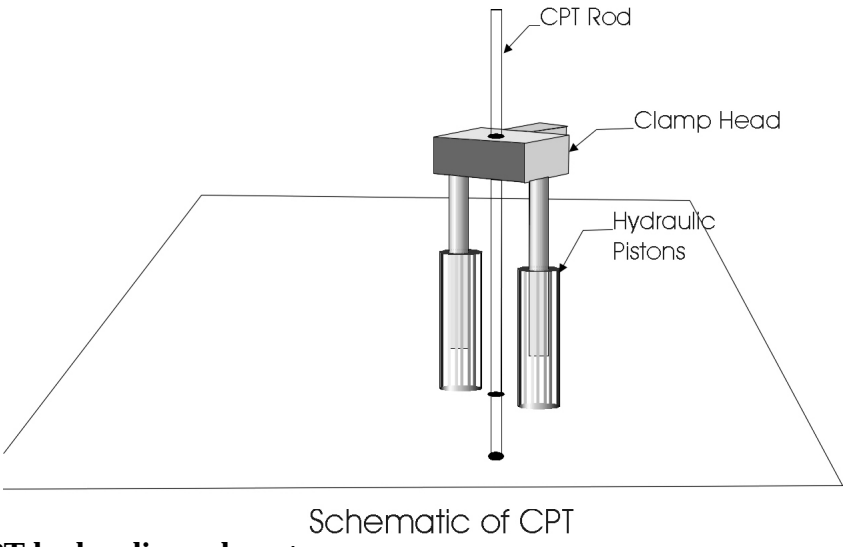

Figure 3.3. CPT hydraulic push system.

B. ELECTRICAL RESISTIVITY TOMOGRAPHY

1. Background

In most environmental restoration applications the role of electrical resistivity is to assist in characterizing a site. The task includes not only specifying the location of contamination, but also mapping the physical and chemical properties of the ground that control their distribution and movement. In the most general sense, mapping electrical resistivity is important for conditioning or constraining the hydrological models of contaminant transport and retention. These models are usually based on drill-hole tests and suffer from the problem of extrapolation of point measurements, made also between holes, to the volume between the holes.

For example, a subsurface channel of high permeability sand that is missed by a drill pattern illustrates the problem of relying solely on drill holes. This channel would be the dominant feature of the site in terms of contaminant transport. Mapping the subsurface distribution of electrical resistivity could reveal the subsurface geometry and drastically change the hydrologic model.

Soil and rock resistivity (or conductivity) measurements have been used in the mining industry for many years, and recently have been used to locate contamination plumes. The

electrical resistivity of most soils and rocks depends on the conduction paths afforded by fluids in the pore spaces. Resistivity is determined by the porosity, saturation, pore fluid salinity, and clay content. Because resistivity is influenced by the dissolved solids in groundwater, mapping it may be the only direct detection method for high concentrations of contaminants that form ionic species.

ARA includes a Resistivity Module in its cone penetrometer instrumentation for measuring resistivity in the adjacent soil. As part of the CPT push rod, the module consists of four circular electrodes in contact with the soil. The electrodes are separated by insulators. The outer two electrodes are used to induce an electrical current into the soil matrix. The inner two electrodes are used to measure the strength of the induced electric field. The amount of voltage potential drop in the electric field is a function of the resistivity of the soil.

Daily et al. [Ref. 8] and *Ramirez et al.* [Ref. 9] at the Lawrence Livermore National Laboratory developed and tested the ERT method for mapping subsurface conditions between boreholes. Applications included monitoring water movement in the vadose zone and monitoring an underground steam injection process for soil decontamination. ERT uses a dipole-dipole measurement technique, similar to those used in conventional surface resistivity surveys [Ref. 10], to measure the bulk electrical resistivity distribution in the soil mass between two boreholes. ARA has collaborated with Dr. Daily to incorporate his research into a CPT ERT system.

Processes such as steam injection can be monitored by taking measurements before the process is started and then repeating the measurements over time as the process proceeds. Each tomographic data set is then subtracted from the original background measurements to produce a "time lapse" image set of resistivity variations between the boreholes.

2. ERT Technical Approach

To image the resistivity distribution between two boreholes, several electrodes are placed in each hole, as shown in Figure 3.4. This particular configuration of borehole electrodes is called a Vertical Electrode Array (VEA). Each electrode must be in contact with the formation.

Two electrodes are driven by a known current, I, and the resulting voltage difference, V, is measured between other electrode pairs. This process is repeated until a predetermined set of linearly independent combinations are measured. Each voltage-to-current ratio is a transfer resistance. The goal is to calculate the distribution of resistivity in the vicinity of the boreholes given the measured transfer resistance.

The ERT image creation process involves solving both the forward and inverse problems. Lawrence Livermore National Laboratory in collaboration with Dr. LaBreque (Refs. 9 and 11) has developed and tested the computer algorithms to transform ERT data sets into tomographic images [8]. The image reconstruction plane is modeled by a finite element mesh, *N* elements wide (between the boreholes) and *M* elements long (along the boreholes). The mesh and the location of the boreholes and electrodes are shown in Figure 3.5. Image resolution is a complicated function of many factors, including data signal-to-noise ratio, electrode and borehole separation, the subsurface resistivity distribution, and the degree to which the resistivity matches the two-dimensional model of the forward calculations. The installed vertical electrode spacing prohibits the resolution from being greater than ½ the electrode spacing. The best resolution is obtained close to the electrodes, and the worst resolution is obtained along a vertical stripe midway between the boreholes. Thus, resolution improves as borehole and electrode spacing decreases.

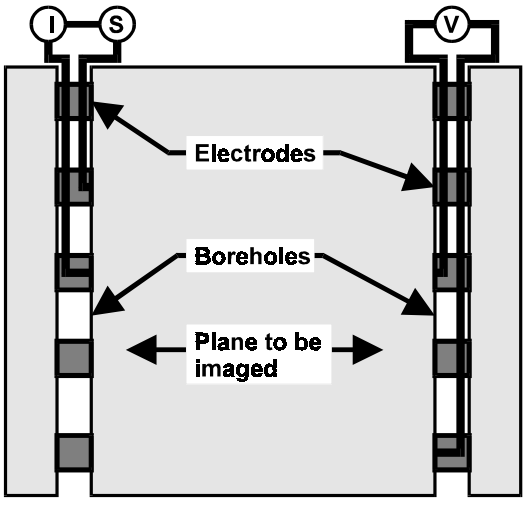

Figure 3.4. Schematic diagram showing data collection approach for ERT measurements.

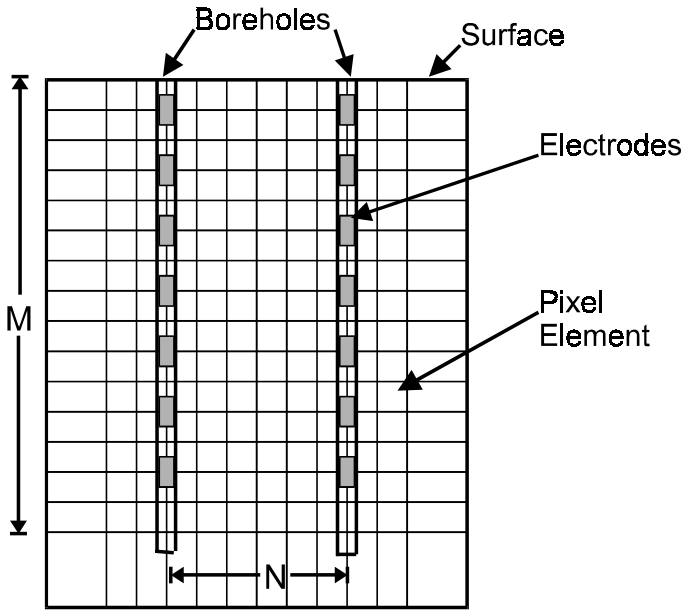

Figure 3.5. The reconstruction plane modeled by a finite element mesh. The pixel elements are the blocks for which electrical resistivity is calculated.

ERT relies on computer processing to form an image from thousands of data points gathered at a site. A technique called mathematical inversion is used to construct an image (tomogram) of subsurface features which have distinct differences in resistance from their surroundings. The analyst creating the tomogram generates a theoretical mathematical model. The object imaged represents what must be present to produce the actual resistance measurement data. This process is illustrated in Figure 3.6.

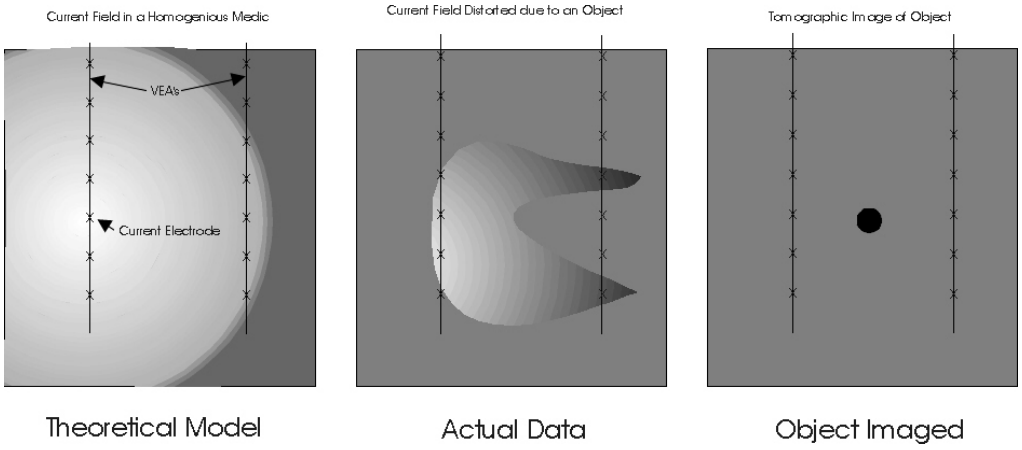

Figure 3.6. The drawings illustrate the process of tomographic imaging.

C. GROUND PENETRATING RADAR TOMOGRAPHY

1. Background

Ground penetrating radar (GPR) has been used for over 20 years (Ref. 12) at chemical and nuclear waste disposal sites (Ref. 13) as a non-invasive technique for site characterization. Standard GPR surveys are conducted from the surface of the ground providing geotechnical information from the surface to depths of 5 to 50 feet, depending on GPR frequency of operation and soil conductivity. Commercially available GPR systems operate over the frequency range 50 MHz to 1000 MHz. The lower frequencies provide better penetration but poor resolution, while the higher frequencies give poor penetration but good resolution. There are many critical environmental monitoring situations where surface GPR does not provide the depth of penetration or necessary resolution.

Borehole radar (Refs. 15 -17) can place the sensor closer to the region of interest, overcoming high signal attenuation in the near-surface soils. However, borehole exploration is invasive, slow and expensive because of the extensive drilling required. The radar logging tool is expensive and, if not properly designed and tested, will give poor results. Drilling and casing the hole disturbs the soil around the hole (Ref. 16) while the air-gap between the antenna and hole strongly influences signal coupling into the formation. Cable noise and attenuation in some borehole radar designs require putting electronics and power downhole (Ref. 18), increasing the cost. The logging cable will distort the radiation pattern putting into question any tomographic analysis (Ref. 18). To overcome logging cable problems, fiber-optic logging cable and a downhole transmitter, receiver and battery-pack can be used, greatly increasing the complexity and cost of the downhole tool.

CPT probes can acquire geotechnical data in soils in less time and at lower cost. For hazardous waste site exploration and quantifying unexploded ordinance (UXO), cone penetrometers are considered minimally invasive, since they do not bring any cuttings to the surface and can be equipped to grout the hole while withdrawing.

As described earlier, existing CPT probes measure soil and groundwater properties, such as resistivity and temperature, in the immediate vicinity of the probe.

Figure 3.7 is a schematic diagram showing possible data collection approaches for GPR measurements. These transmission measurements include hole-to-hole and hole-to-surface measurements. At each downhole position the surface antenna is scanned radially from the hole. For cross-hole tomography (GPRT), one CPT antenna is held stationary while the other unit is moved. The process is repeated until the volume between the holes is covered.

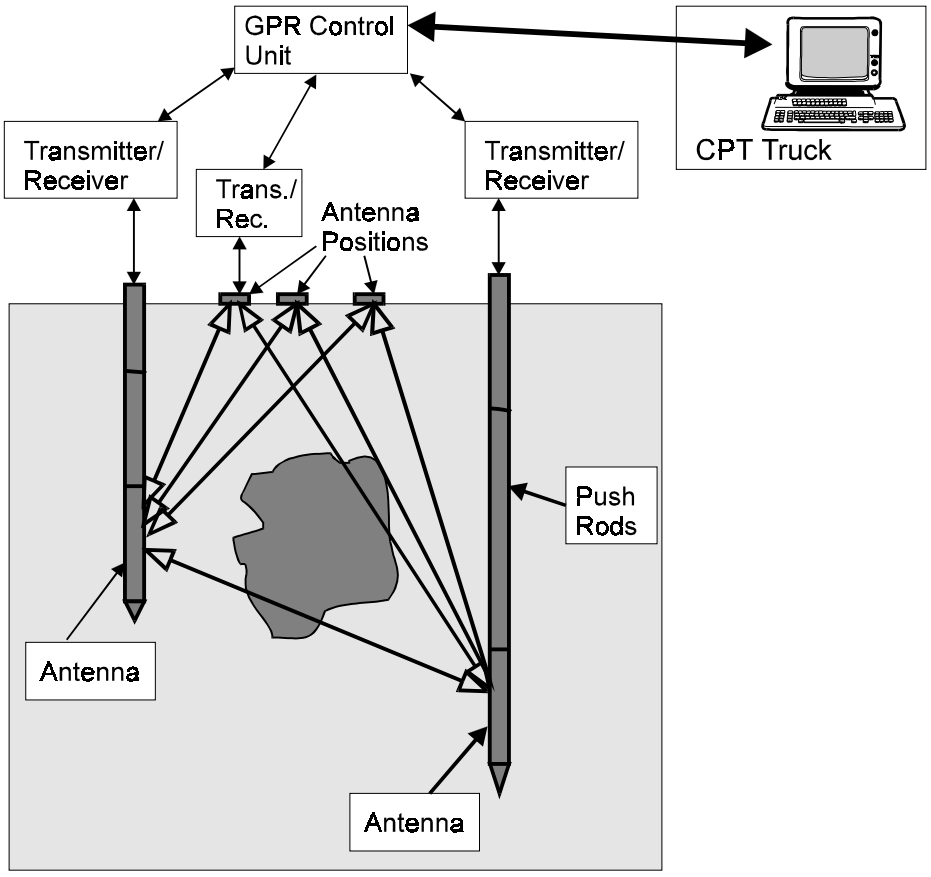

Figure 3.7. Schematic diagram showing data collection approach for GPRT measurements. Several ray paths are shown for typical transmitter-receiver positions on the surface and in the holes.

The interpretation of cross-hole radar data parallels the approaches used in cross-hole seismic studies. However, cross-hole data from GPR is less complicated than seismic data because the radar wavelet propagates as a single mode rather than the multitude of mode conversions that occur with seismic methods. As the radar pulse propagates, it is attenuated due to conductivity and slowed due to the dielectric constant. Therefore, GPR tomography maps

variations in conductivity and velocity from which it is possible to estimate soil characteristics, such as water content, density and contamination.

For GPRT data, a tomographic reconstruction is attempted using first arrival times in an simultaneous iteration reconstruction tomography (SIRT) algorithm, initially with straight ray paths. However, if difficulty is experienced with convergence, then a perturbation method is used which allows for curved ray paths. (In the near-surface zone, the air/soil boundary may have a significant effect on shallow tomographic reconstruction and must be taken into consideration.) The region under investigation is divided into a regular grid (similar to ERT, see Figure 3.5), and the radar wavelet velocity and attenuation are iteratively calculated for each cell and combined to generate a color map of the region between the holes. Spatial resolution is governed by the dominant wavelength of the pulses in the medium; at 100 MHz resolution is on the order of 0.5 to 1.5 meters.

2. GPR Technical Approach

The performance of ground penetrating radar is estimated from the following set of equations. Maximum radar range is a function of radar system parameters, target parameters, and the electromagnetic properties of the materials being probed. Soil conditions govern the attenuation and velocity of the radar signal. The radar range equation appropriate for GPR is:

$$Q = 10\log[\frac{P_{\min}}{P_t}] = 10\log(\frac{E_t E_r G_t G_r v_m^2 g e^{-4\alpha R}\sigma}{64\pi^3 f^2 R^4}) \qquad (1)$$

where Q is the system performance factor in decibels (dB) and the various components are:

System dependent:

P_{min}	=	minimum detectable power
P_t	=	transmitter output power to antenna
E_t and E_r	=	antenna efficiency
G_t and G	=	antenna gain
f	=	frequency of operation

Media dependent:

v_m	=	velocity of propagation in medium
α	=	attenuation coefficient of medium

Target dependent:

g	=	back scatter gain of target
σ	=	target scattering cross-section area

Range Dependent:

R	=	distance to target from antenna.

Commercially available GPR systems advertise Q values from about -100 dB to -150 dB, the lower value is without computer processing while the larger value (-150) is with processing. Antenna efficiency and antenna gain are influenced by the type of soil and the coupling of the antenna to the soil. Part of this project was to optimize the antenna design in relation to the medium it is immersed in for maximum gain and efficiency. The operating frequency is a design parameter that was investigated for various operational and deployment configurations.

Velocity of propagation in the soil is a function of the soil mixture dielectric constant (Refs. 19 and 20)and is primarily governed by water content. Radar signal attenuation is controlled by soil conductivity. Clay soils are conductive, thus radar range is limited to a few feet. Sandy soils are much less conductive and penetration depths are on the order of 100 feet. Dielectric mixture theories (Ref. 19) are used to calculate the complex dielectric constant of four-phase soil mixtures for modeling the radar propagation response and interpreting measurement results. Mixing models take into account soil density (solid particle and air volume), water volume, and contaminant volume.

Figure 3.8 is a plot of maximum radar range as a function of frequency for three different target types -- a smooth plane reflector, a rough plane reflector, and a point scatterer. As frequency of operation decreases, the maximum range increases for plane reflectors, such as boundaries between soil and bedrock or between dry and wet soil. For discrete targets, such as boulders or metal drums, maximum range increases with frequency because the target radar cross-section is larger relative to wavelength at the higher frequencies. However, at even higher frequencies the target is no longer a point scatterer and its response approaches a plane reflector.

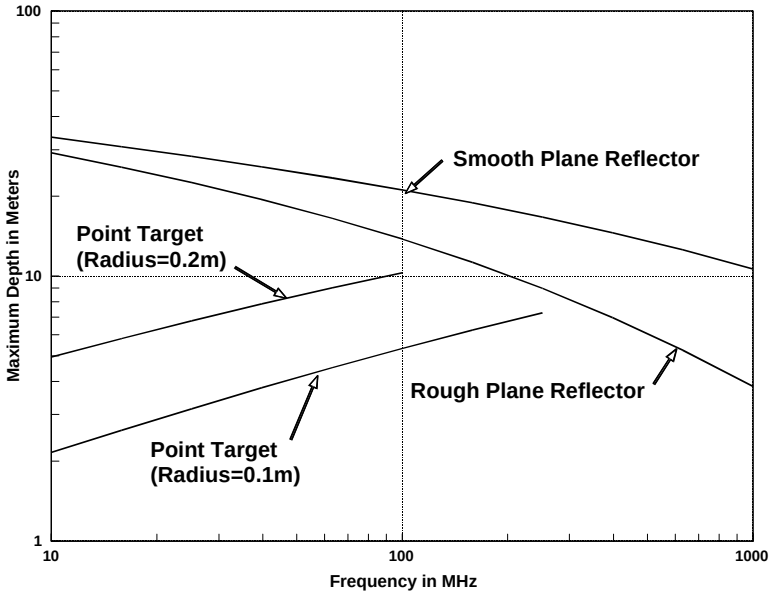

Figure 3.8. Maximum radar range for three target types. (Q = -110 dB, dielectric constant = 6, and conductivity = 0.001 S/m.)

Figure 3.9 shows the influence of soil conductivity on maximum radar range at three frequencies for a rough plane reflector. Note that low conductivity sands are much more transparent than clays. Water content is not as important as the conductivity of the water. Penetration depth is roughly the same for moist and saturated sand as long as the conductivity is the same.

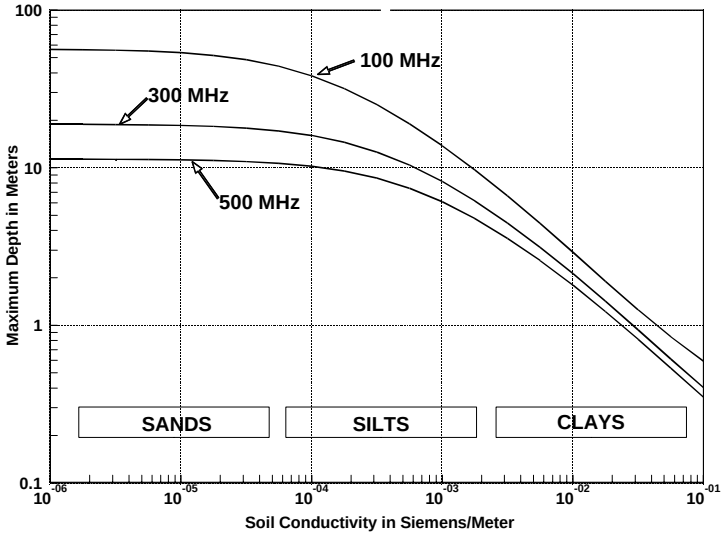

Figure 3.9. Radar range to a rough plane reflector, such as bedrock. The soil types are general designations. (Q = -110 dB and dielectric constant = 6.)

D. SOIL MOISTURE SENSOR

A Soil Moisture Sensor (SMS) was used during the field evaluation tests of the ERT and GPR systems. The Soil Moisture Sensor logs the moisture content of the soil surrounding a borehole as the probe is advanced down the hole. Since radar propagation in soils is strongly influenced by moisture content, SMS measurements help with GPR interpretation.

Measurement of soil moisture and electrical resistivity with the Cone Penetrometer Probe can provide ground truth data for use in the electrical resistivity and ground penetrating radar tomography analysis. Analysis of ERT and GPR tomography data to date has not incorporated the use of detailed ground truth data as can be gathered by the CPT. As will be shown in a later section, incorporation of this data can greatly enhance the quality and accuracy of the inversion process. Under other programs, ARA has developed a soil moisture and electrical resistivity probe which was used on this project. A summary of the ARA soil moisture probe operation principle and results of field evaluations of the probe is given below. Soil moisture data is a key parameter in any environmental or geotechnical site investigation.

1. Soil Moisture Probe Background

It has been recognized since the work of Selig (Ref. 20) and Topp (Refs. 21 and 22) that the dielectric properties of a soil are closely related to the soil moisture content. Dry soil has a dielectric constant of roughly 3 to 6, and adding water to dry soil will increase the dielectric constant as water has a dielectric constant (80). Using this phenomena, Topp developed a technique using Time Domain Reflectometry (TDR) technique to measure the soil dielectric.

Conventional TDR measures the dielectric at very high frequencies (several hundred MHz) using specialized equipment, and has been demonstrated to minimize the effect of soil electric conductivity and soil type. This technique has been confirmed by Topp (Refs. 21 and 22), Baker and Goodrich (Ref. 23), and Zegelin (Ref. 24). We initially examined using TDR as a CPT technique to measure the soil dielectric. After preliminary laboratory evaluations, this approach was rejected because TDR can only be used over relatively short cable distances (generally less than 100 ft) and high conductivity soils will attenuate the TDR signal, making interpretation difficult. To minimize these effects, we developed a soil moisture probe that uses

downhole electronics to minimize the effect of signal attenuation and that has been designed to be insensitive to soil electrical conductivity.

2. SMP Operation Principle

ARA developed the soil moisture sensor using a Resonant Frequency Modulation (RFM) approach to determine the soil moisture content and dielectric constant (K_d). This approach consists of installing a custom PC board in a CPT probe which is then interfaced with standard CPT equipment, eliminating the need for specialized measurement equipment. An advantage of this approach is that cable distances are unlimited as all conditioning and processing of the signal occurs downhole, eliminating the effect of cable length induced signal attenuation.

The RFM approach uses the probe and surrounding soil to determine the resonant frequency of an oscillator. The RFM circuit frequency varies from 100 MHz in air to approximately 75 MHz in tap water. The basic principle of the probe is that a portion of the soil between two rings in contact with the soil will form part of an electronic circuit that has a frequency of:

$$f = \frac{1}{2\pi\sqrt{LC}} \qquad (2)$$

where: L = inductance and
C = capacitance

The capacitance has two components that set its value: 1) fixed parameters of the probe that equal a constant "C_k," and 2) a value that changes with the surrounding soil moisture, C_v. The combination of C_k and C_v will change by ≈30 pf from air to water with the soil moisture probe (SMP).

The final equation relating the frequency of oscillation of the circuit to the capacitance of the soil is:

$$f = \frac{1}{2\pi\sqrt{L(C_K + C_v)}} \quad (3)$$

A critical choice in a soil moisture probe is the frequency at which the system operates. At low frequencies, the electrical conductivity of the soil can have a significant influence on the measured dielectric. In addition, examination of work by other researchers indicated that as the measurement frequency is increased, the soil conductivity influence on the measured value is greatly reduced.

The SMP module, shown in Figure 3.10, is installed directly behind the CPT probe. The combined probe measures the conventional CPT tip, sleeve, and pore pressure in addition to the simultaneous acquisition of electrical resistivity and dielectric constant. From these data, a wide range of geotechnical properties can be calculated. For resistivity measurements, the array operates at a frequency of either 40 Hz or 1000 Hz to avoid soil polarization effects. The SMP electronic package outputs a 0-4 volt DC signal, which is compatible with any standard CPT electronic cable and data acquisition system.

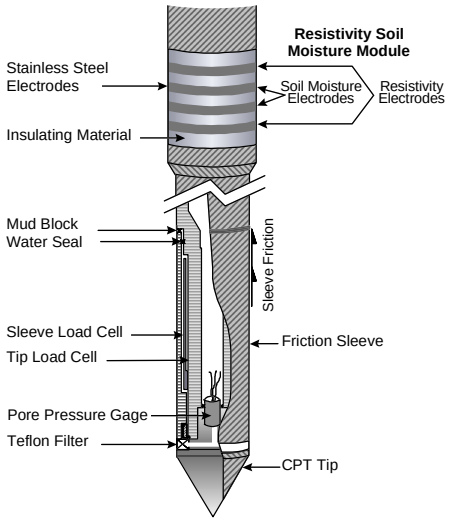

Figure 3.10. Schematic of ARA's soil moisture probe (SMP).

3. Field Evaluation Series

An evaluation of ARA's SMP probe and two other CPT soil moisture probes was conducted by the DOE Argonne National Laboratory. The objective of the field evaluation program was to define the limits of these three CPT soil moisture probes. The reader is referred to the evaluation report from Argonne National Laboratory (Ref. 25) of the soil moisture probe for details of this test program. Testing of the SMP probe was conducted at the DOE Savannah River Site, located in Aiken, SC. The CPT soil moisture probe evaluations were conducted at the TNX and M Basin Areas. A brief description of the TNX and M Basin Areas' geology (summarized from reference 1) is given below.

4. Geology Description

TNX. Shallow sediments that comprise the near-surface aquifer at TNX are Tertiary to recent in age and consist of interbedded fine sands, silts, and clays of mainly terrigenous and marine origin. The shallow aquifer at TNX can be subdivided into a semi-confined unit and an overlying unconfined unit. The two hydrologic units are separated by a 10-ft thick, clayey silt layer that is present throughout TNX except in the floodplain, where only a single unconfined aquifer is present. Geologic core data and geophysical logs obtained at the TNX site indicate that the bottom of the unconfined aquifer is approximately 65 ft bgs. The water table varies from 35 to 50 ft below the ground surface (bgs) and discharges mainly to the Savannah River.

M Basin Area. Sediments at the M Basin Area consist of Middle to Upper Eocene sands, clayey sands, and sandy clays. The sediments of interest for this study belong primarily to the Upland Unit Formation and the top of the Tobacco Road Sand Formation. The Upland Unit is less than 60 ft thick and overlies the Tobacco Road Sand Formation which forms the top of the Upper Eocene Barnwell Group in the study area. The upper 15 ft of sediment collected at the M Basin Area soil boring consisted of red-brown sand with some silt, grading into red-brown silty, clayey sands. The sediments became more sandy with depth. At 54 ft bgs, the sediments became increasingly more sandy and changed in coloration. This change in composition and coloration may indicate that these lower sediments are part of the upper Tobacco Road Sand Formation. The upper 150 ft of sediment consists of four major clay layers. The upper two layers are

discontinuous, whereas the lower two layers have more lateral continuity. The lowest clay unit acts as a confining layer separating the upper semi-confined aquifer from the lower confined aquifer. The upper aquifer has a static water level that ranges from 117 to 140 ft bgs.

5. Collection of SMP and Soil Sample Data

Two sites at the TNX area and one at the M Basin Area were selected for testing of the SMP. These locations had enough distinctive geologic variability to test the SMP under a variety of lithologic and moisture conditions. The sites were characterized by Westinghouse Savannah River Company (WSRC) personnel to determine the site geology and geotechnical properties and to insure that the sites were uncontaminated. Characterization of the site consisted of collecting undisturbed Shelby tube soil samples, which were field logged. The samples were carefully wrapped and transported to a geotechnical laboratory for determination of the soil wet and dry density, specific gravity and gravimetric soil moisture. The gravimetric water content and dry density were used to calculate the volumetric water content, θ, as:

$$\theta = w*\gamma_d/\gamma_w \qquad (4)$$

where w = gravimetric water content
γ_d = dry density
γ_w = specific gravity of water

The three core hole locations were used as the SMP data collection sites. Each SMP probe was pushed twice, a minimum of 25 diameters apart (about 3.5 ft) centered around each core hole. The general configuration for conducting the SMP test is shown in Figure 3.11. Where possible, the sensor readings were collected prior to drilling to eliminate the possible effects of the soil disturbance on the sensor reading. The first push of one of the SMPs (1a) was at any point along the circumference of an imaginary circle. The second push (1b) with the same moisture probe was directly opposite the first push. This sequence was done for each of the three soil moisture sensors. The tip and sleeve readings were collected in addition to data from each moisture sensor. Collection of the CPT data was done to help in data interpretation should the geologic conditions change substantially between the sampling locations. Only the ARA SMP probe data is presented in Figure 3.12.

The SMP data was analyzed and compared to laboratory measured volumetric soil moisture contents. A comparison for all three test locations is given in Figure 3.12. Plotted on the figure are the laboratory and field measured soil moistures as a function of the SMP output voltage as well as fits to the laboratory and field data. As can be seen, the laboratory calibration curve was fairly accurate for low values of volumetric soil moisture; however, for volumetric soil moisture values greater than 25%, the laboratory curve begins to underestimate the best fit to the field data. This is in part due to the previously described limitations of the laboratory test program.

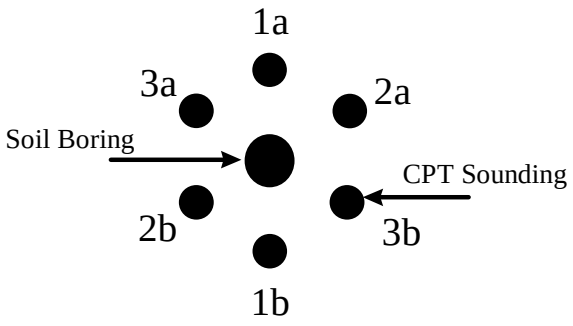

Figure 3.11. General configuration of the SMP testing around the soil sampling boring.

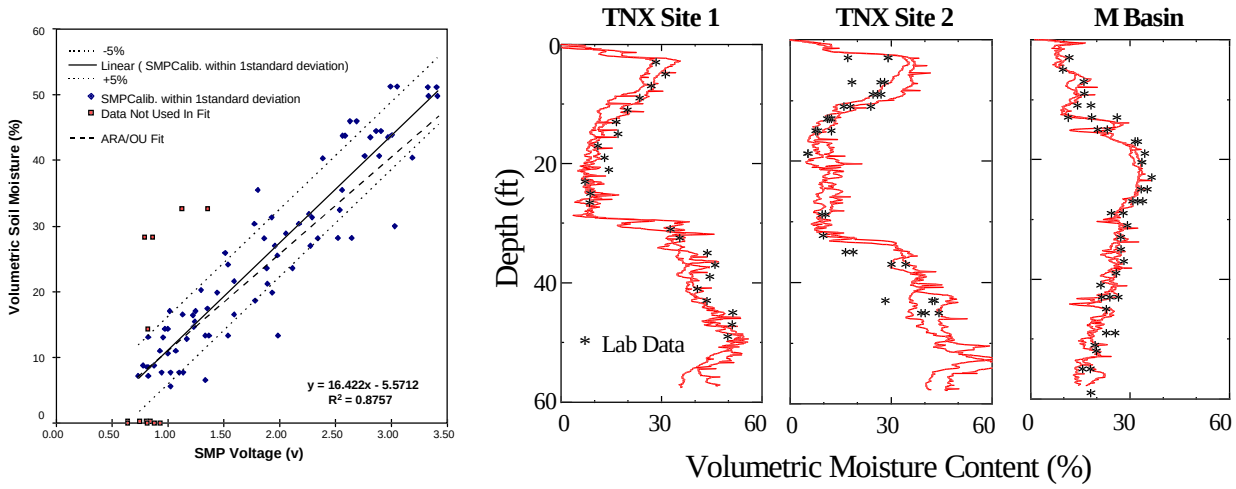

Figure 3.12. The field test results at the three TNX sites predicted the volumetric soil moisture content within the range of the calibration curve shown at left.

Also plotted on the left of Figure 3.12 are the ±5% bounds for the test data. The bulk of the data falls within these bounds, indicating for the sites tested that soil type is a secondary variable. It should be noted that the clay component of the SRS soils is dominated by kaolinite,

which has a low CEC (Cation Exchange Capacity). More active soils may show a wider range of response than was evident at the SRS site. As the field derived curve was based on a higher quality data set, it was decided to use the best fit to this data as the SMP calibration curve.

As can been seen on the right in Figure 3.12, the CPT soil moisture profile shows rapid changes over short depth intervals. At the TNX area the water table was encountered at a depth of 30 to 35 ft. At this depth the soil becomes saturated and the volumetric soil moisture content and porosity are equal. Hence, below the water table the measurement can be interpreted as both the soil volumetric moisture content and porosity.

For use in the ERT inversion analysis the ARA soil moisture probe determined electrical resistivity can be used directly, as will be shown in Section 5. For the GPR analysis, an estimate of the soil dielectric constant is required. A commonly used relationship between soil moisture and the dielectric constant was proposed by Topp, et al. (Refs. 21 and 22):

$$\theta = -5.3 + 2.92K_d - 5.5 \times 10^{-2} K_d^2 + 4.3 \times 10^{-4} K_d^3 \qquad (5)$$

where: θ = volumetric moisture content, %
K_d = dielectric constant

This equation is known as the Universal (Topp's) equation and has been applied to all soil types. ARA inverted the above equation and used the CPT probe measured soil moisture to calculate an estimate of the soil dielectric constant.

SECTION 4.
HARDWARE DEVELOPMENT

A. ERT SYSTEM DEVELOPMENT

ERT system development consisted of three primary tasks:

1. Vertical Electrode Array (VEA) design for CPT installation.
2. ERT electronics hardware.
3. Software for control and imaging.

1. VEA Design

CPT is routinely used by ARA to rapidly install PVC monitoring wells. The PVC pipe is placed on the outside of the push rod and is attached to the push rod only at the bottom. This allows the PVC to be pulled down into the hole to eliminate compressive forces and minimize breakage. However, this installation process stresses the threaded joint between PVC pipe sections, limiting the installation method to relatively low friction soils, e.g. sands and clays. (Since the GPR borehole system requires a plastic lined hole for the antenna, this CPT method is used for the VEA.)

PVC well installation follows a two stage procedure. First a "dummy" hole is formed using 1.75-inch diameter rods, and the rods are then extracted, leaving an open hole. The crew switches to 1.4-inch CPT rods. Threaded sections of PVC are then slid over each section of rod and the central rod is are pushed down the pilot hole pulling the PVC casing with it. The inner push rods are extracted leaving the outer PVC well casing, or a VEA.

The VEA design consists of installing alternating sections of PVC tubing and stainless steel electrodes. 0 shows the components for this design: the 1-1/2 inch PVC (2 inch OD) pipe, the stainless steel electrode element and the wired-spring contacting assembly. This contactor is installed after the PVC-SS VEA has been pushed into the ground and the CPT truck clears the site. Sections of ½-inch-diameter PVC pipe, alternating with each spring contactor, are threaded,

bead-like, onto a central cable. The entire assembly is put together on site as it is being inserted down the VEA "well". The drawing in 0 illustrates the final installation.

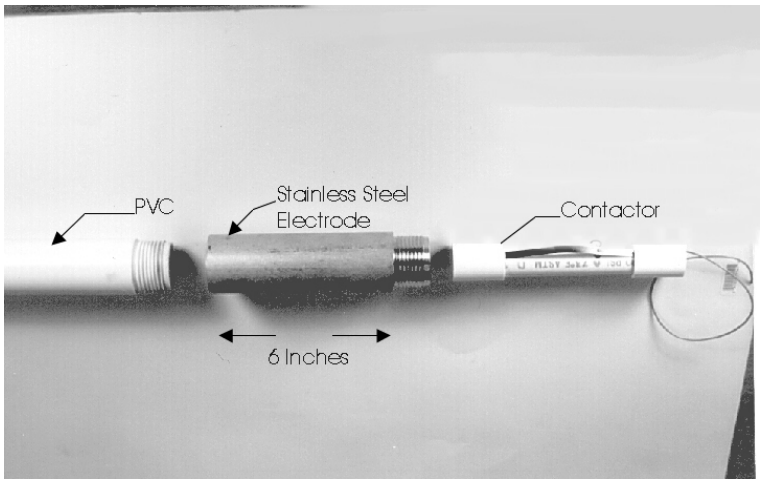

Figure 4.1. PVC and stainless steel electrode assembly.

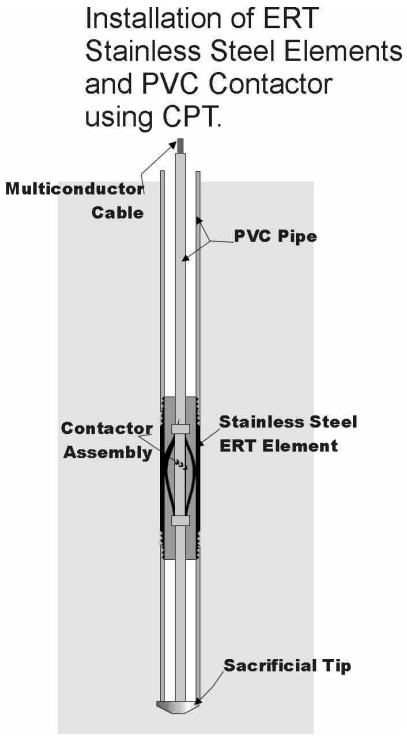

Figure 4.2. PVC-SS electrode VEA illustration.

Initial field testing indicated that the contactor assembly was too fragile and too difficult to remove without breaking the ½-inch-PVC pipe. Also, the spring contactor surface in contact with the inside of the SS ERT element was limited to essentially a two-point contact. A second, interim solution was to use the existing stainless steel fingers on the signal cable without the ½-inch PVC pipe. While this design did work and imaging data were successfully taken, other

issues such as ruggedness over repeated deployments, strain on the multi-conductor cable, storage problems, and low electrode contact area made this design less desirable.

A second contactor assembly was designed, built and tested. The preliminary design shown in 0 was drawn up and a prototype built out of aluminum. The machining for this design was felt to be excessive, so a cost reduction analysis was made, and the final design shown in 0 was selected.

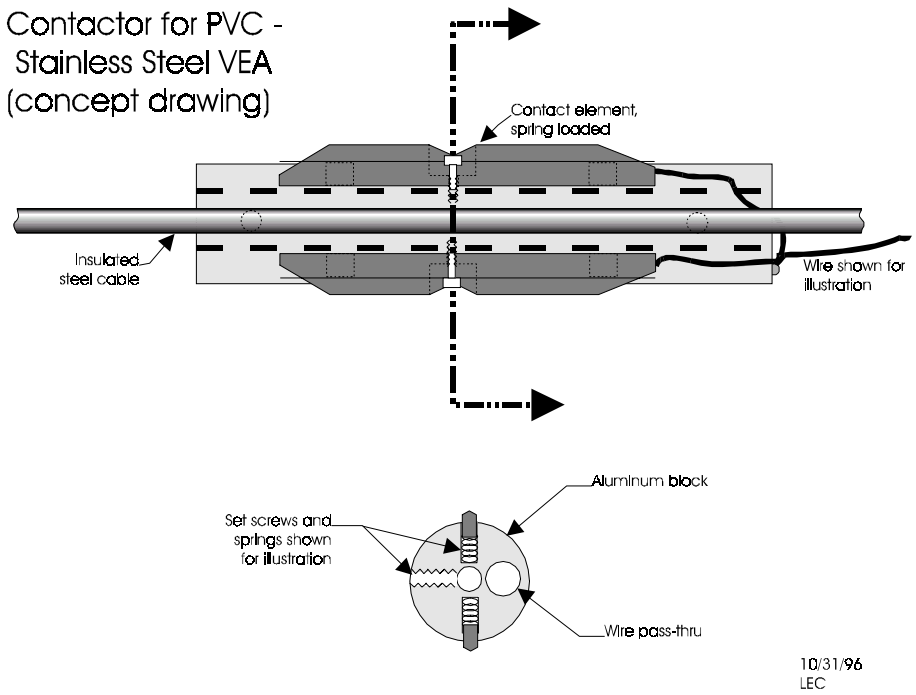

Figure 4.3. Preliminary ERT contactor design.

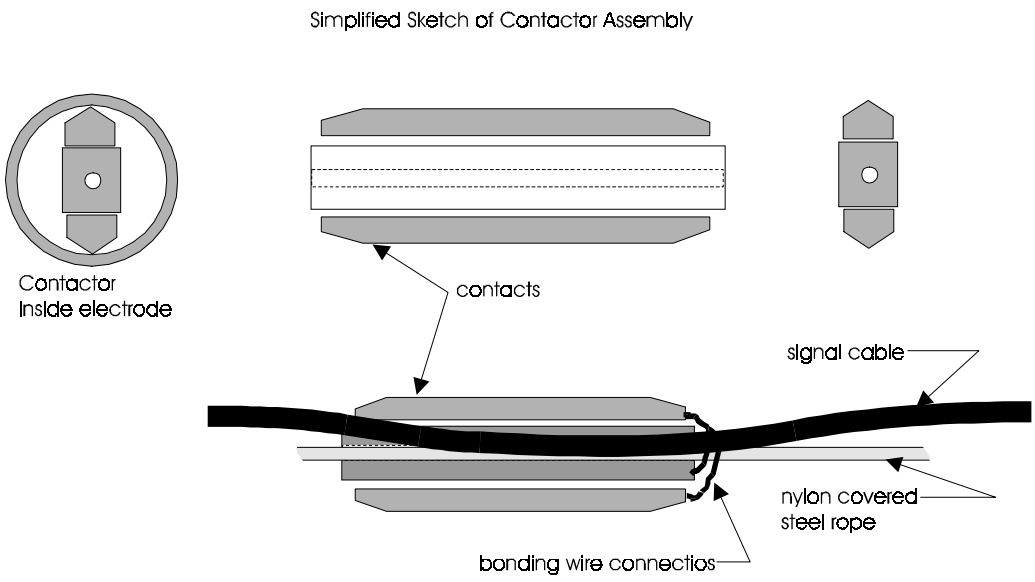

Figure 4.4. Final ERT contactor design.

The two contact units are spring loaded to the central cable housing, thus forcing the contactors against the inside of the electrode. A prototype was built and springs were sized using a friction pull scale. Contact resistance tests were made with a VEA mockup and the contactor performed well. Forty contactors (for four VEA's with 10 electrodes each) were built and firmly attached to the nylon covered steel rope at intervals corresponding to VEA electrode spacing. Each contactor was then connected to the appropriate wire in the cable bundle for electrical connection to the ERT electronics. A weight was attached to the lower end of the steel rope to counter the contactor friction as the final assembly was lowered into the VEA.

0 is a picture of the contactor assembly being lowered into a GeoWell. (The term GeoWell is used for the CPT installed PVC/SS-electrode well that was also used for the GPR cross-hole measurements. In other words, a GeoWell is a well in which multiple sensors can be deployed.) No significant problems were encountered as the contactors were deployed into the GeoWells. The contactor arrays are easily removed, wound up on wire reels, and stored when not in use. They are easily redeployed and relocated back in the GeoWells and indexed to the

proper electrode location in a matter of minutes. 0 is a schematic of contactors deployed in a GeoWell.

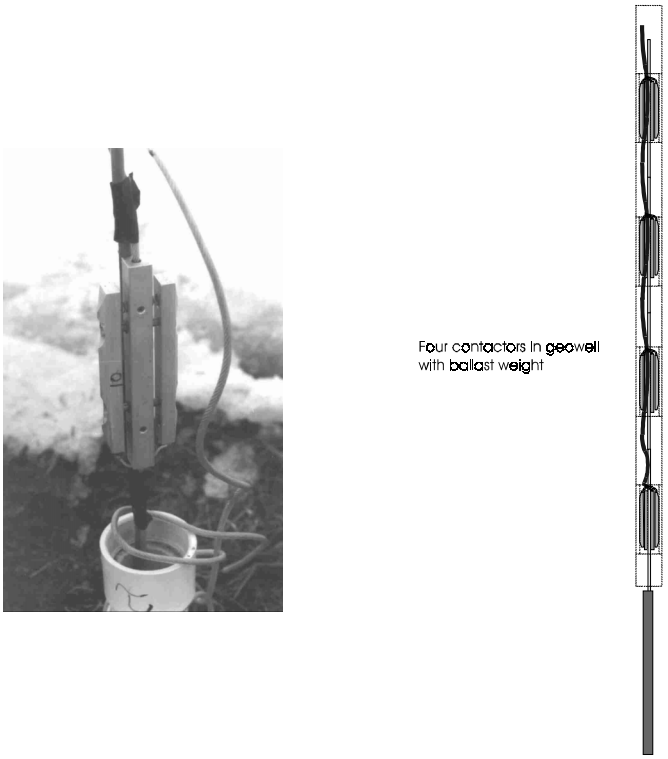

Figure 4.5. ERT contactor entering and as installed in GeoWell.

There are several important advantages to this CPT installation method of VEA GeoWells:

- The electrodes are in ***intimate*** contact with the soil formation by virtue of being pushed into the soil; whereas, in a borehole environment, they need to be grouted in place and fluid sometimes injected to minimize contact resistance.
- Installation ***costs*** are substantially reduced over that of borehole techniques, thus allowing more measurement holes using CPT. With more holes surrounding the soil volume, the resultant tomographic images are clearer and less ambiguous.
- Standard PVC well installation procedures can be used with no need to grout the hole.
- A hollow well is left in the ground for other possible uses, such as GPR tomography and the soil moisture sensor.
- Long-term robust installation.

- Sonic-CPT methods may be used in difficult gravely soils, i.e. Hanford, WA, which require vibratory methods for coarse geologies.

Disadvantages include:

- Electrical connection to the SS electrode using spring contactor requires a clean hole.

- Two CPT pushes are required per VEA installation.

2. Electrode Testing

Various tests are routinely performed on VEAs once they have been installed and prior to data acquisition to test various aspects of an ERT network. Some of these tests are checks that wiring and installation have been performed properly while other tests estimate data quality. Some tests are between electrodes within a vertical array -- termed intra-array tests -- while others are performed between two or more VEAs -- termed inter-array tests.

An intra-array test (loosely termed the "pole-to-pole" test) which checks the wiring to each electrode was conducted on each VEA. This test identifies problems such as: 1) the wiring to two electrodes being inadvertently reversed, and 2) wire insulation being accidentally scraped during installation, thereby creating a current injection or potential measurement point in a location not intended. The test also checks the contact impedance between each electrode and the surrounding soil to assure that sufficient electrical energy is imparted to the ground. Results of these tests demonstrated that the electrodes and wiring for each VEA were functioning properly.

To detect spurious signals from sources such as nearby electric lines, the wave forms of received signals from the VEA electrodes were inspected using an oscilloscope. Although spikes of an unknown origin were observed, there was no 60 Hz interference as might be expected from buried electrical lines or overhead power lines.

The degree to which electrical data can be successfully inverted by tomographic methods to produce an accurate image of the subsurface resistivity structure depends largely upon our knowledge of data quality. Several tests are frequently performed to determine the quality of

ERT data. These are checks on the electrode environment and the subsurface resistivity structure, not the data acquisition electronics. For example, these tests determine the degree of electrical coupling between the electrode and the surrounding soil. They also help to determine the stability of the subsurface resistivity environment during the time of data acquisition These tests are as follows:

- Repeatability
- Reciprocity
- Superposition
- Linearity

Although none of these tests quantitatively define the measurement error, an estimate of that error is given. There is no way to directly detect measurement error *in situ* without prior knowledge of the subsurface resistivity structure. Therefore, the strategy is to devise schemes, using the above tests, to estimate error with as few measurements as possible.

Repeatability involves taking the same measurement many times without changing the measurement system. When repeatability is used as a noise estimator, it is conducted as an inter-VEA test. The experience with repeatability has been as follows:

- It is an easy method to use and can generate substantial information in a relatively short time.
- It is difficult to guarantee that the subsurface resistivity structure is not changing. It is best therefore, to repeat the measurements as close in time as possible when the subsurface can be expected to be nearly static.
- Repeated use of transmitting electrodes within a short period of time can under some conditions, electrically polarize them as a result of electrochemical reactions at the metal-electrolyte interface. This polarization degrades the measurement in a way that does not happen normally, yielding a biased error estimate.

Another test that may be conducted as either an intra- or inter- VEA test is reciprocity. This test consists of repeating the measurement but with the transmitter and receiver dipoles interchanged. In an ideal linear system, i.e. when Ohm's law holds, each measurement and its reciprocal will yield identical results. Perfect reciprocity of this kind is a fundamental

assumption enabling the measurements to be inverted for the resistivity structure. Experience with reciprocity tests shows that:

- Although not as easy to perform as repeatability, it can generate statistical information on errors in a reasonable time period.
- Between the time the normal and reciprocal measurements are made, it is necessary to assume that the subsurface resistivity structure is static.
- The method is sensitive to polarization of the transmitting electrodes as explained in the discussion on repeatability.

From experience, reciprocity has been found to be the best estimate of measurement error for ERT data. Due to its importance, the normal and reciprocal measurements are automatically collected as a standard part of the acquisition measurement schedules.

Another test that checks the data quality is based on the principle of superposition. Superposition must be satisfied for any linear system. For a given transmitter dipole, potentials on three electrodes *a*, *b*, and *c* will be such that

$$f_{ac} = f_{ab} + f_{bc} \qquad (6)$$

where *f* is the potential drop between two electrodes. This states that the potential differences measured between electrode *a* and electrode *c* must equal the sum of the potential differences measured between electrodes *a* and *b* and electrodes *b* and *c*. The degree to which this equality is not true is an estimate of data error.

The experience with error analysis from superposition measurements is as follows:

- It is difficult to use because it required at least three measurements and several calculations to get a single error estimate. Also, it is not easily configured in the acquisition measurements schedules.
- As with the other methods of error estimates, it is assumed that the subsurface resistivity structure is static during the time of the measurement.

Experience has shown that the error estimates obtained from applying the method of superposition are similar to reciprocity estimates. It is used primarily when a problem is found to

involve a few known electrodes. This fact combined with the application difficulties results in low usage of the law of superposition for error analysis.

As mentioned above, superposition tests the ERT system, including the subsurface, for linearity. For a system to be linear, the potential drop measured on a particular receiver dipole must be linearly related to the amount of current being transmitted on another particular dipole. To check for linearity, the transmitting current must be changed as consecutive measurements are made for each dipole pair. Consequently, checks for linearity are made only when other test methods indicate that it is required.

3. ERT Electronics Hardware

Several commercial manufacturers of resistivity measurement equipment were evaluated. Apparently, none of these systems are specifically suited to cross hole applications. All of the vendors offer equipment which works well with surface electrodes. One manufacturer, Zonge, has recently added a multiplexer to its product line which specifically addresses cross hole measurements, and the Zonge system was purchased for the DOE field demonstrations, as it was the most powerful, rugged, and flexible. For the Vermont field test, the Zonge system components were unavailable. Table 4-1 shows a comparison of features and capabilities of the systems examined. Manufacturer commentary for these products is reproduced in Appendix B.

Table 4.1. ERT Data Acquisition Hardware Comparison Chart

	IRIS	OYO	Zonge A	Zonge B	U of AZ	Keithley
Cost ($)	11K	50K	56k	85K	25K	22K
Channels	1	32	4	30	30*	50
Cost/Channel	11K	1.5k	14K	2.7K	0.78k	0.5K
Size/Weight	10 lbs	40 lbs	100 lbs	100 lbs	200 lbs	40 lbs
Automatic/Manual	Manual	Auto	Manual	Auto	Auto	Auto
Battery Portable	Yes	Yes	Yes	Yes	No	No
Upgradable/Expandable	No	No	Yes	Yes	Yes	Yes
Flexibility for Research (1-10)	1	3	8	8	10	10
Tech Support	Yes	Yes	Yes	Yes	No	No
Field Repairable	No	No	No	No	Yes	Some
All the above data acquisition systems would require a computer workstation to generate tomograms. (~$5k)						

We decided to use a multiplexer and a source/measurement system from the commercial test equipment industry. Hewlett Packard, Tektronics and Keithley equipment were reviewed. The Keithley equipment has the best overall value and some of it could be rented. Therefore, a Keithley Model 238 source/measure instrument was rented. Purchasing the multiplexer, a Keithley 7002 with 8 each 4X5 relay matrix cards, was necessary since no matrix equipment could be found in the rental market. TestPoint ™ general purpose test instrumentation software was purchased to run the equipment via the GPIB (IEEE-488).

The Keithley equipment performed well using dummy loads in the laboratory. However, in the field, the wide dynamic range of currents required to excite the electrodes (500 microamps to 100 milliamps) made data gathering very difficult. A second Model 238 was ordered and integrated into the system such that a constant voltage could be applied to the electrodes and the induced voltage measured from the other Model 238. However, noise levels were found to be unacceptable. We decided to use an Iris Syscal Junior connected to a computer for automatic data acquisition and the Keithley multiplexer to switch between electrodes.

A Syscal Junior was rented and integrated into the system. Still, reciprocity noise levels were found to be unacceptable. We discovered that the battery powered Syscal Junior, linked to the computer via the RS232 port, had a ground connection to the power grid and earth ground. So, in effect, there was always an extra electrode in the array which seriously affected the noise level and would invalidate any possible imaging data. This noise problem was eliminated after the AC power ground line was lifted from the computer.

4. Hardware System Design

Manufacturers of resistivity measuring hardware have not designed their equipment for borehole, cross hole configurations. The essential ingredient in such a system is a flexible relay matrix with a high channel count. Economical commercial field portable hardware does not exist in the market today. Perhaps the reason is that subsurface resistivity measurements require higher amounts of power to produce the required high current densities. The Syscal Junior at 50 watts power would be the minimum transmitter required. Zonge, for instance, offers a 1,000 watt unit. At these power levels, the relays for the matrix would have to be quite large, heavy and

expensive. An interim and flexible solution is to use a commercially available relay matrix system which could be reconfigured upon demand for the number of VEAs at the site and the total number of electrodes.

The relay matrix system selected for the ERT field tests is manufactured by Keithley Instruments, Inc. A mainframe chassis (Keithley Model 7002) houses the switching cards (Keithley Model 7052). The 4 X 5 matrix card in 0 has four inputs and five outputs and in this case, allows the four signal lines from the Syscal Junior to be multiplexed to any of five electrodes. Two cards are required for each VEA of ten electrodes, and eight cards total for the four VEAs used in the Vermont field tests. With eight 4 X 5 matrix cards, each electrode in the array of 40 electrodes can be connected to any of the four Syscal Junior signal lines, as partially depicted in 0.

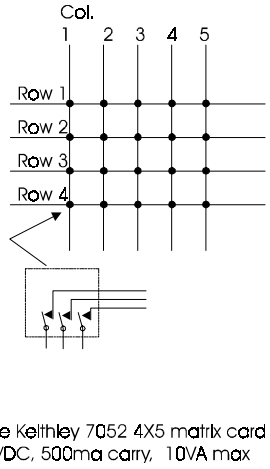

Figure 4.6. Schematic of the 4 X 5 matrix card.

The matrix cards are housed in a chassis which furnishes relay actuation power and control logic. The chassis (Keithley 7002) accepts inputs manually, or in this case over the GPI Buss. The 7002 has a 500 location local memory. A sequence of relay patterns can be loaded into each location and saved even after power is shut off.

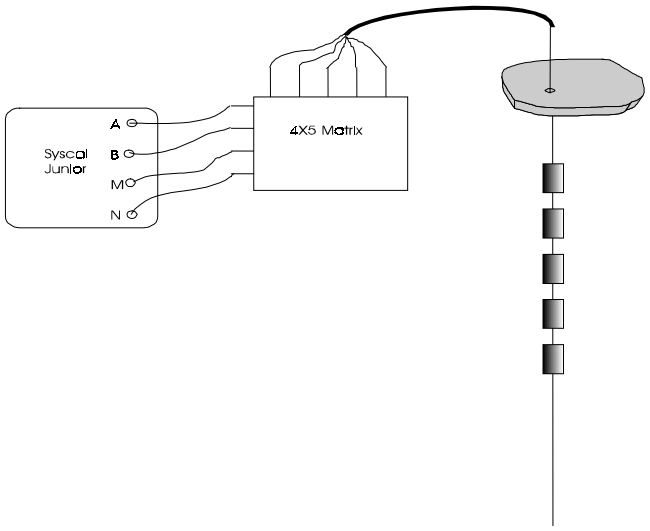

Figure 4.7. Partial system schematic.

0 shows a PC, running Windows and the TestPoint application software, controlling the Keithley 7002 relay matrix over the GPIB. The PC asynchronously starts the IRIS Syscal Junior and then receives ERT data over the RS232 port. Though this is not an optimized system, it works well enough to allow one measurement to be taken every 30 seconds.

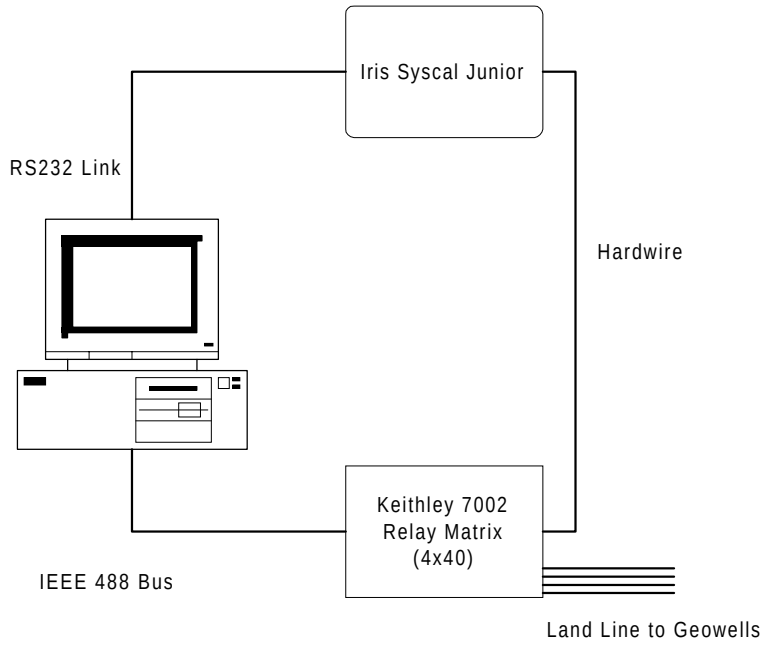

Figure 4.8. ERT system diagram.

0 is a software/hardware flow diagram. An Array Schedule File is set up depending upon the ERT measurements to be made. Generally, all possible independent combinations of nearest neighbor electrode pairs are measured. The total number of independent measurements is equal to $\frac{n(n-3)}{2}$, where n is the number of electrodes. Thus, for two VEAs with 10 electrodes each, n=20 and the total number of independent ERT measurements is 170. The reciprocal of each independent measurement is also made in order to quantify the noise level for the forward inversion and imaging program. Therefore, the Array Schedule File will contain a sequence of 340 measurements in our example. For this example and the equipment used, the total measurement time for one borehole-to-borehole ERT measurement is about three hours.

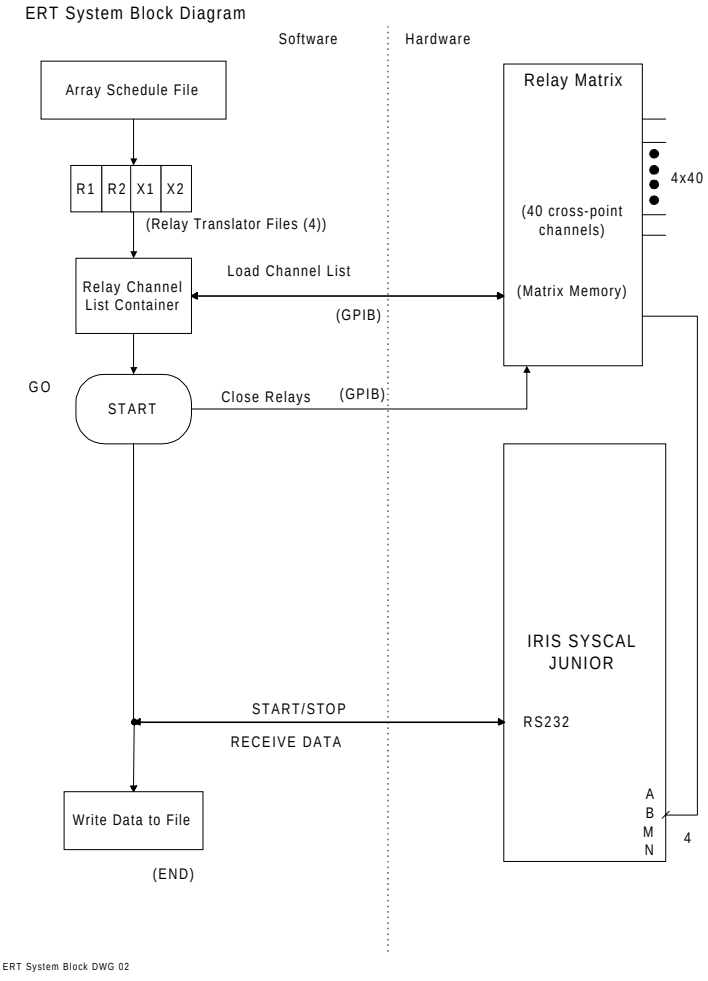

Figure 4.9. ERT software/hardware flow diagram.

A Zonge system was purchased after the first ERT tests were conducted at the Vermont test site. The Zonge system has more power and was used to conduct the second two field tests at the DOE/Savannah River Site.

5. Zonge System for Geophysical Data Acquisition

Initial testing using the Keithley system was less than satisfactory. The system did not have enough power for high resistivity soils. Therefore, we purchased the commercial Zonge system. This system performed well and was used for the remainder of the project. The geophysical data acquisition equipment manufactured by Zonge Engineering Inc. is designed to obtain virtually any type of electromagnetic or electrical data with the DC to 8 kHz bandwidth. The equipment for a typical Dipole-Dipole Resistivity Phase test with a reference electrode is made up of a multichannel receiver (GDP-32), a battery powered transmitter, a power supply capable of generating 100V, an isolation amplifier, a multiplexor, and a laptop computer to control the test. A schematic of the components and layout of the test is shown in 0.

The GDP-32 multichannel receiver is designed to obtain data for resistivity, induced polarization, (frequency or time domain) spectral IP, complex resistivity (CR), controlled source audio-frequency magnetotellurics (CSAMT), transient EM (TEM), NanoTEM, and natural source MT and AMT. The receiver operates both in frequency domain and time domain. Twenty four frequencies can be selected in binary intervals between 0.0007 Hz and 8 kHz. The GDP-32 is designed for multiple channel data acquisition. One to 16 channels can be used and multiple receivers can be used together for n-channel acquisition. The receiver has automatic software control for control through a serial port to a computer. Data may be manually or automatically logged based on a schedule of measurements. The GDP-32 is connected to the ZT-30 transmitter and controls the cycling speed of the transmitter during a test.

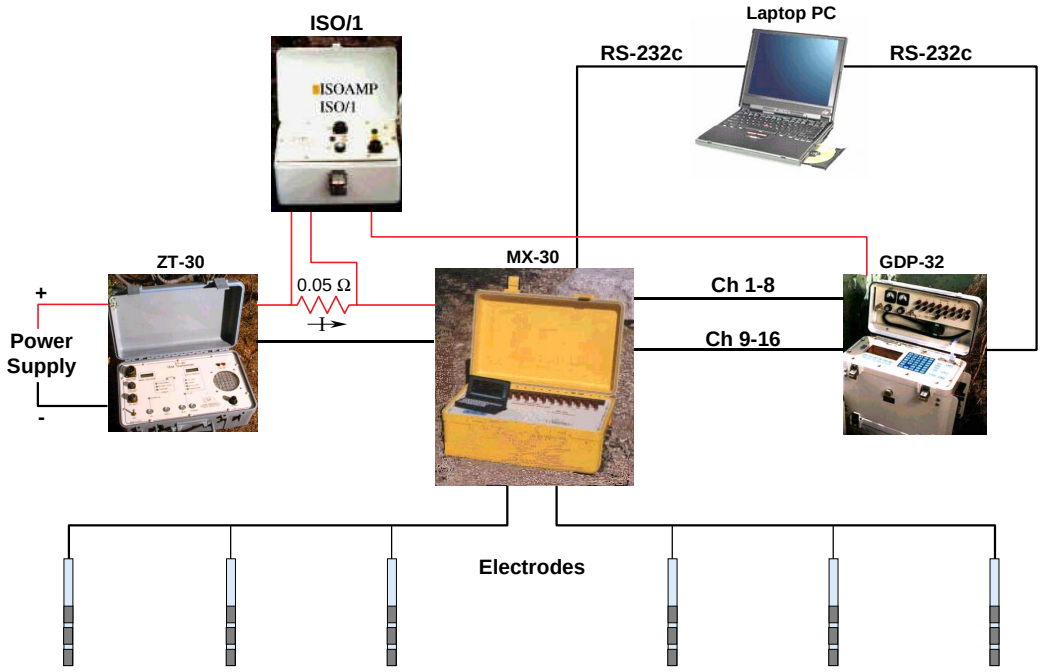

Figure 4.10. Zonge's geophyscial data acquisition system set up for a dipole-dipole electrical resistivity test.

The ZT-30 transmitter is a battery powered transmitter designed to transmit a time domain signal between DC and 32 Hz and a frequency domain signal from DC to 512 Hz. It can be synchronized with the GDP-32 receiver for synchronous measurements. It has a transmitter signal and a polarity signal for controlling the output polarity of the transmitter and transmits the signal through one-quarter period cycling. The ZT-30 contains a shunt resistor of 0.05 Ohms so that the current can be measured in the circuit. It is connected with an isolation amplifier which sends the actual current in the circuit during a transmit cycle to the GDP-32 receiver. The ZT-30 transmitter transmits the signal generated from the power supply.

The multiplexor (MX-30) is used to allow automatic switching from one electrode pair to another during a measurement schedule. Each electrode is hooked directly to a position in the MX-30 and the computer software uses the information from the MX-30 electrode locations to interpret and store the data from the GDP-32 receiver.

An electrical resistivity test is conducted from the software schedule that is supplied to the GDP-32 receiver. This tells the receiver which electrode pair connected to the MX-30 will be

the transmitter pair (the electrode pair as part of the transmitting circuit) and which pairs to measure the potential difference of during the transmission of the signal across the transmitter pair. Since the GDP-32 has eight channels, one channel is used for the transmitter pair and the other seven are used to take measurements of potential across the receiver pairs. The potential across the receiver pairs is divided by the value of the transmitter current pair and then stored in the computer. The schedule moves to the next transmitter pair and receiver pairs and in this way a schedule of measurements is taken. After examining numerous systems, the Zonge system was the most powerful, rugged and flexible of all the geophysical data acquisition systems we investigated.

6. ERT Software

The software used for processing the ERT data was supplied by Abe Ramirez and Bill Daily of Lawrence Livermore National Laboratory. The underlying algorithms are described in (Ref. 26 and 27). Here we summarize some of the key features.

The geophysical inversion process uses finite element model methods that solve the inverse problem posed by minimizing an objective function made up of iterates of a forward model and the data collected. The goal of this process is to make the final forward calculation match the field data to a certain specified degree of accuracy. The code solves for the resistivity structure in a half space based on electrical resistivity measurements taken between discrete electrodes residing in two or more co-planar boreholes. The code is loosely referred to as 2.5D, which means that the earth resistivity structure is assumed to be two dimensional (i.e. resistivity varies only in the plane defined by the boreholes), yet the problem is solved at some level in three dimensions to allow for the fact that the electrodes used for injecting and receiving measurement signals are discrete points in 3-D space. This mixture of 2-D and 3-D philosophies is implemented via a Fourier transform technique. This improvement over a pure 2-D method allows the electric field around the electrodes to be modeled properly, yet avoids the difficulties and time constraints of solving a pure 3-D problem. The boundary conditions used in this method are (1) no current flow out of the ground at the earth/air interface (Neumann condition) and (2) a constant zero potential at the other three subsurface mesh boundaries (Dirichlet

condition). The three subsurface mesh boundaries are set at a large distance from the measurement boreholes.

The general problem of tomographic inversion of electric potential data for the resistivity structure from boreholes in the earth is both ill-posed and non-unique. This problem stems partly from the fact that full surrounding coverage of the region of interest is not possible. Therefore, some additional constraints referred to as "regularization" must be placed on the solution for the inversion to converge. In this implementation of the problem, the most desirable solution is one that (a) gives a minimal difference between the forward calculation and the measurements, and (b) has the smoothest spatial variability in the resistivity structure consistent with (a). This additional constraint is sufficient to allow the inversion to converge to a stable and repeatable result. The method requires that an estimate be made apriori of the variance of each measurement, that is the variability or scatter to be expected if many repeated identical measurements were to be made. This variance is necessary to calculate a weight or degree of confidence in the particular measurement, so that one or more noisy measurement values will not unduly affect the results. Actually estimating the variance of each measurement by repetition is impractical due to time constraints, but experience has shown that the difference between each measurement and its reciprocal is the most useful estimate of this parameter.

B. GPR HARDWARE DEVELOPMENT

GPR borehole system development consists of three primary tasks:

1. Antenna design for CPT installation;
2. GPR electronics hardware; and
3. Software for control and imaging.

1. Antenna Design

GPR systems require antennas that can radiate temporally short, wide-bandwidth pulses in the 50 MHz to 1000 MHz frequency range. Therefore, the antenna should have the following characteristics:

- The radiated pulse should be a faithful reproduction of the transmitter output.
- There should be little pulse distortion and ringing on the radiated pulse.
- The reflected signal at the input to the antenna should be small, on the order of 30 dB or more below the input pulse.
- The amplitude of the radiated pulse should be as large as possible.

An infinitely long biconical dipole is the ideal radiator for short, ultra-wideband pulses, meeting all the above criteria. Resistively loading a finite length biconical dipole provides the most practical antenna design for pulse radiation (Ref. 28). The resistive loading is meant to eliminate or greatly reduce the reflections from the ends of the dipole, creating a traveling-wave antenna. When placed in a borehole, antenna characteristics, modified by the surrounding medium, are quite different from that in free space (Ref. 29).

Several antenna design approaches were studied, including making the antenna an integral part of a CPT push rod assembly. From the electromagnetic (EM) prospective the antenna should be intimately coupled to the surrounding soil to maximize energy transfer, yet maximally decoupled from any metallic control cables and CPT push rods. Mechanical loads on the radar probe restrict the design considerations and the types and thickness of dielectric materials. Also, if the antenna is built into a CPT rod assembly, a CPT truck is required as part of the GPR data acquisition process. The truck is needed to move the antenna/push rod assembly up and down the hole.

After careful consideration it was decided to design the GPR antennas to operate independently of the CPT truck, except that CPT methods are used to install the GPR boreholes much like the ERT installations. In fact, tests were run to demonstrate that the same PVC/SS-electrode-lined holes could be used for GPR measurements – the GeoWells. Using GeoWells for both ERT and GPR is an important development which improves data fusion and reduces survey costs.

The antenna is constructed from a 7-foot long piece of 1-inch diameter PVC pipe over which copper foil is glued to form the dipole elements. The antenna is connected to the surface

with a low-loss coaxial cable. At the cable-antenna connection a ferrite balun is inserted to transform the unbalanced cable currents to the balanced dipole. A properly designed balun decouples the cable from the antenna, thus reducing distortions in the radiation pattern due to the presence of the metallic cable. The antenna assembly is covered with plastic to provide a moisture resistant protective coating. 0 is a picture of the two GPR borehole antennas and 0 shows an antenna prior to deployment in a borehole. Vertical radiation pattern measurements were made in the ground indicating that the antennas are well behaved.

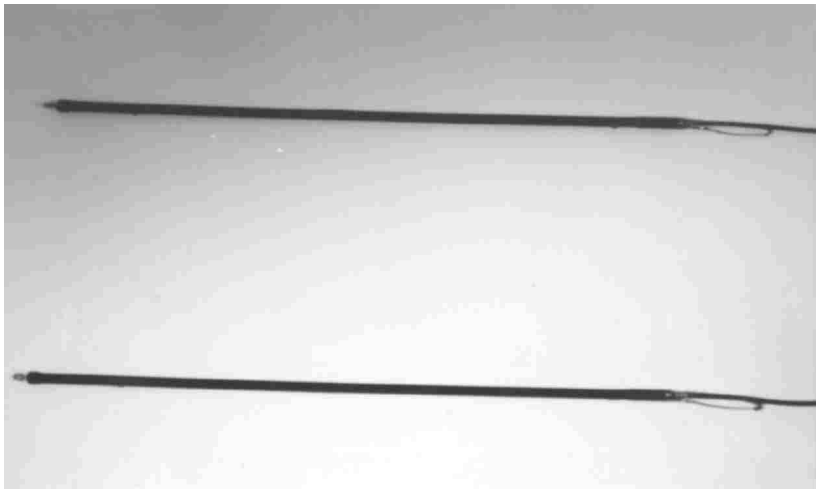

Figure 4.11. Picture of GPR borehole antennas.

Figure 4.12. GPR borehole antenna ready for deployment.

2. GPR Electronic Hardware

Several manufacturers of GPR equipment were evaluated. Apparently none of the vendors sells a borehole system suitable for our application. All the vendors offer equipment which works with surface antennas.

Table 4.2. GPR Equipment Comparison Chart

Manufacturer	GSSI-SIR2	Sensors &Software pulseEKKO 100A	RAMAC/GPR
Cost	**$53,350.00**	**$44,005.00**	**$33,500.00**
Control Unit	$23,000.00	$27,000.00	included
Antenna Set, 120MHz	$16,000.00	$10,000.00	included
Software*	$7,700.00	included	included
Accessories	$1,650.00	$2,005.00	$2,500.00
Computer Workstation	$5,000.00	$5,000.00	$5,000.00

*GSSI has quoted both RADAN and WINRAD-ACT software which will automatically pick datapoints and enter them into a spreadsheet.
Sensors and Software includes an integral software package which picks datapoints automatically.
RAMAC/GPR from Sweden is a complete system for taking surface GPR measurements and would require some modifications / additions to perform borehole measurements.

A GSSI SIR2 electronics system was rented and used to perform the initial testing of the borehole antennas. 0 is a picture of the equipment and antennas. The antennas are partially shown in the foreground and the 100-foot downhole cables are coiled in the background.

Figure 4.13. Picture of GPR borehole test equipment.

The GSSI system is optimized for surface measurements where the antennas are towed across the ground; this equipment was not well suited for borehole measurements. Therefore, Sensors and Software PulseEkko1000 electronics equipment was used for the GPR borehole testing program. The radar control unit was interfaced with a laptop computer as shown in Figure 4.14. A 100 MHz monocycle, short pulse transmitter was used. Transmitter parameters and data acquisition settings were set via the laptop computer (Toshiba Tecra500). Received waveforms were stored on this computer's hard drive.

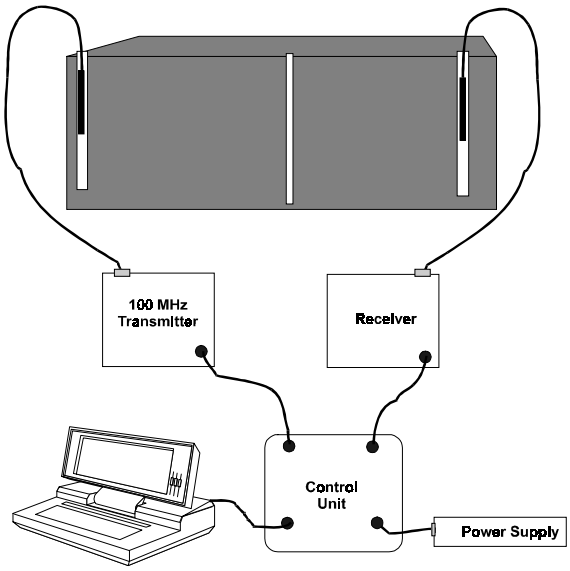

Figure 4.14. GPR equipment setup for tomographic measurements.

3. GPR Software

Several steps are followed to assure GPR data quality for software processing. The radar data acquisition software permits the viewing of individual return wavelets in oscilloscope format in order to verify system integrity. In this viewing mode, we can observe excessive noise due to hardware problems or cable distribution as well as return signal amplitude values. While data is actually collected in "wiggle trace" viewing mode, we examine the return wavelets in oscilloscope mode before actual data collection of each borehole pair and a number of times during collection. In order to improve signal-to-noise ratio, a fixed number of consecutive scans (e.g. 64) are averaged for each transmit/receive location. Each averaged scan is stored in a separate computer file and the file name and test conditions recorded.

After field data collection is finished, each data scan is preprocessed using a bandpass filter to remove high frequency noise and low frequency offsets. The power envelope of the scan is calculated and compared with the average amplitude. If the maximum value of the power is less than three times the average value then the scan is removed from the data set.

The software used for processing the GPR borehole data to generate tomographic images is 3DTOM [30]. 3DTOM is a DOS compatible computer program developed by the U.S. Bureau of Mines for three dimensional tomographic imaging of the subsurface at mine sites. The program uses the simultaneous iterative reconstruction technique (SIRT) to invert travel time data and produce maps of wave velocity, or to invert amplitude data and generate maps of wave attenuation coefficients. The SIRT algorithm employs an initial guess model. The corresponding travel times for the ray paths are then calculated and compared to the experimental data. The differences between the calculated and experimental travel times are used in calculating correction factors to be applied to the initial model. This procedure is repeated until some convergence of limit criterion is reached. The correction factors are calculated for all path simultaneously. Either seismic or electromagnetic wave data may be used.

Ray tracing in 3DTOM uses several different methods, including ray bending, network theory, and a combination of these. User-defined constraints are important in reducing the mathematical non-uniqueness of inversions based on limited data. 3DTOM permits the use of hard constraints, or soft constraints based on fuzzy logic, to allow for uncertainty in the constraints.

SECTION 5.
RESULTS AND DISCUSSION

A. FIELD DEMONSTRATIONS

Site conditions and soils may prohibit the usefulness of GPR or ERT when used alone. Highly resistive soils for ERT and highly conductive soils in the case of GPR make it difficult to design and use these methods individually for improved site characterization and monitoring. However, CPT data and deployment methods can overcome the problems soil types and conditions may present to ERT or GPR and improve these types of imaging methods by providing additional information on the subsurface. Three test sites were chosen for technology demonstration of integrated CPT, ERT and GPR. Each of these field demonstrations presented a unique opportunity to test the benefits of these integrated technologies in a variety of soil conditions and soil types, in both the unsaturated and saturated zones.

The first site, the Vermont Test Site, was used to field test the prototype electrodes and designs, CPT installation of the vertical electrode arrays, and ERT and GPR data acquisition and imaging, before going to a DOE site. The Vermont field test was the first field implementation of the CPT/ERT and GPR demonstration. After this test the electrode designs were improved and new ERT equipment was purchased. The ERT results from the Vermont test site indicated that the equipment was insufficient to transmit the necessary electric current through high resistivity soils. For the DOE field demonstrations a more powerful Zonge system was purchased. The second and third tests were conducted at DOE's Savannah River Site, the second in an uncontaminated aquifer, and the third in a contaminated aquifer undergoing remediation. The results are very encouraging and indicate the benefits of using integrated CPT, ERT and GPR for site characterization and monitoring.

ARA's Vermont site was chosen as the field test site because it is close to our offices and we had some previous CPT experience at this site. However, a more important consideration was that it contained inter-bedded sands and clays with variable moisture content; thus it contained a range of electromagnetic subsurface conditions for testing the ERT and GPR capabilities.

The MWD site at SRS was chosen as the second test site. The test area was an uncontaminated area of the unsaturated zone and the unconfined portion of the Upper Three Runs aquifer. These strata are the upper part of the Floridian Aquifer System at the Savannah River Site. Our field demonstration at the MWD site included; field deployment of Geowells with CPT, integrating CPT data to improve inversion model imaging, ERT and GPR data acquisition, and using CPT, ERT and GPR to image the changes exerted on the aquifer during a pumping test.

The TNX area at SRS was chosen as the third test site. The test site is located near the Geosiphon (TGSC-1) that is used for an on-going groundwater remediation effort using *in-situ* iron filings surrounding the Geosiphon. The Geosiphon is a passive flow treatment well utilizing zero valent iron reduction to treat contaminated groundwater. It is located in the floodplain below the TNX facility. The test area was the saturated zone very near the Geosiphon. Our field demonstration at the Geosiphon site included; field deployment of new electrodes modified to also serve as sample ports for discrete layered sampling, conducting a tracer test, ERT and GPR data acquisition before and during the tracer injection, ERT imaging of the tracer movement and consequently preferential flow patterns toward the Geosiphon, and verifying the results with the samples taken from the electrodes during the field test.

B. ARA'S VERMONT TEST SITE

1. Site Description

The ARA Vermont Test Site is an open grassy field on a hill approximately 160 ft above the White River in South Royalton, VT. The soil is inter-bedded sands with clay lenses and thin clay layers; the water table is about 160 ft bgs. The test plan included installing four GeoWells on a square grid with an infusion well at the center of the square. ERT and GPR tomographic data would be taken before and after the infusion of about 100 gallons of salt water.

The surface topography was measured and a GPR surface survey was performed to map the near-surface soil stratigraphy. An initial interpretation of the GPR profiles indicated that the possible flow direction of the water from the infusion test would be in the northwesterly

direction. The position and orientation of the GeoWell grid was chosen from these GPR survey results. A reasonable push depth for our tests is 60 feet, which then dictated a maximum hole spacing of 30 feet for the ERT tests . (A rule of thumb is to have the well spacing ½ the depth or length of the ERT array.) The CPT truck installed the four GeoWells and the infusion well along with three additional monitoring wells. A photograph of the test site is shown in 0. The heated instrumentation trailer is in the background with the GeoWells and Monitoring Wells identified in the foreground. 0 shows the dimensional layout of the test site. 0 shows the site topography.

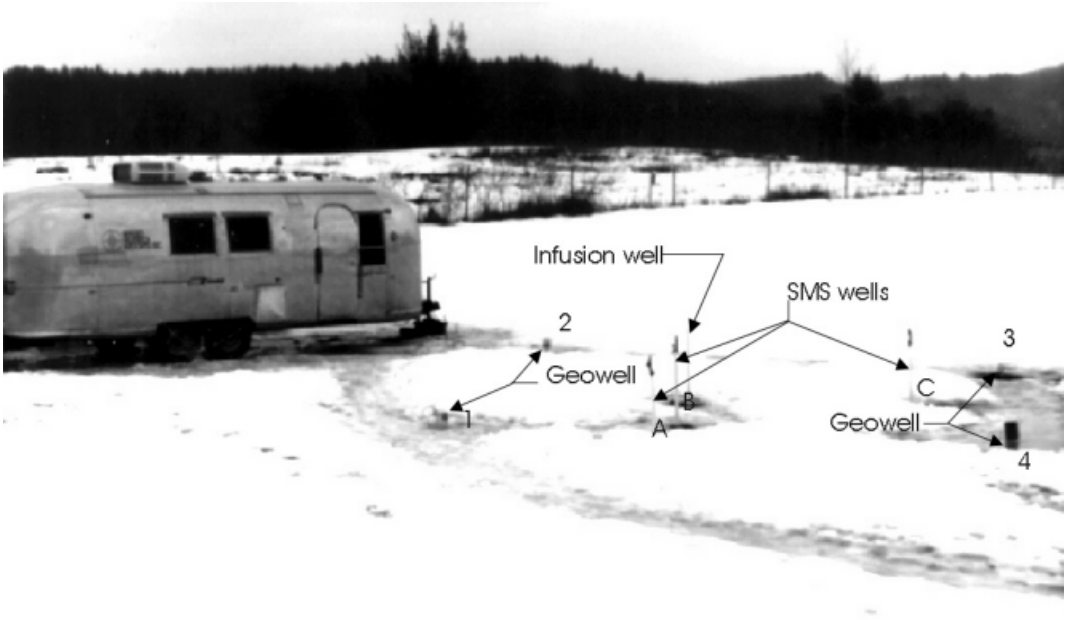

Figure 5.1. Picture of the Vermont Test Site.

2. GPR Surface Survey Results

Prior to making the survey and installing GeoWells, the site was staked out and grid lines 10 feet on center were laid out over a 100 x 100 foot square centered about the well site. Theodolite data were taken and surface features plotted (see 0).

A GSSI ™ GPR system with a 500 MHz antenna was used for the survey. Scans were made in both the North-South and East-West directions. Event markers at each 10-foot interval were placed in the data record by the operator during the scan. 0 shows two examples of radar profiles with the GeoWell locations superimposed on the “raw” radar records. These profiles are

orthogonal to each other. The prominent reflection features are thin clay layers; the blank areas are homogeneous sand. The radar profiles were interpreted to produce a 3D map of the major subsurface layers to a depth of about 20 feet as shown in 0. 0 is a contour map of the first major clay layer. The location of the monitoring wells and holes 1 and 4 were selected to intersect the projected direction of the salt water plume.

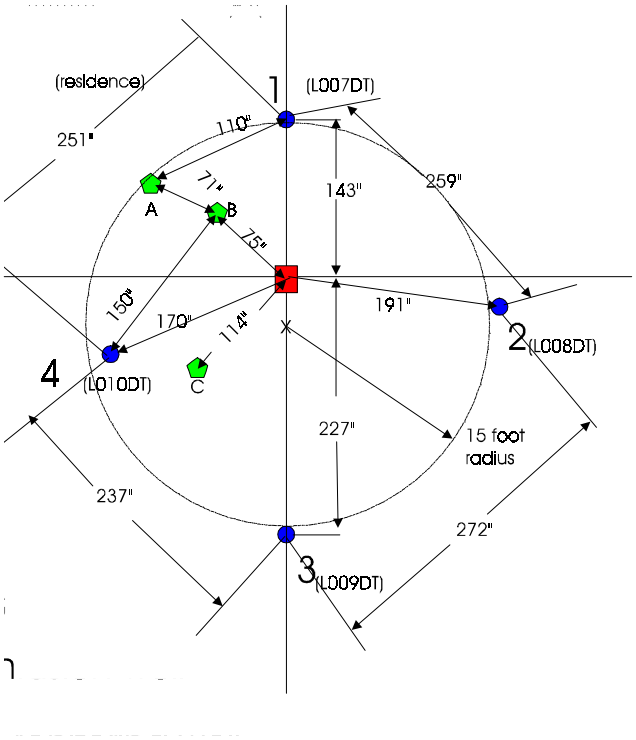

Figure 5.2. Layout of GeoWells at the Vermont Test Site.

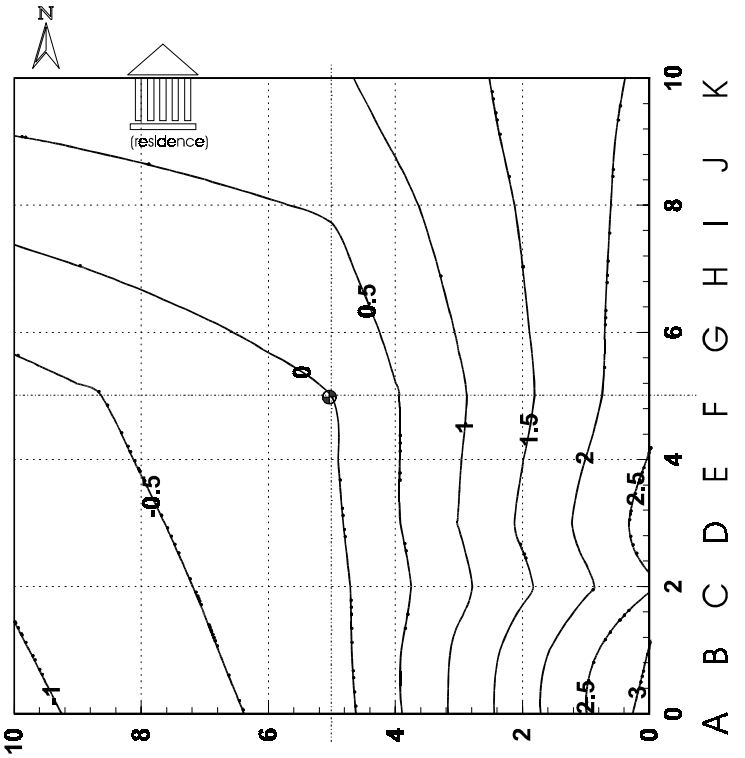

Figure 5.3. Surface contours in feet at Vermont Test Site.

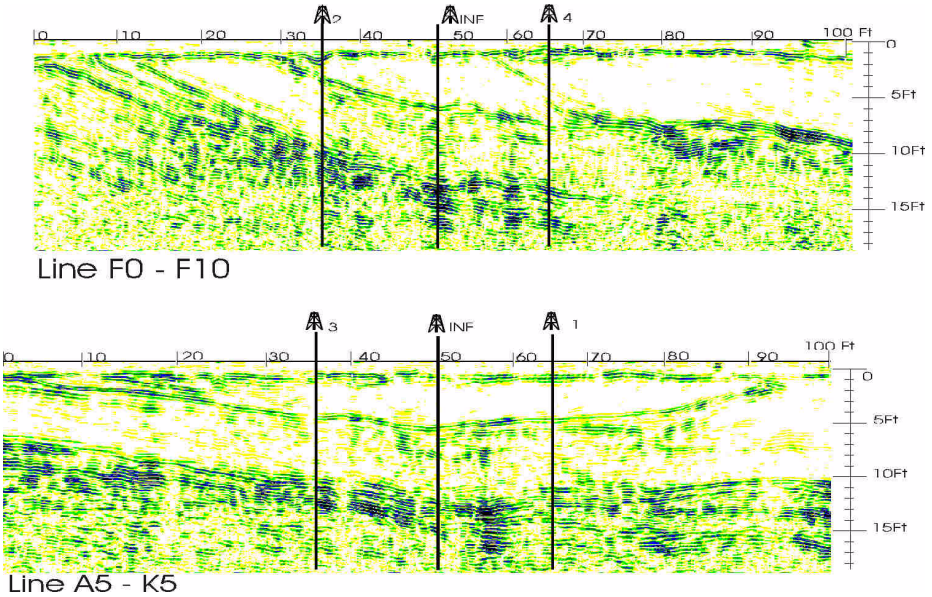

Figure 5.4. Examples of GPR profiles.

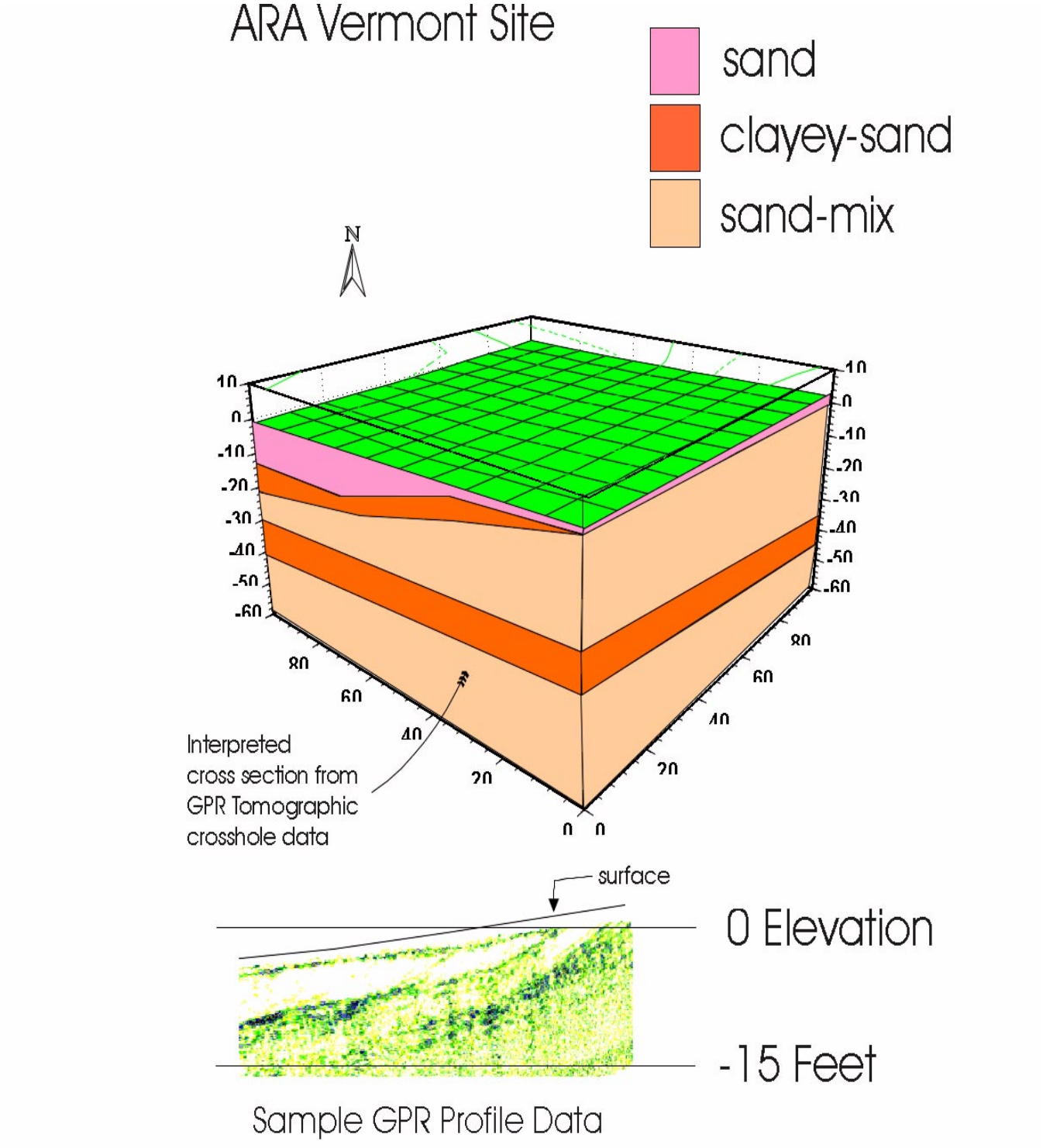

Figure 5.5. 3D map of major subsurface layers.

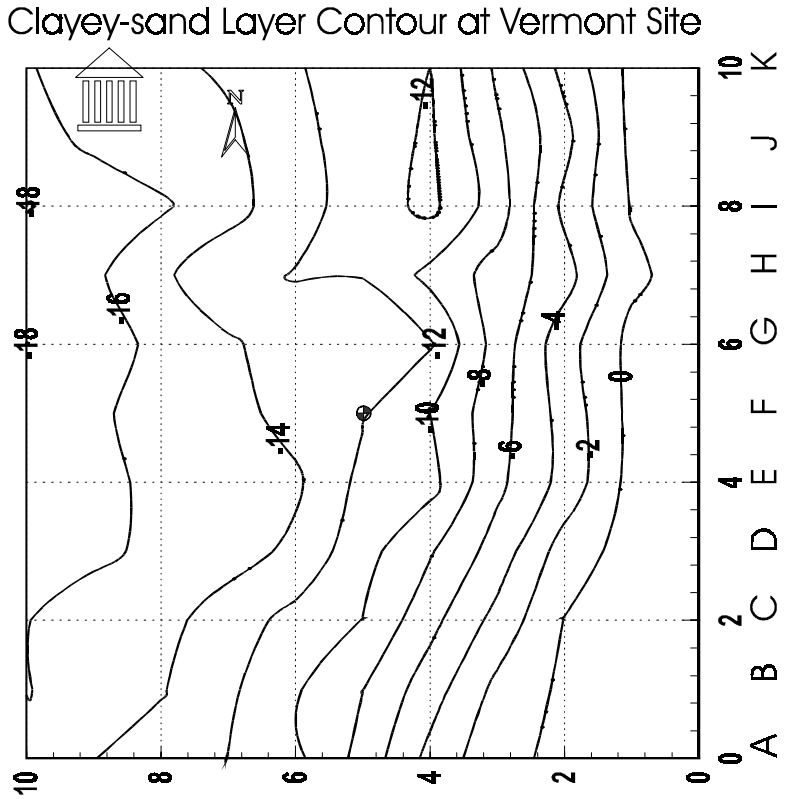

Figure 5.6. Contour plot of first clay layer from radar profiles.

3. CPT Results

Standard CPT pushes were made at each of the GeoWell locations prior to installing the GeoWells. CPT logs of tip, sleeve, pore pressure, and resistivity data were recorded at each well location. The CPT logs are plotted in Appendix B. Figure 5.7shows the soil classifications calculated from the CPT logs. These CPT data are eventually compared to GPR and ERT data. Note that the depths to the inter-bedded clay layers are fairly consistent from hole to hole. The pore pressure logs (Appendix B) indicate that the clay layers are very wet.

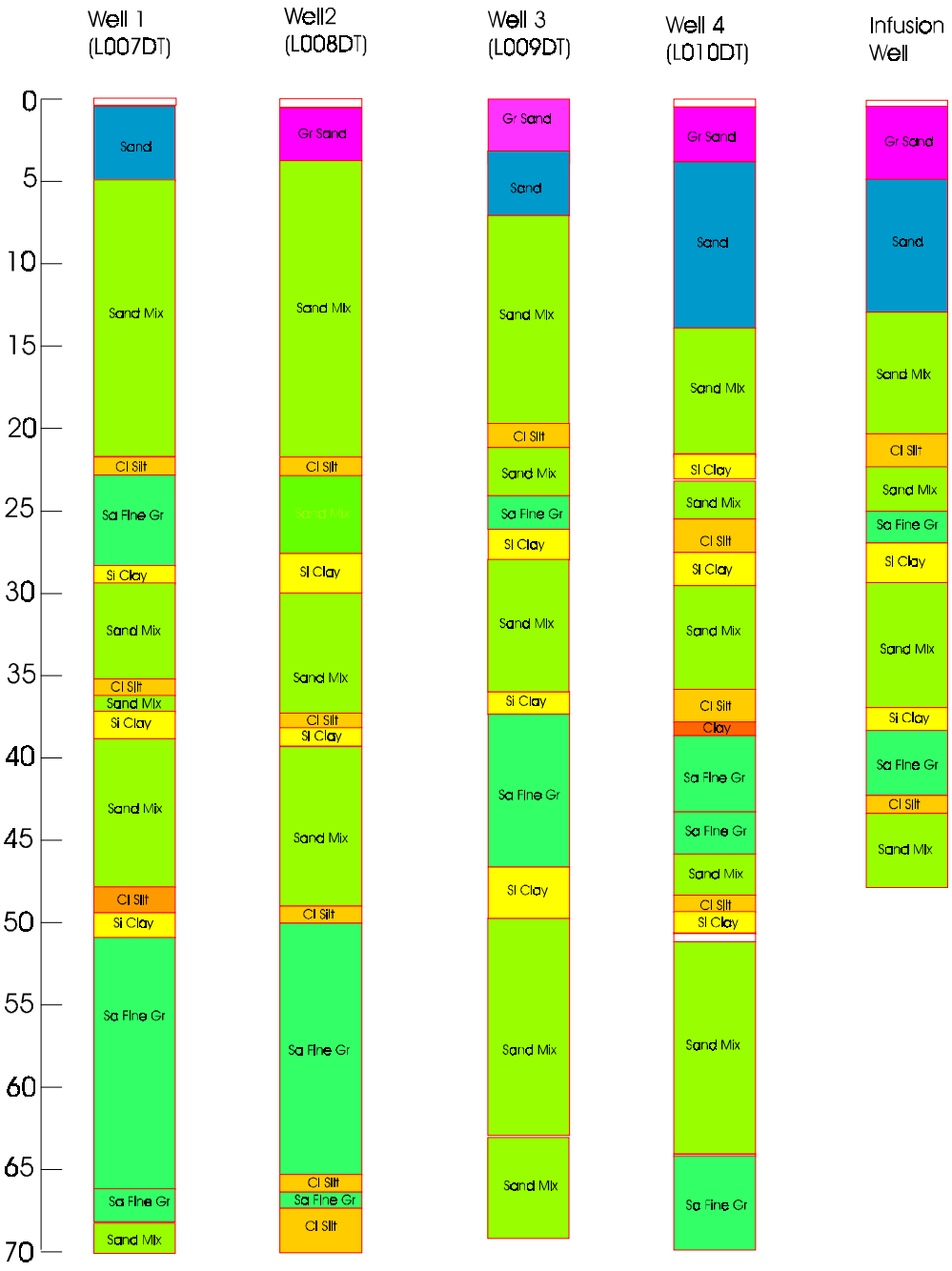

Figure 5.7. CPT soil classification logs at GeoWells.

Combining the surface topography plot and the GPR profiles with the CPT data, the depth to soil interfaces from a horizontal datum plane is calculated. The top of the first clay layer is at approximately 15 ft bgs at the center of the grid. Using real-depth measurements from CPT records and contiguous records from GPR data, this clayey layer was easily located and mapped (Figure 5.6). (In the CPT logs, this boundary is between the Sand and Sand Mix classification.)

This clayey layer dips towards the northwest while the surface contour dips towards the south. Based on this information, we speculated that the saline water introduced at the infiltration well should flow in the northwesterly direction.

4. GeoWell Installation

Several field trials were made to determine the most effective method of installing GeoWells. During these procedures, two types of well casing material were tried: PVC and reinforced fiberglass. The goal was to install a GeoWell in a single push versus reoccupying a well hole after a "dummy" CPT push. Four condition sets were attempted:

- Single push with standard sacrificial tip;
- Single push with oversize tip;
- Reoccupying with standard sacrificial tip; and
- Reoccupying with oversize tip.

A schematic of the CPT well push configurations for the standard oversized tips is given in 0. In both cases using the oversized tip, no difficulty was encountered installing the GeoWell to a desired depth (0). For the case using the standard tip, both PVC and fiberglass separated from the tip, causing the push to be abandoned. The case of reoccupying a "dummy" hole with using the standard tip produced marginal success as stress fractures were noted at the threaded joint connecting the tip with the well pipe.

Results for both PVC and reinforced fiberglass were identical, though the fiberglass has a much higher tensile strength (approximately five times that of PVC). The side-wall friction forces created tension; forces at the tip joint were higher than either material could withstand. The tip joint failed in all trials with the standard tip. Note that these trials were made at a relatively "easy" site where CPT push forces were one-fourth to one-half of capacity.

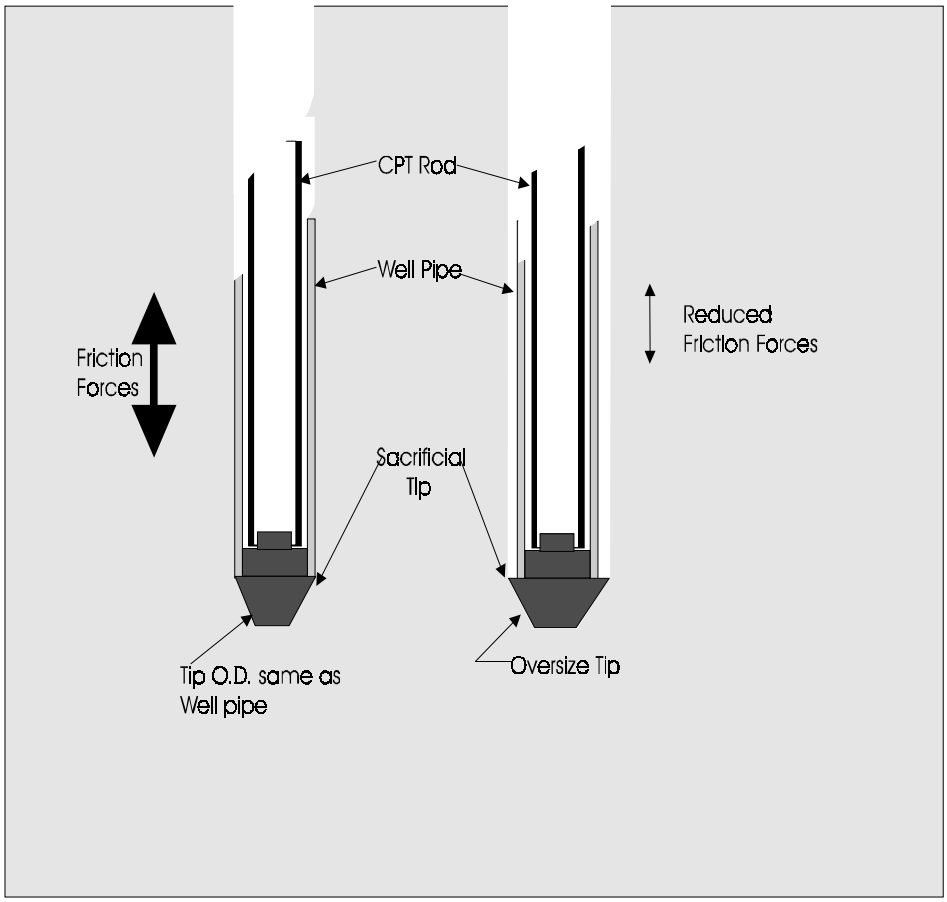

Figure 5.8. GeoWell installation test configurations with a standard and an oversized tip.

It was decided to do a standard CPT push at each well location while gathering CPT data, and then reoccupy these holes with the GeoWell using the oversize tip to insure successful installation. A schematic of the well locations is shown in Figure 5.2. No particular difficulties were encountered during the GeoWell installations. Tests were conducted using a 12-volt DC power source and a multimeter to determine the extent of electrode contact with the soil.

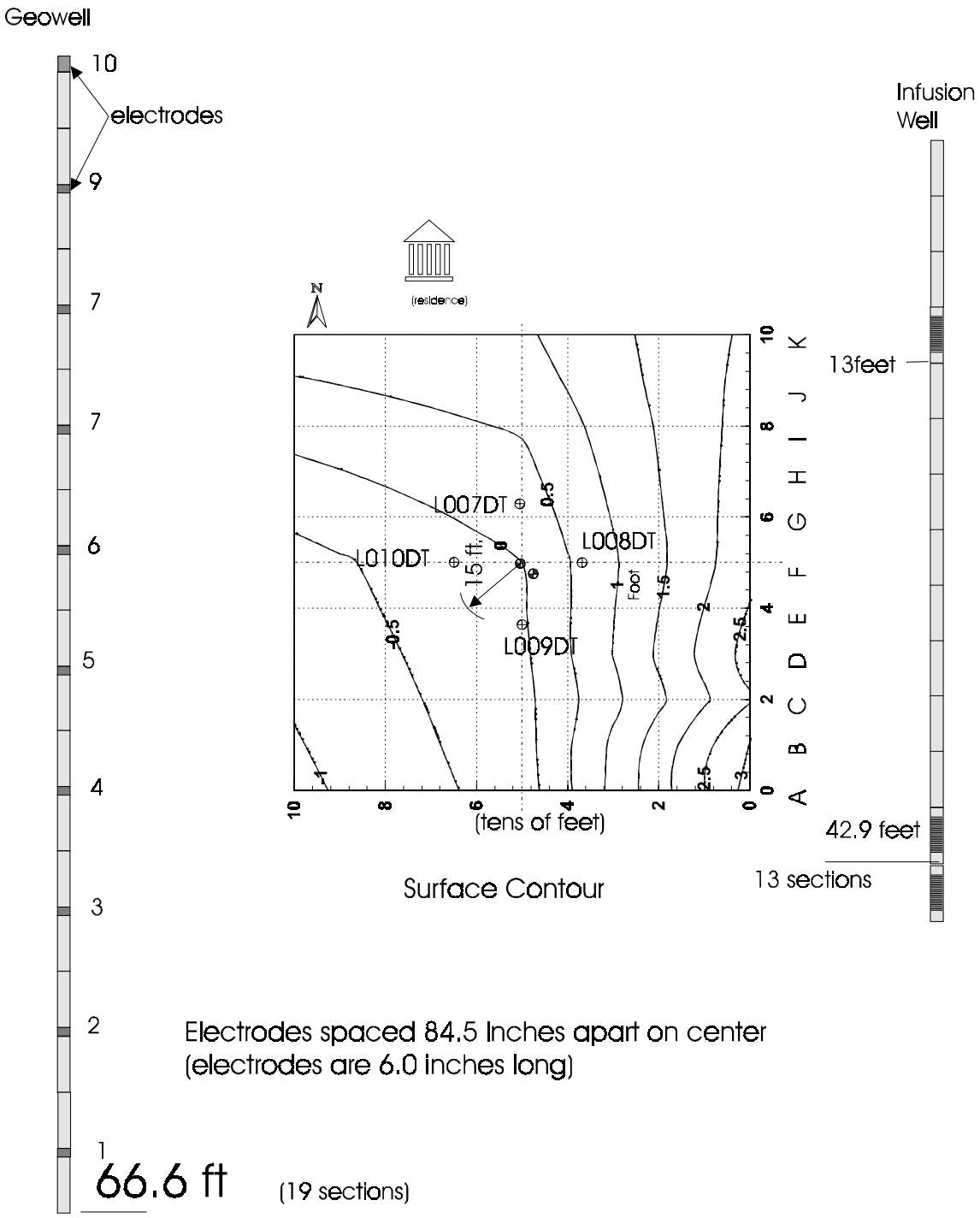

Figure 5.9. Dimensional schematic of the GeoWell, showing electrode numbering, and infiltration well.

5. GPR Borehole Antenna Testing in the GeoWell

One objective of the field testing program was to demonstrate that the same hole could be used for both ERT and GPR. GPR borehole antennas were used in PVC-lined well casings and

showed good results. However, the GeoWells had the addition of stainless-steel sections of threaded tubing, six inches long, spaced between PVC-threaded sections. The potential effect of a steel electrode on GPR borehole antenna tuning was not initially known. A scale mockup of two GeoWells, in air, was made in the laboratory. One set of borehole antennas was set up to operate with a 100MHz monocycle pulse; a digital oscilloscope was used to examine the received signal on the other antenna. Both antennas were moved along the GeoWell, past the electrodes, over their full length. The GeoWell's stainless steel electrodes have negligible effect on the radar signature. Further examination of the GPR tomographic images taken in the CPT installed GeoWells confirmed this conclusion.

6. Borehole Test Results

The test program called for making cross-borehole measurements with both the ERT and GPR system from the same GeoWells before and after salt water infusion. The salt water infusion was designed to create a migrating plume to be imaged by the two techniques. The GeoWells had to be occupied sequentially by the electrode contactor strings and the GPR antennas. Each measurement set took several hours for both the ERT and GPR. The pre-infusion measurements were made over several days; however, the post-infusion measurements had to be made as quickly as possible to capture the migrating water plume.

Table 5.1 shows the ERT GeoWell measurement schedule.
The GPR measurements are interleaved with this schedule. Each ERT tomography experiment is controlled by an "Array Schedule File." This ERT measurement sequence is a list of all combinations of 4 electrodes (2 for the transmitter and 2 for the receiver) which would be accessed during an experiment.

Table 5.1. Vermont Test Site ERT Measurement Schedule

	Actual: Feb, 1997	
Well	Pre Infusion	Post Infusion
1 to 3	2/12	2/17, 2/17, 2/18
2 to 4	2/12	2/17, 2/17, 2/19
1 to 4	2/12	2/17, 2/19
1 to 2	2/13	2/19
2 to 3	2/13	2/19
3 to 4	2/13	2/19

Resistivity data were taken several days before the salt water infusion process. Several sets were repeated to see if the data were repeatable and to determine the noise characteristics for the site, GeoWells, and ERT instrumentation. After a full suite of data were taken, the contactor strings were removed and GPR borehole data were taken in the same GeoWells. Based upon the good quality of the ERT images, it was decided to proceed with the salt water infiltration. As soon as the 100 gallons of water were injected through the infusion well, another set of GPR measurements were made. Because the GPR required a full day, additional resistivity data were taken the following day which yielded another set of images showing the progress or flow of the saline plume.

a) Transmit and Data Acquisition Settings

Data was acquired using a time window of 750 nanoseconds (ns) over 1071 points (700 psec/pt). In order to improve signal to noise ratio, we averaged 64 consecutive received signals (64 stacks) for each transmitter-receiver position.

Four cross-hole scans were taken at the following GeoWells:

Transmitter	Receiver
4	1
1	2
4	2
1	3

Prior to making the tomographic measurements, a cross-hole scan was made wherein the transmitting and receiving antennas were kept at the same elevation and moved up the holes together. Figure 5.10 is an example of the received waveforms. The time and amplitude information of the “first arrival wavelet” was used in the 3DTOM software to create the tomographic images. Note the increase in travel time and decrease in amplitude between 20 and 30 feet. This was due to the wet clayey layers in that region.

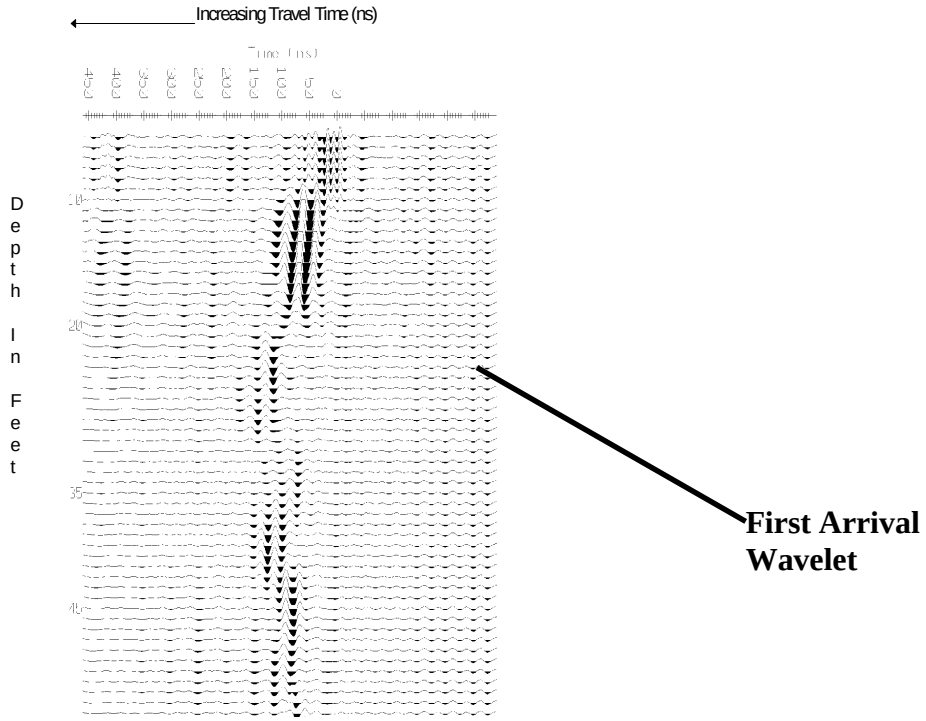

Figure 5.10. Example of GPR cross-hole data.

b) Antenna depth placements for tomographic measurements

For each cross-hole scan, the transmitting antenna was placed at a depth from 10 feet to 50 feet. For each transmitter antenna position, the receiving antenna was placed at depths corresponding to the transmitter position plus and minus 20 feet in one or two foot increments (depending on desired resolution). The upper and lower limits of the receiving antenna were 5 feet and 60 feet respectively. After the receiver sequence was completed, the transmitting antenna was moved down one of two feet (depending upon desired resolution).

c) Air media calibration

Before each cross-hole scan was performed, the two antennas were held above ground over the GeoWell. Approximately 10 transmit-receive wave forms were acquired and stored on disk.

d) Synchronization of antenna position with stored waveforms

Each cross-hole scan sequence (for example the data acquired between holes 1 and 3) was stored on a separate computer file. For each sequence, a written chart was maintained to assure that each position was recorded. At preset intervals, usually the start of each new transmitter position, an electronic tic mark was placed on the data file. At the same time this position was marked on the chart.

e) Matlab Analysis

Each raw data file was input to a software package (written in Matlab) which performs the following operations:

1. Bandpass filter (butterworth) the data to remove any high frequency noise or low frequency trending.
2. Cosine taper the signal to give less weight to information at the edges of the scans where we do not expect to find valid signals.
3. Calculate the power envelope of the signal to give equal weight to positive and negative values.
4. Monitor and note the presence of an electronic tic mark.
5. Determine the time of arrival of the first signal maximum.
6. Compare the amplitude at the maximum to the average value of the waveform.
7. Generate a new file storing the following parameters:
    1) Trace Number
    2) Tic mark presence flag
    3) First maximum onset time.
    4) Maximum vs. Average value flag
    5) Amplitude at the first maximum.

f) Correlation of processed signal trace with antenna position

The file generated by the Matlab software was read into an Excel worksheet. Here, known electronic tic mark locations are lined-up with the tic mark flags on the data file. Data was then checked to see if resulting positions lined- up. Usually any discrepancy was due to a double acquisition at the point of electronic marking (easily observed by clearly similar values).

For each waveform, the maximum value vs. average amplitude flag was checked. If the value was zero, indicating that the maximum value was less than three times the average value, that waveform was removed from the set. For each cross-hole scan, the travel time values measured in air were determined (via the Matlab software). This value was subtracted from the raw time value recorded on the data file.

Finally, the data was reformatted to be read by our tomographic software (described below). The following 8 columns were stored to a new file:

1. A unique ID number for each waveform.
2. X coordinate of the transmitter
3. Y coordinate of the transmitter
4. Z coordinate of the transmitter
5. X coordinate of the receiver
6. Y coordinate of the receiver
7. Z coordinate of the receiver
8. Measured time at the position of the first maximum minus the air-wave time.

g) GPR Tomographic Imaging Software

Antenna-pair position and arrival-time data as described above were input to Tomographic Imaging software 3DTOM beta version 1.0. This software, developed and provided by the U.S. Bureau of Mines, uses the simultaneous iterative reconstruction technique (SIRT) which repeatedly modifies an initial model to obtain the best possible fit to the data to a three-dimensional region.

7. ERT Results

The ERT data were processed using the LLNL software described earlier in Section IV. 0 is an example of ERT images before and after the salt water infusion. These results are very encouraging. The blue areas are high resistivity and the red are low resistivity (see the Colormap Key of Log Resistivity). These areas correlate well with the CPT logs where the sands have a higher resistivity than the clays, as would be expected. Note in the "after" image between 30 and 40 feet the major decrease in resistivity (red) due to the low resistivity salt water plume. Figure 5.12includes the CPT soil classification logs for holes 1 and 3. The three clay zones (29 feet, 36-38 feet, and 50 feet) are represented by the yellow/red areas in the "before" ERT image. Being able to delineate between high and low resistivity layers is important, even though ERT does not have the resolution to map thin soil layers. Also being able to map resistivity changes for environmental monitoring purposes is an important result of this project.

0 shows the before and after ERT images for the plane between holes 1 and 4. Again note the changes in the region between 25 and 40 feet and three red zones in the "before" image that correlate with the clay layers. The saline plume seems to be centered at about 38 feet. The results in 0, for the plane between holes 2 and 4, indicate that there was not much of a change due to the plume. Referring to the GeoWell site layout plan and the discussion on expected plume flow direction, these results are consistent. The plume is moving in the northwesterly direction away from the plane between holes 2 and 4 and toward the plane between holes 1 and 4.

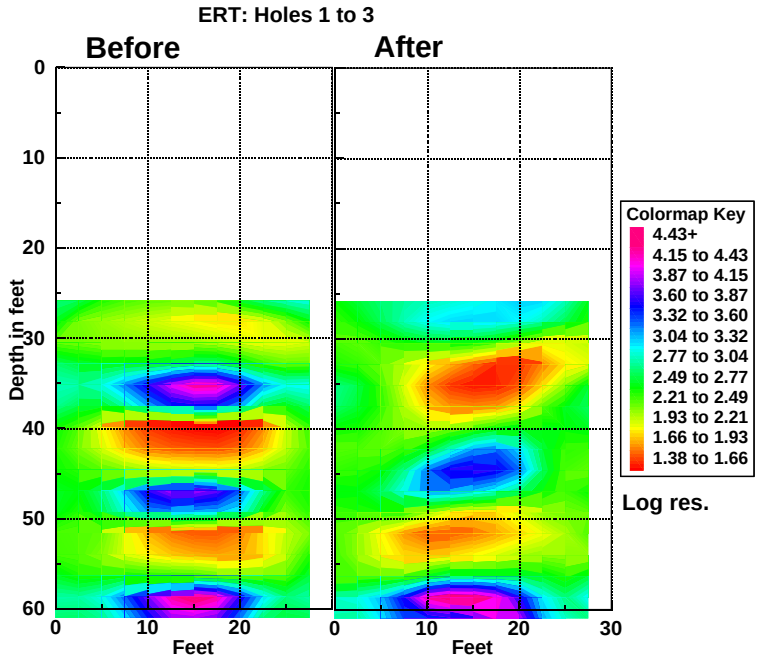

Figure 5.11. ERT tomographic images before and after salt water infusion for plane between holes 1 and 3.

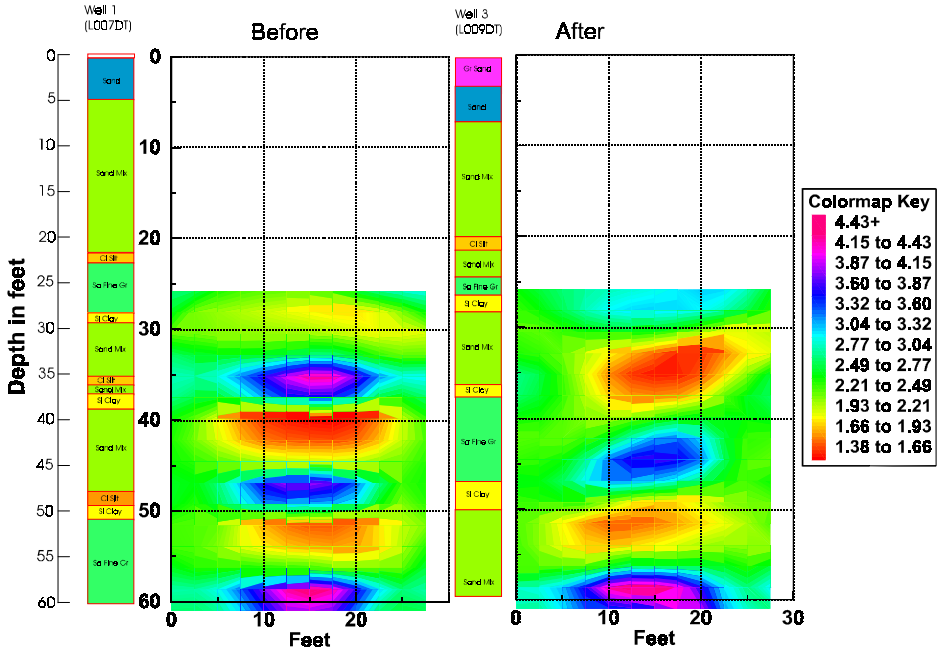

Figure 5.12. ERT images with CPT soil classification logs.

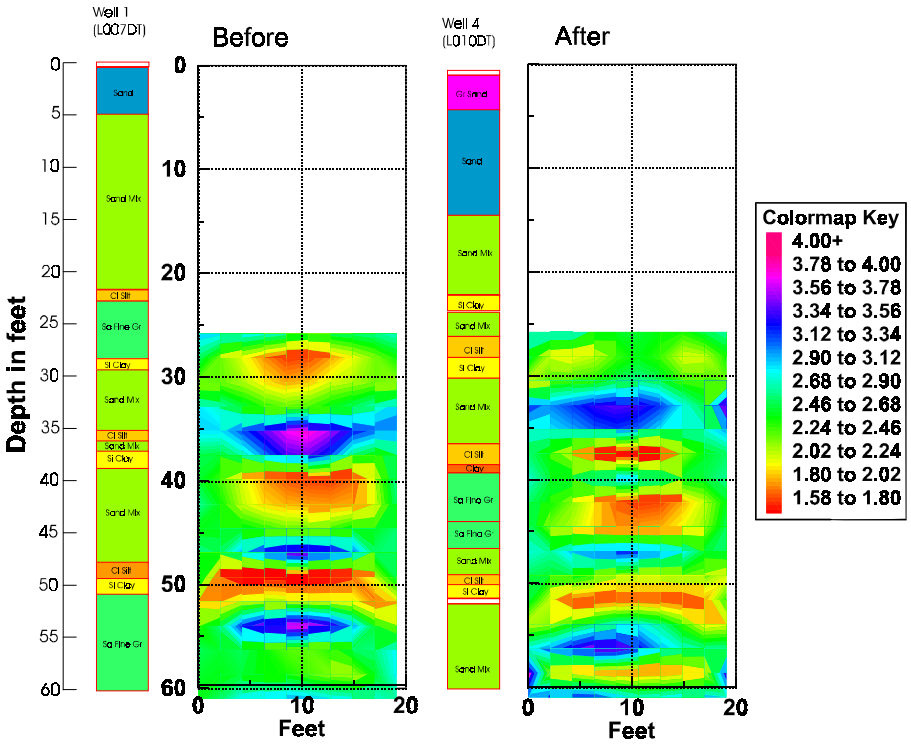

Figure 5.13. ERT images between holes 1 and 4.

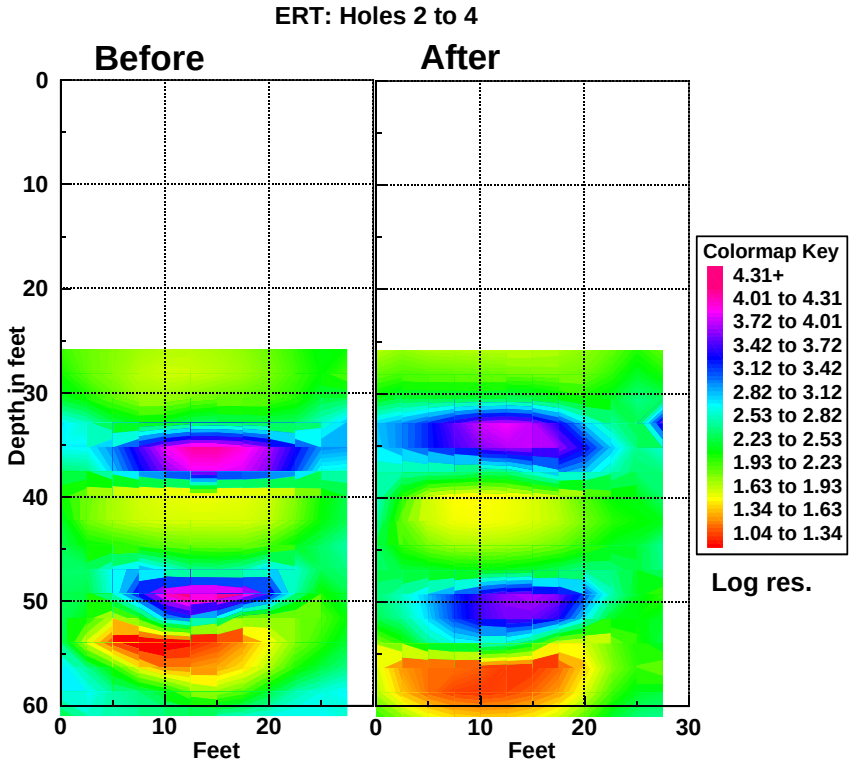

Figure 5.14. ERT image between holes 2 and 4.

8. GPR Results

The GPR data were processed using 3DTOM as described above. Figure 5.15 shows the before and after tomographic images for the plane between holes 1 and 4. The plume is quite evident in the "after" image. These GPR images are plots of radar signal velocity through the ground. Relatively high velocities, e.g. 0.4 feet/ns, represent dry or frozen sand, while low velocities, e.g. 0.1 feet/ns, are due to wet soils. Note the change in the region between 20 and 40 feet where the velocity has decreased (red/yellow) due to the increased water content from the water infiltration process.

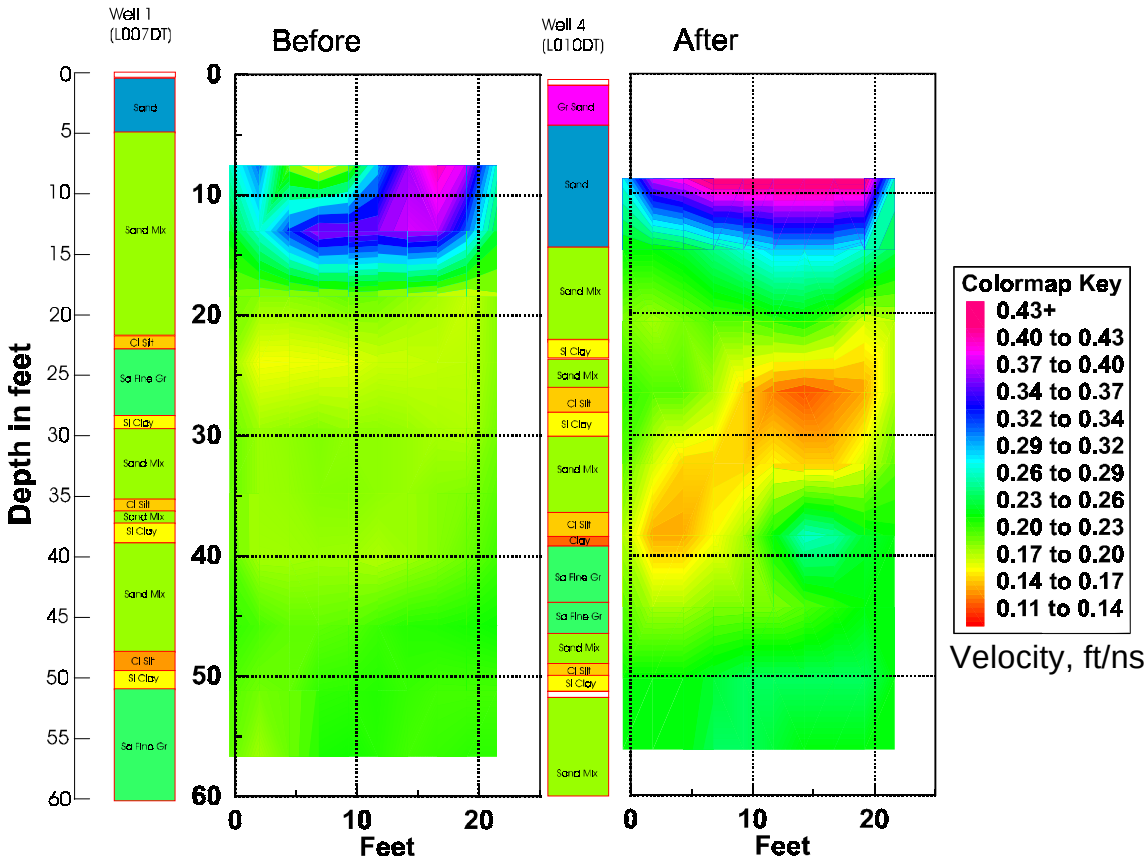

Figure 5.15. GPR tomographic images between holes 1 and 4.

Figure 5.16 is a comparison between ERT and GPR images. Even though the two methods respond to different electromagnetic soil properties, similar changes with depth are evident in the two images. The three wet clay regions are represented by low resistivity (red)

areas in the ERT image and by the low velocity (red) areas in the GPR image. These results are consistent with the theory.

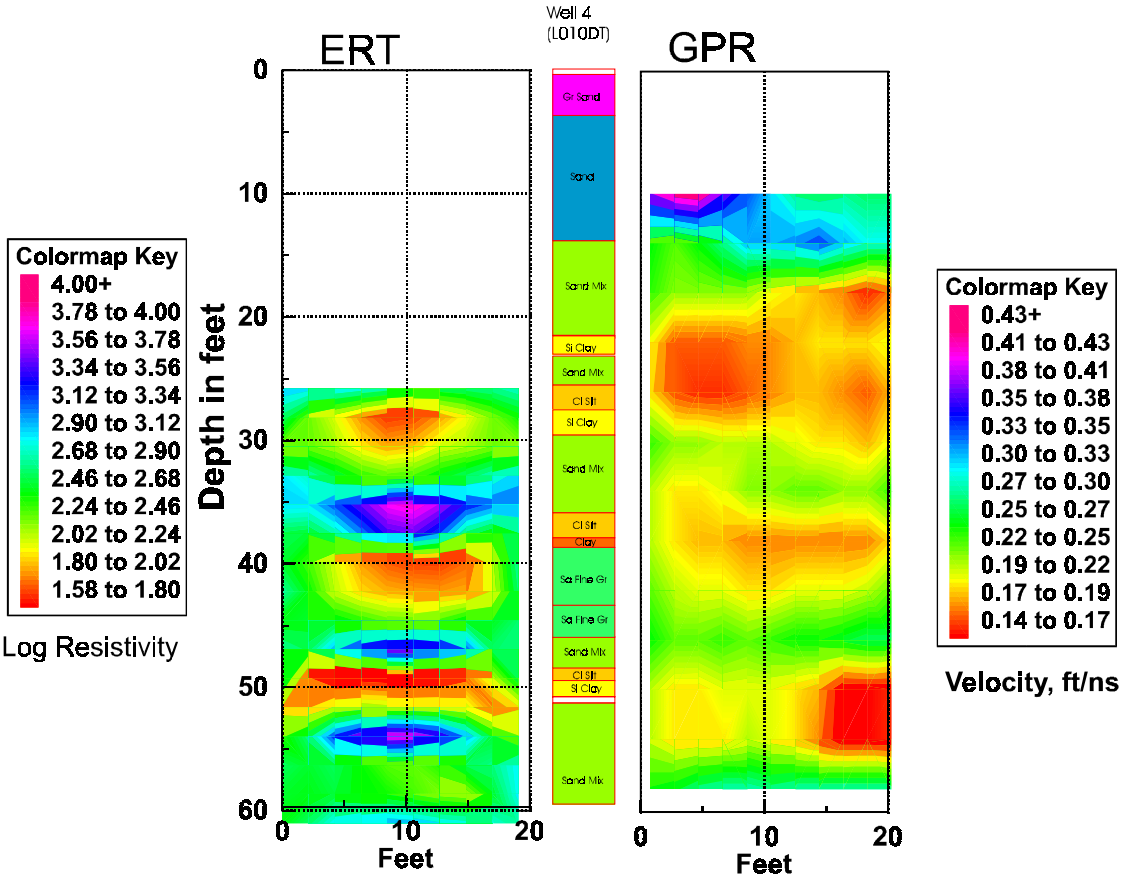

Figure 5.16. ERT and GPR comparison images between holes 1 and 4.

9. Soil Moisture Sensor (SMS) Results

The SMS was used to measure the soil moisture at the Monitoring Wells as a function of depth. Figure 5.17 is an example of a soil moisture log from Monitoring Well A compared with the CPT pore pressure log from GeoWell 4. The SMS results confirm that the clay layers are very wet. Where there was high pore pressure, e.g. at 22 and 28 ft, the recorded moisture content was also high. Well constrictions prevented the SMS from going deeper than about 35 ft.

One purpose of using the SMS in the Monitoring Wells was to detect the presence of the water plume over time. However, for the SMS measurements that were made, there was no noticeable change with time. This may have been due to not logging deep enough (below 35 ft)

or the sensitivity of the SMS instrument or the plume not intersecting the wells at the time of the measurements.

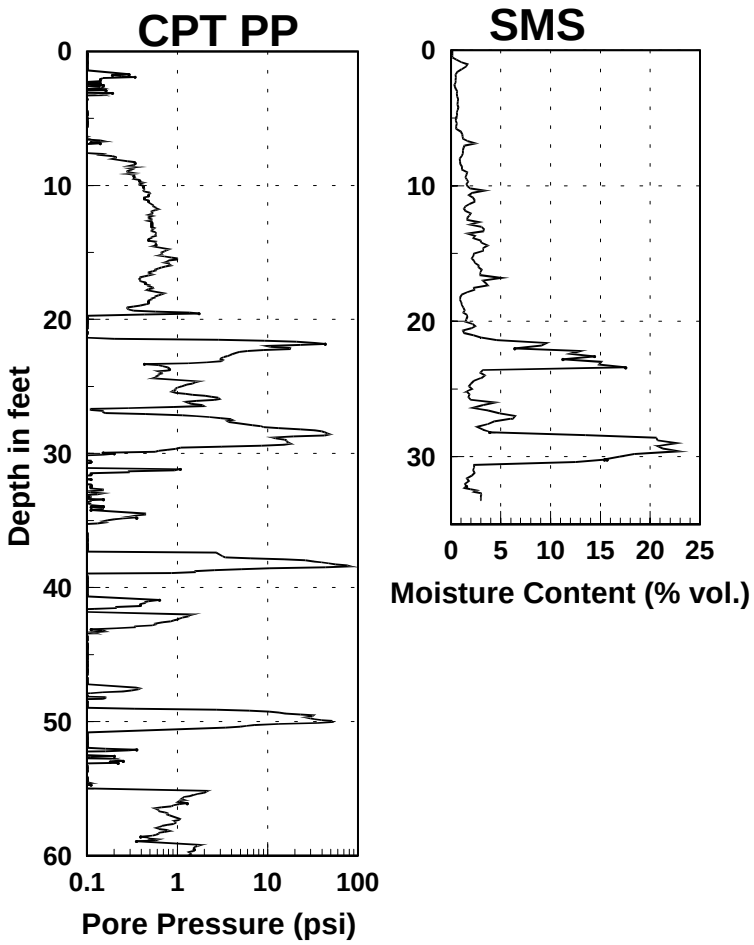

Figure 5.17. Pore pressure and SMS borehole logs.

C. MWD TEST SITE

1. Site Description

The test area was an uncontaminated area located at the Savannah River Site (SRS) in Aiken, South Carolina in the unconfined portion of the Upper Three Runs (UTR) aquifer. The UTR is part of the upper strata of the Floridian Aquifer System at SRS. The test site is located in a field of monitoring wells (MWD) installed and used for field demonstration purposes by Clemson University.

Examination of the CPT data and the MWD well logs from this site reveal it is made up of a few layers, with the water table beginning at approximately 72 ft bgs. The layers are made up of alternately quartzitic sand and clay with the sand containing varying amounts of silt with depth. The first clay layer appears at 8 feet bgs and extends with small intermittent layers of sand, to 35 feet. At 35 feet a highly resistive layer of sand appears and extends to approximately 70 feet where a lower resistivity clay exists between 70 and 74 ft bgs. Fine grained sands with varying amounts of clay and silt are found between 74 and 125 feet where the top of the UTR – Semi Confined Unit (SCU) begins. The clay layers are very similar in resistivity; however the sand bearing strata's resistivity is more variable. Figure 5.18 shows a CPT log with soil classification from the MWD uncontaminated test site.

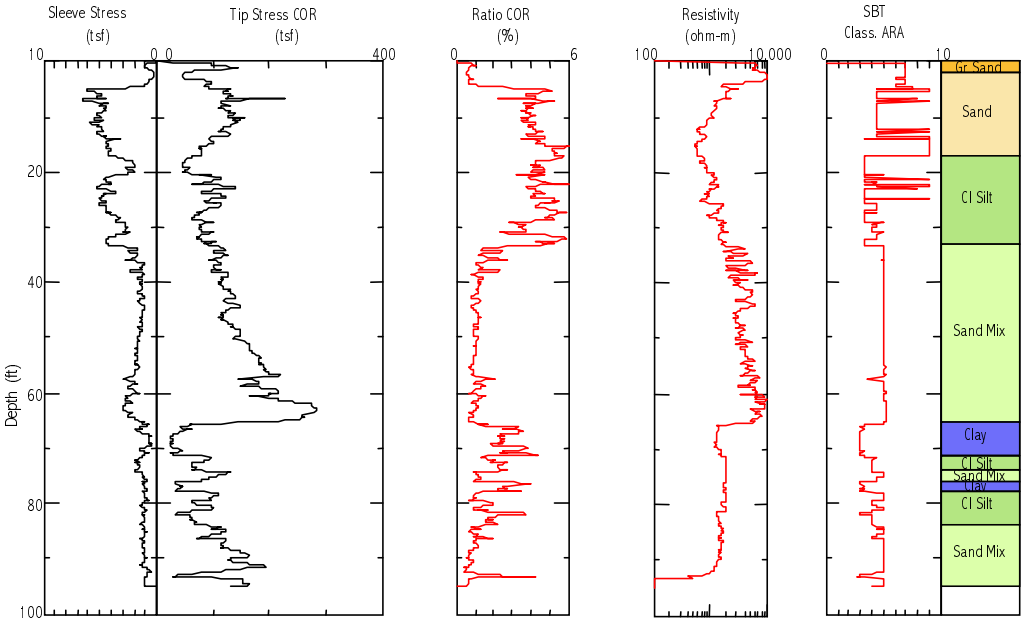

Figure 5.18. CPT Profile from the MWD test site at SRS.

2. Field Test Objectives

The objective of the field demonstration was to integrate CPT, ERT and GPR to successfully image changes in the subsurface due to an event that would produce changes in the soil's properties. Specifically, electrodes were placed in the subsurface surrounding a pumping well and images were constructed from test data taken before and during a pumping test event using CPT, ERT and GPR techniques. CPT was used to install the electrodes, reducing

installation costs and enhancing information about the subsurface conditions at the site to be used in a data fusion process with the ERT results. Installing ERT electrodes is an advantage because it is relatively non-invasive, reducing disturbance to the site, and once the electrodes make good contact with the soil, they may be left in place for long term monitoring.

3. Field Test Layout

Six Geowells were installed in a circular pattern around MWD-14 (Figure 5.19), a monitoring well at the site which extends to the base of the UTR boundary between the semi-confined and unconfined units, a clay layer located approximately 100 ft bgs. Each Geowell installation was preceded by a CPT push which measured tip and sleeve stress, determined soil classification, resistivity and soil moisture as a function of depth.

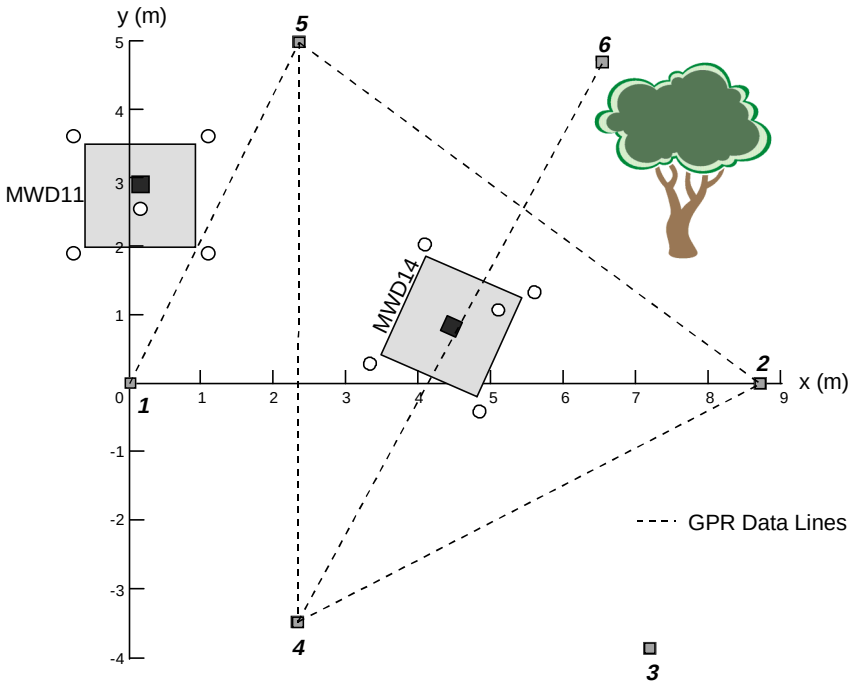

Figure 5.19. Geowell Layout around MWD-14 at the SRS MWD Test Site

The Geowells were placed approximately 15 feet in a circular pattern around MWD-14 which was to serve as the pumping well. GPR and ERT surveys before and during pumping were used to image the changes in the saturated zone due to pumping. MWD-14 is a four inch Schedule 40 PVC cased well 30 slot screened from 69 to 109 ft bgs with a filter pack set from 60

to 113 feet. Previous pumping tests at this well pumping approximately 70 gallons per minute resulted in a determination of hydraulic conductivity of 8.07 ft/day and a drawdown in a well 125 feet away, screened in the same zone, of 7.8 feet. The Geowells for this experiment were installed to 100 feet and 15 feet radially from the pumping well. Since a drawdown cone of depression was the object to be imaged, it was determined that a pumping rate of 22 gallons per minute would be sufficient enough to produce an expected drawdown of 20 feet in the saturated zone between the Geowells and the pumping well. Since this is an estimate (Thiem equation for unconfined radial solution to a pumping well) under non-ideal conditions, tests were conducted once the pump was installed in MWD-14. A pumping rate of approximately 35 gallons per minute produced a drawdown of 18 feet in the pumping well, which was determined to be sufficient of the test. This pumping rate was maintained during the pumping test portion of the ERT test. The pump was installed to a depth of 104 feet.

Borehole GPR data was gathered between cross sections that would include MWD-14 in the center of the slice before and during the pumping test. ERT surveys were also conducted between Geowells. The cables of electrode were installed into each Geowell and checked for electrode connection with the stainless steel in the Geowell. Two 12 Volt batteries were used to induce a current through each electrode contacting stainless and then ground. If the electrode was making good contact, a small current could be measured. If the electrode was misaligned and contacting only PVC, no current could be measured. It was noted that below the water table relatively large currents were measured. This could be due to standing water in the Geowell which was not observed during cable installation, or, the lower resistivity of the soil water mixture next to the stainless steel.

The ERT survey was conducted using equipment designed and built by Zonge Engineering Associates. The equipment consisted of a power amplifier, a transimitter, a resistor to allow measurement of the current through the circuit under observation, a multiplexor, a receiver and a computer to coordinate communications between the receiver, transmitter and multiplexor. The tests were conducted in order to observe the resistivity in vertical slices through the soil sometimes including the pumping well. Dipole measurements involving one pair of electrodes in current transmission and other pairs in the measurement of potential

difference due to the current pair were set up in a schedule. The test were then conducted automatically switching from one transmitter pair to another using the receiver and multiplexor, down one Geowell and up the next while taking measurements at other receiving pairs. The Geowells are equidistant from the pumping well. The vertical slices which include the pumping well are Geowell pairs #1 and #2, #3 and #5, and #4 and #6.

4. Numerical Simulation using CPT data in the ERT Inversion

In general, ERT data are analyzed using finite element model methods that solve the inverse problem posed by minimizing an objective function made up of iterates of a forward model and the data collected. The algorithm will find an acceptable minimum value of the objective function that satisfies explicit criteria set forth by the user and determined by the nature of the data. An initial guess of the site resistivity is needed, and it can be shown that the better the initial guess, the more likely the inversion technique will find the optimal solution. Since CPT gives estimates of the resistivity of the site with depth, it is hypothesized that a better solution will be obtained by inputting a CPT profile as the initial starting condition. Studies were conducted to test this hypothesis, both with numerically generated and actual electrical resitivity tomography data collected at the MWD SRS test site. To invert the data, we used the publicly available inversion model OC2D3D as written by Douglas LaBreque.

Two studies were conducted using the zoned CPT resistivity logs from the site to help design the ERT site test, evaluate the expected results and sensitivity of the method for this site. The first study involved using the zoned CPT resistivity logs as input to the forward model, to predict data pairs such as would be collected during an ERT survey at the site, then use those predictions as input data for the inverse model. The forward model input is shown on the left in Figure 5.20. The middle and right profiles in Figure 5.20 are tomographic inversions using the 300 numerically generated data pairs and two different initial guesses.

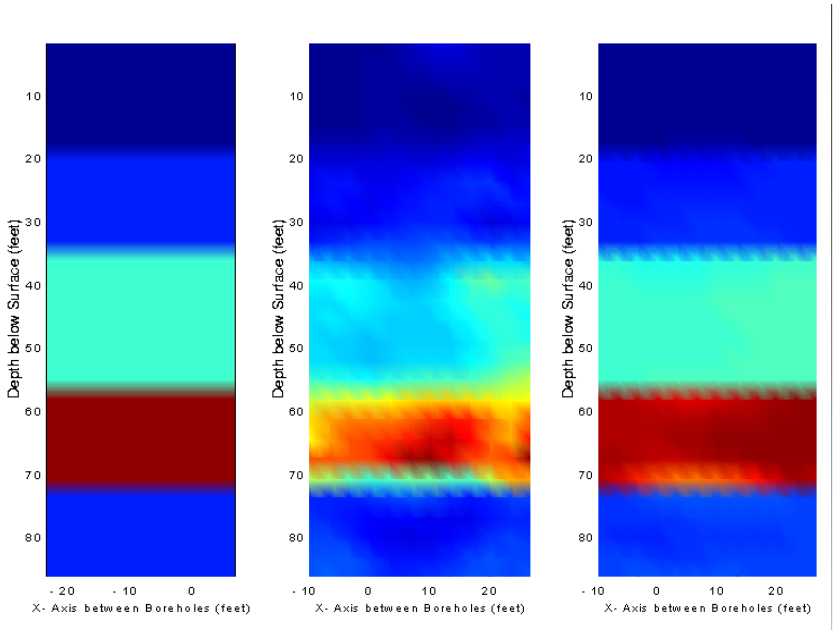

Figure 5.20. Middle and right images indicate the importance of a good initial guess for numerical inversion modeling to obtain the true initial soil profile (shown on left).

The middle profile in Figure 5.20 was inverted using a homogeneous initial guess of 2000 Ohm-meters (as if there was limited information about the subsurface resistivity) and the right profile in Figure 5.20 was inverted using zoned CPT resistivity logs as the initial guess. The calculation using an initial guess of 2000 Ohm-meters reproduces the main features of the profile, however, delineation of sharp layer interfaces was not possible. Numerically, the inverse model tends to smooth the interfaces between the layers but does a better job the closer the initial guess is to the actual resistivity. The profile using the zoned CPT resistivity logs is in good agreement with the input profile, including the sharper interfaces between zones, which proves the ability of the model to correctly invert the data, and the importance of a good initial guess. The model does not numerically force a solution to the initial guess, it holds the data to be true, therefore it can avoid spurious optimal solutions if given a good initial guess.

The numerical study was conducted from numerically generated data, free of noise that would be expected from ERT survey data collected in the field. Data obtained at the SRS site were analyzed with and without the zoned CPT resistivity profiles as the initial starting point.

The experimental setup for at the MWD site allowed 300 ERT data pairs to be collected per vertical slice.

5. Integrated CPT, ERT, and GPR Results

CPT, ERT, and GPR data were collected before and during the pumping test at the MWD site. Several Geowells surrounding MWD-14 were used to collect the data and image vertical cross sections. ERT survey data was analyzed without using initial CPT zoned resistivity profiles as is shown in Figure 5.21 an image of the section between GW04-GW06 before pumping. At this location, 300 ERT data pairs were collected, but only 79 were used in our analysis due to noise. This is not surprising given the high resistivity values observed in the sands at this location.

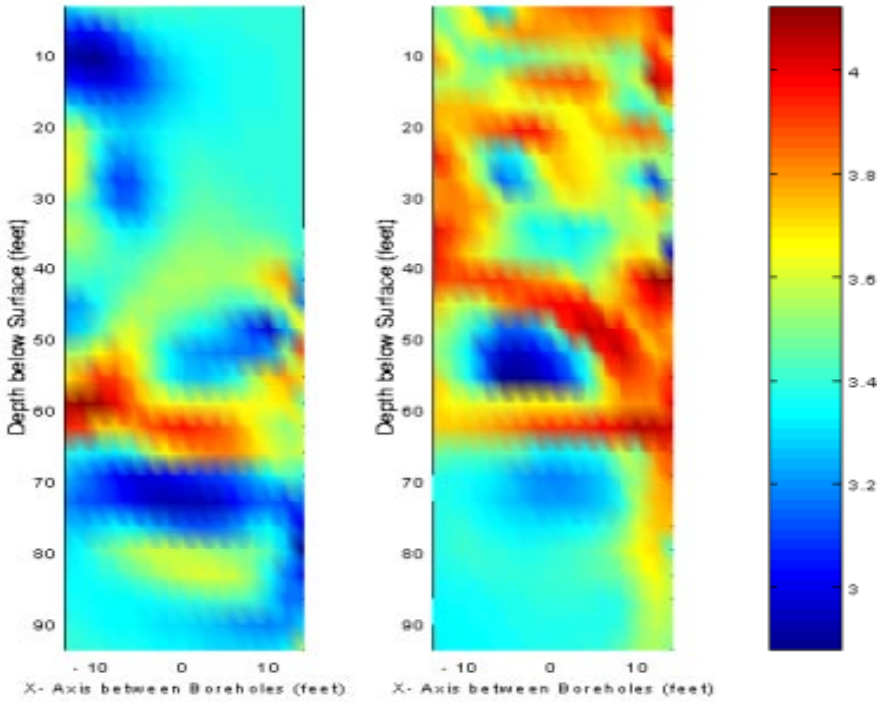

Figure 5.21. Tomographic Section between GW04-GW06. Initial guess 2000 Ohm-meters. No CPT data.

The two profiles in Figure 5.21 are the tomographic images from inverting two ERT data sets using a homogeneous initial guess. Much like the numerical simulation conducted

previously, the images are fuzzy and the layers indistinct. The tomographic image derived from the ERT data using the zoned CPT resistivity logs as an initial input is plotted in Figure 5.23. This image is in much better agreement with the CPT data. Note the two CPT profiles taken from the boreholes on either side of the section. The upper clay layer is well defined. An important point is that the input CPT data were horizontally layered over the section; however, the inverse model predicts the clay layer to be dipped from 15 feet depth at GW04 to 22 feet at GW06. This is in excellent agreement with the actual CPT data and indicates that the ERT method can verify subtle dips in geology, given a good initial guess of the resistivity profile. Inputting a more statistically likely initial guess following the CPT logs, instead of layering zones horizontally, may further improve the fidelity of the resulting image.

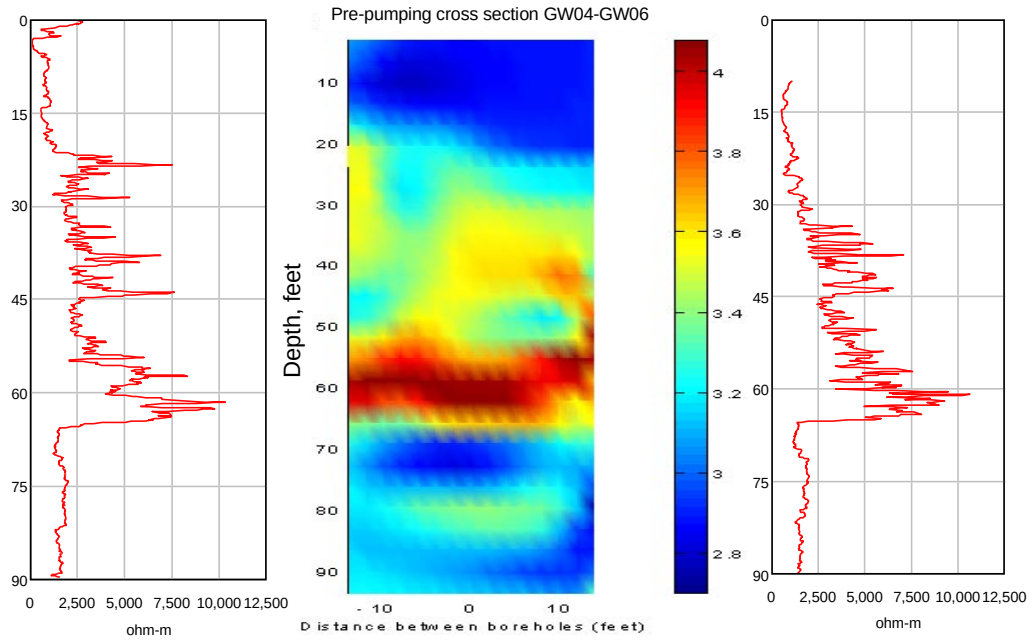

Figure 5.22. Tomograph between GW04-GW06. Zoned CPT resistivity logs (shown) used as initial guess.

The results shown in Figure 5.22 are tomographic images from ERT data taken before pumping began from MWD-14 and using CPT data for an initial guess. The saturated zone begins at approximately 72 ft bgs and the image shows a sharp decrease in resistivity where the water table begins. During the pumping test, ERT surveys were again conducted in this cross

section. For comparison, the images from data taken before and during the pumping test are shown in Figure 5.23. The image from data taken during the pumping test shows a considerable decrease in resistivity in two places near GW-06, in a previously high resistivity area, this is attributed to a significant rain event that occurred during the pumping test and the subsurface near GW06 might have been affected. However, the rest of the image is nearly the same as obtained before pumping except for an increase in resistivity over the entire saturated zone area. Since the pumping rate had reduced the water level in MWD-14 by 18 feet and the pump was installed to 104 ft bgs, the increase in resistivity shown in the tomographic image is attributable to the pump removing the water from this zone.

Since analyzing ERT data requires estimating the uncertainty associated with a measurement, only images that have the same level of uncertainty are compared. One method that can be used to estimate the uncertainty of an ERT measurement is to look at it's reciprocal value. This means that if a potential measurement was taken between electrode pairs 1 and 2 in GW-04 due to a current pair of electrodes 5 and 6 in GW-06, then the potential measurement between 5 and 6 in GW-06 must also be measured due to the current pair of electrodes 1 and 2 in GW-02. If these two sets of measurements are within a required tolerance, then they meet the criteria of reciprocity and are used in the numerical inversion. Each of the images shown in Figure 5.23 were created using the same number of measurements obtained using the same reciprocity criteria. In addition, the numerical inversion model requires that estimates be made of the amount of smoothing desired, and the weight of each measurement. The smoothing parameters were kept the same between images, and the weight associated with each ERT data pair was it's reciprocity value.

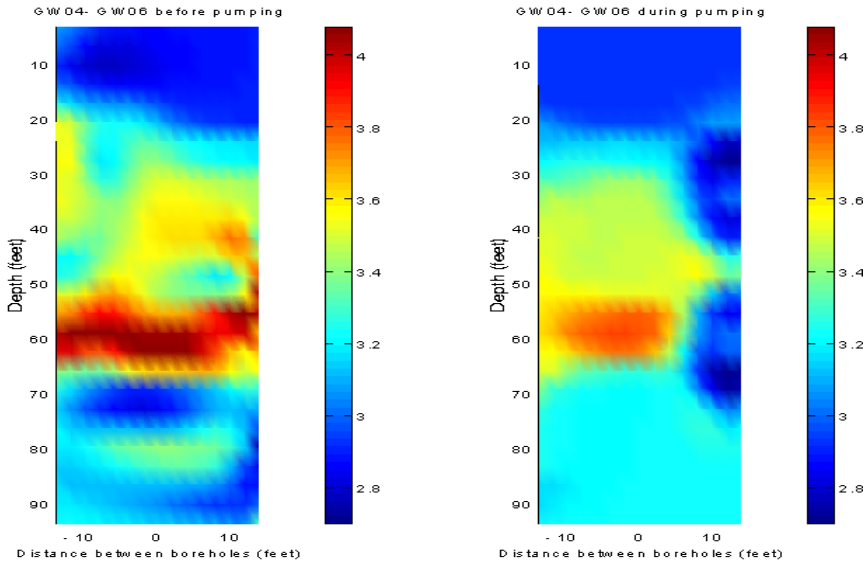

Figure 5.23. Images from ERT surveys taken before and during the MWD pumping test.

The results of the borehole GPR testing compared favorably with the ERT and CPT results at the MWD site. GPR data were collected over the cross sections indicated in Figure 5.19. Figures 5-24 through 5-27 are the results of the borehole GPR taken before and during the pumping tests. The images are similar to the results obtained from the ERT surveys but in general are fuzzier and had difficulty delineating the changes in soil type. The high resistivity sand layer observed in both the ERT and GPR images corroborates with the CPT probe.

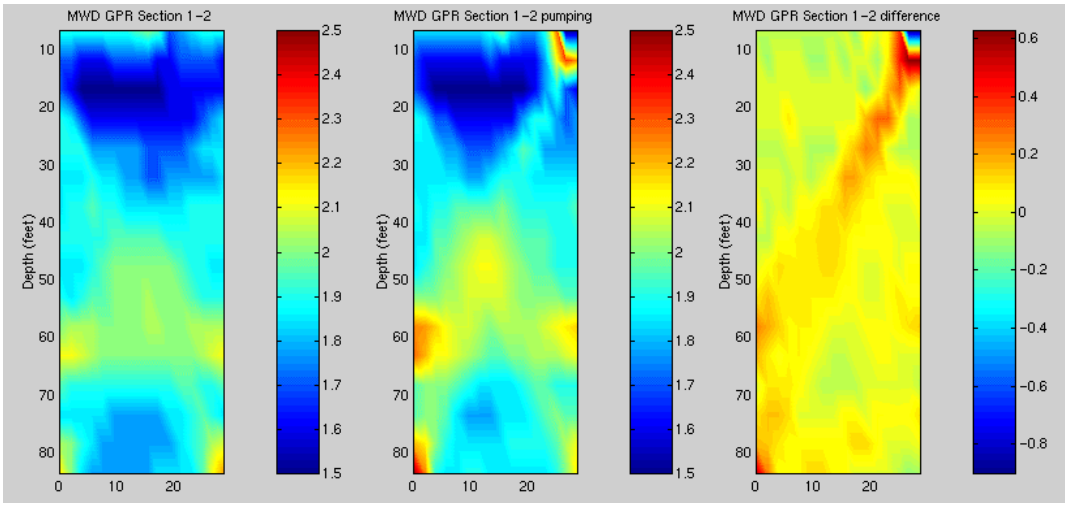

Figure 5.24. GPR Section 1-2 taken before and during the pumping test.

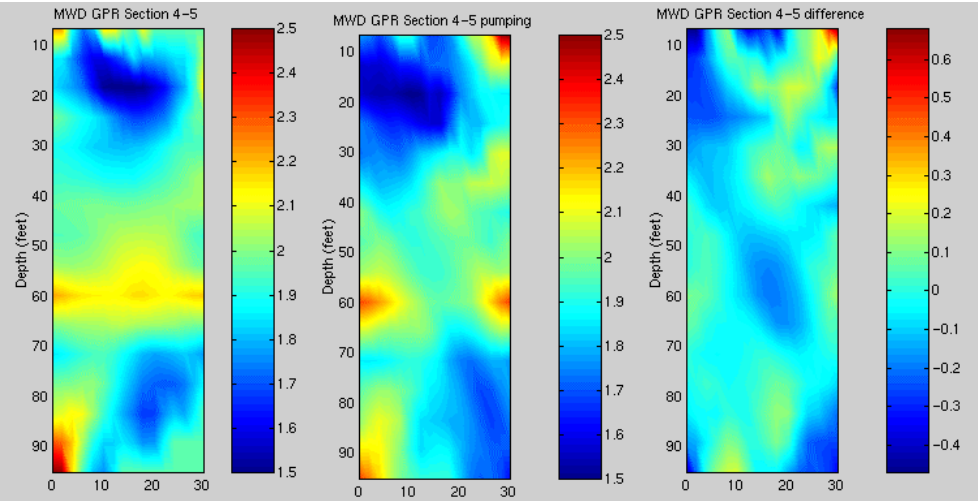

Figure 5.25. GPR Section 4-5 taken before and during the pumping test.

The images on the right in Figures 5-24 through 5-27 are the time lapse differences of GPR taken before and during pumping.

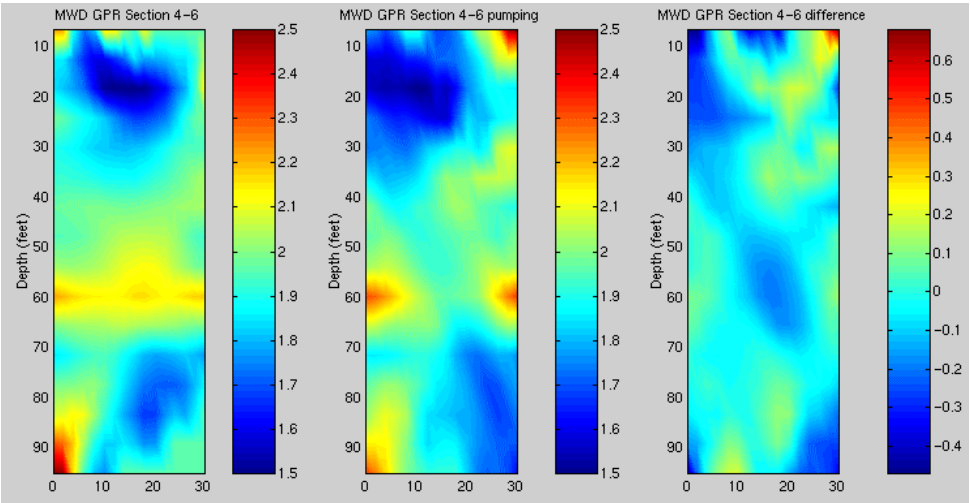

Figure 5.26. GPR Section 4-6 taken before and during the pumping test.

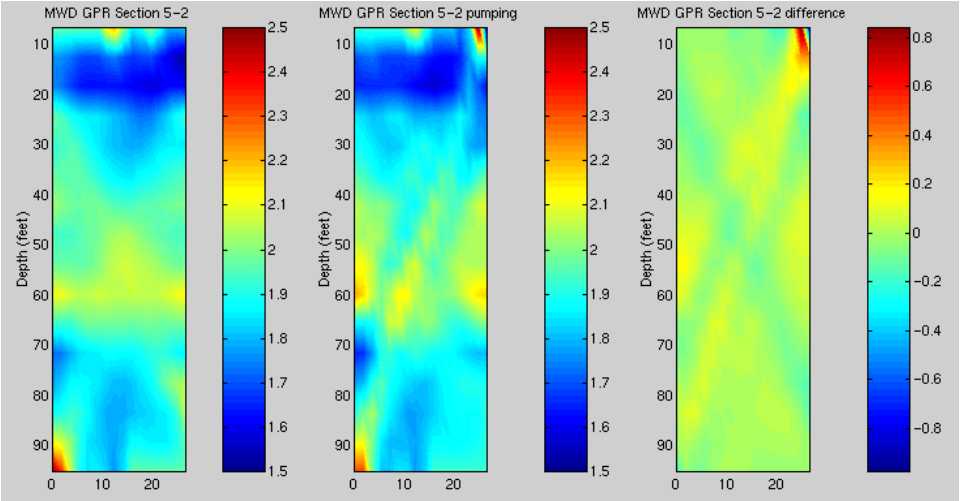

Figure 5.27. GPR Section 5-2 taken before and during the pumping test.

The GPR time lapse differences did not indicate a change in the resistivity of the soil matrix due to pumping; however, the combination of CPT and ERT was able to resolve the resistivity change due to the pumping at MWD.

D. TNX AREA TEST SITE

1. Site Description

The test area is located at the TNX Area of SRS where a Geosiphon is being used as part of a remediation system to clean groundwater. The Geosiphon cell is a passive flow treatment well utilizing zero valent iron reduction to treat contaminated groundwater. It is located in the floodplain below the TNX facility. The Geosiphon treats contaminated water abiotically by drawing the water through iron filings using the natural groundwater head differences to replace pumping in a well. The treated water is siphoned and discharged to the receiving body of water. The Geosiphon is located in the center of the cage containing the iron filings, and the iron filings extend out from the siphon horizontally by approximately four feet and are fully screened to the aquitard. Due to the geometry of the Geosiphon it is difficult to estimate the Geosiphons's radius of influence, or which layers are providing the majority of flow through the treatment cell. Figure 5.28 shows the layout of the Geosiphon (TGSC-1) with respect to the TCM monitoring

wells and the location of the electrode strings. TGSC-2 is another Geosiphon that was to be installed after this field test.

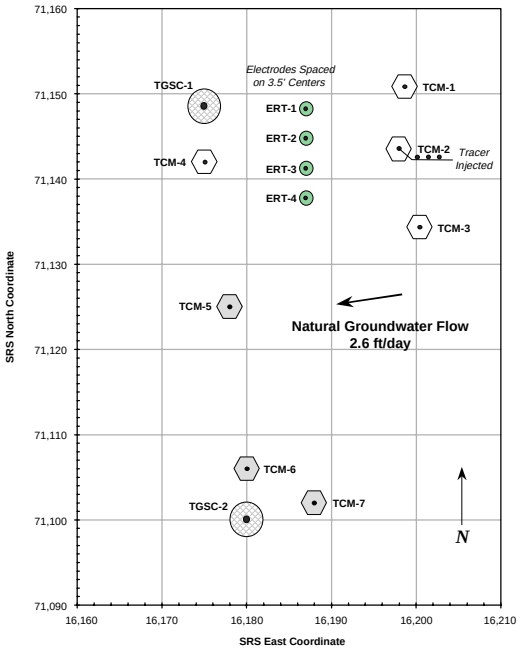

Figure 5.28. Layers at TNX area showing Geosiphon (TGSC-1), injection well (TCM-2) and electrode string locations.

The geology of the upper water table in this area is mostly unconsolidated sands with a few clay layers and discontinuous cemented sand layers. The water table aquifer begins at approximately 4 ft bgs and there is a clay layer located at 20 ft bgs separating the upper water table aquifer from the aquifer below the clay layer. The contaminants in the aquifer are located above this clay layer, and the Geosiphon cell was installed to the clay layer at a depth of 20 feet. The total porosity is estimated to vary between 36 and 50 percent (based on soil moisture CPT data) and the apparent resistivity varies between 100 and 20 Ohm-meters.

2. Field Test Objectives and Expected Benefits

This field test is part of a demonstration of an integrated CPT, ERT and GPR tomography system extended from success at a clean site, to aid in characterization of a possibly contaminated site, or a site involved in remediation activity. Through the use of a tracer, which alters the pore fluid salinity of the aquifer, and the combination of CPT with ERT and GPR, the preferential flow patterns surrounding the Geosiphon in its zone of influence were monitored

over time. ERT and GPR surveys were taken before, during and after tracer injection. During this process, samples were extracted from the electrodes to determine the salinity content of the groundwater at discrete depth intervals. As the tracer plume moved nearer the Geosiphon, changes in resistivity were detected and used to develop images of the groundwater flow field. The expected results of the field test design were estimated using numerical flow modeling and mass transport modeling for determining the mass of solute that can be expected during the monitoring phase. The images resulting from the modeling process helped design the field layout of the tracer test for optimum results. A pictorial view of the test is shown in Figure 5.29.

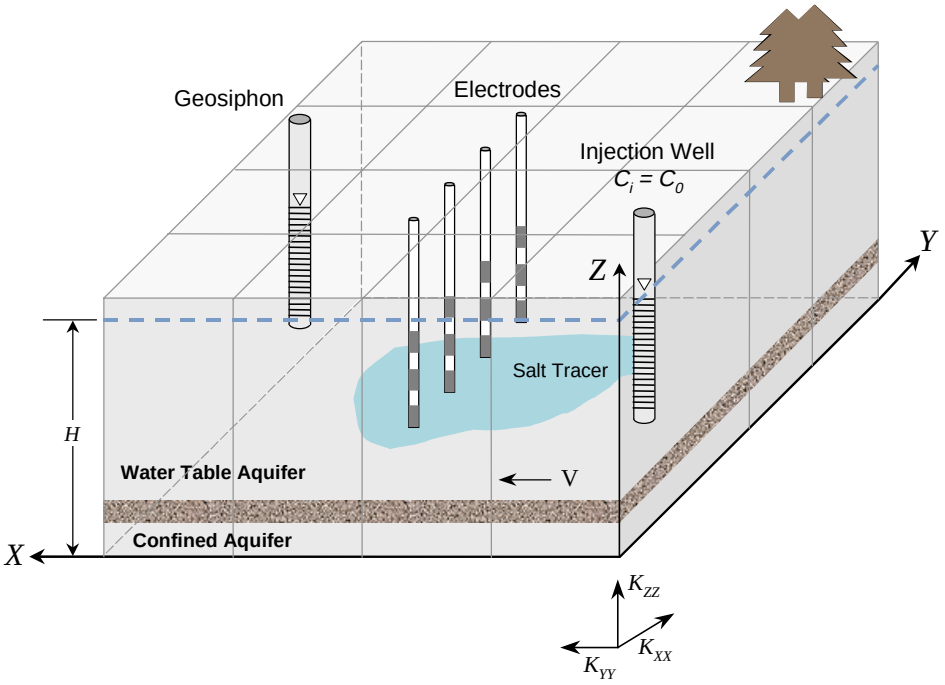

Figure 5.29. Orthographic view of tracer test at TNX area. The Geosiphon, monitoring wells, and electrodes were installed to 20 feet bgs. Confining layer shown is at 20 feet bgs.

Expected benefits from the tracer test at the TNX area demonstrate the increase in information that integrated CPT, ERT and GPR can add to a subsurface monitoring or site characterization effort. Through imaging the salt tracer, new information about the flow patterns toward the Geosiphon can be estimated such as the capture zone, dispersion and preferential flow through particular layers. The combination of CPT installed electrodes that have a dual purpose of extracting water samples at a particular depth validates the findings of the ERT and GPR surveys. The methods may also be used without interfering in the performance of the Geosiphon

or the remediation activity that the area is experiencing, and provide a means of overcoming the under-representation due to costs from typical tracer tests allowing only a limited number of observation points.

3. Numerical Modeling and Field Experimental Design

Electrodes were installed upgradient of the Geosiphon in a configuration to monitor the approach of the salt tracer toward or around the Geosiphon, as shown in Figure 5.28 and Figure 5.29. The injection well was used as a continuous source for the saline solution to enter the aquifer and was heavily concentrated with a Potassium Bromide solution for 36 hours. In order to estimate the effect of the salt solution on the apparent resistivity, calculations involving changing the pore water salinity of the bulk conductance were used to determine the field experimental design of the tracer test.

If we desired to change the observed resistivity by a factor of 3 to 5, which we estimate can be resolved with ERT, we would have to decrease the resistivity or increase the observed specific conductance. The observed specific conductance can be related to the bulk conductance of the material as a function of the saturation and porosity as in Equation 1,

$$\sigma_t = \frac{\sigma_b S^b n_t^m}{a} \tag{7}$$

where *n* is the porosity; *a*, *m* and *b* are empirically derived constants and approximately equal to 1, 1.5 and 1 respectively; *S* is the degree of saturation and equal to 1 for the Geosiphon site; and

where *n* is the porosity; *a*, *m* and *b* are empirically derived constants and approximately equal to 1, 1.5 and 1 respectively; *S* is the degree of saturation and equal to 1 for the Geosiphon site; and σ_t is the total observed conductance of the media and pore fluid and σ_b = bulk conductance of the pore fluid, colloidal conductivity, and double layer conductivity. Assuming a porosity of .36 and that the conductivity of the site is 500 μmhos/cm, Equation 1 yields a σ_b of 2,300 μmhos/cm. If σ_b is made up of the conductance of the pore water, double layer effect and colloidal conductivity, as in Equation 2.

$$\sigma_b = \sigma_w + \sigma_{xx} \tag{8}$$

where σw is the bulk conductance of the water and is equal 50 μmhos/cm, then the conductance due to interfacial conductivity, colloidal conductivity, and other sources, (σxx) can be determined. For the TNX area, the conductance due to colloidal or these effects is about 2,250 μmhos/cm.

Calculations have shown that if the pore fluid conductivity could be increased by a factor of 3 to 5, the tracer could be easily observed by ERT. Thus, it is desirable to induce a large change in the pore fluid conductivity. To alter the observed conductance by a factor of 5 would mean increasing the specific conductance to a new value as shown in Equation 3.

$$\sigma_{bnew} = \sigma_b \times F \tag{9}$$

If $F = 3$, σ_{bnew} = 6,900 μmhos/cm
If $F = 5$, σ_{bnew} = 11,500 μmhos/cm

Subtracting would leave the conductance of the saline water solution that would produce a factor of 3 to 5 change in observed resistivity or specific conductance.

$$\sigma_{bnew} - \sigma_{xx} = \sigma_{saltsolution} \tag{10}$$

If $F = 3$, $\sigma_{saltsolution}$ = 4,650 μmhos/cm

If $F = 5$, $\sigma_{saltsolution}$ = 9,250 μmhos/cm

Therefore, from Equation 4, the saline solution the pore spaces must have a specific conductance of at least 4,650 μmhos/cm and, at most, 9,250 μmhos/cm to invoke a change that would be readily observable by ERT.

According to Carmicheal, a salt solution of approximately 6 g/l will exhibit specific conductance between 4,650 and 9,250 μmhos/cm. Therefore, the concentration of the tracer entering the formation as a continuous source must have a concentration of about 6.0 g/l to observe between a factor of 3 and 5 change in total resistivity.

4. Estimate of Tracer Movement

Estimates of the salt tracer's movement through the saturated zone can be estimated by solving the convective dispersive equation for uni-directional mass transfer in groundwater (Equation 11)

$$D\frac{\sigma^2 C}{\sigma x^2} - U\frac{dC}{dx} = \omega R\frac{dC}{dt} \qquad (11)$$

where D is the dispersion tensor, C is the concentration of the salt mass, x is the location, U is the velocity of the groundwater, ω is the total porosity, R is the retardation factor and t is time. If the salt tracer is injected into the saturated zone upgradient of the Geosiphon, as a continuous source, the time it would take the bulk of the front of the tracer to break through to the location of the electrodes can be estimated by solving Equation 11 in the x-direction between the injection well and the Geosiphon. Using the analytical solution for Equation 11 (Ref. 30)and the hydrogeologic parameters determined from site investigation, examples of the breakthrough of the salt tracer for this experiment are displayed as a curve in Figure 5.30. The curve represents the concentration of salt at the electrode locations as a function of time for the recommended groundwater gradient of 0.007 ft/ft. This gradient was measured under natural conditions with no flow through the Geosiphon. For this example, the dispersion coefficient, D, is estimated at 10 ft^2 per day; the retardation factor, R, is assumed to be 1; the total porosity, ω, is 0.3; the distance from the injection well to the electrodes is 15 ft; and the initial concentration is estimated at 6 g/l as a continuous source.

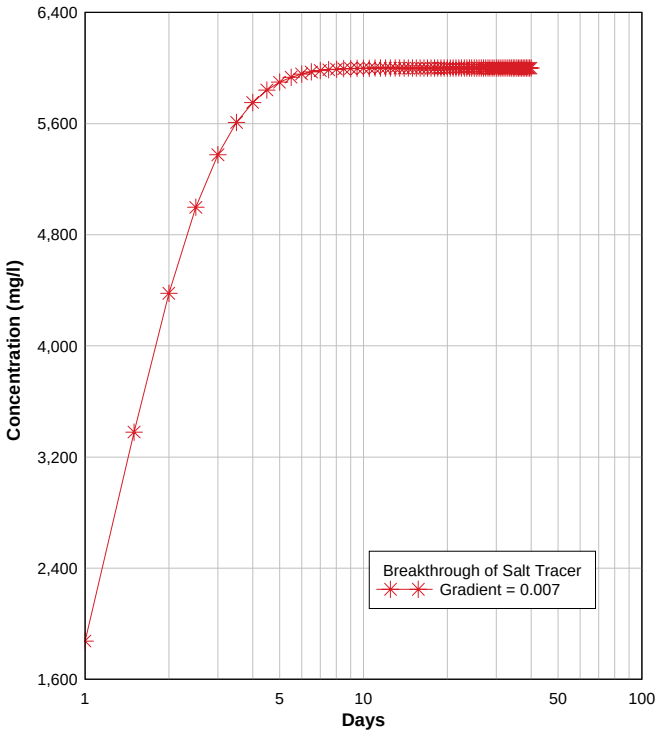

Figure 5.30. Estimated breakthrough of the salt tracer at the electrode locations. The groundwater gradient assumed was natural groundwater conditions.

During injection of the salt tracer, monitoring well TCM-2 (Figure 5.28), upstream of the Geosiphon, will be loaded with a salt solution and maintained at a constant flow rate of 0.5 gallons per minute for 3 days. In 3 days, a total of 2,160 gallons of salt solution would be injected and the beginning of the salt front should be passing the first set of electrodes. To estimate the well pressure head needed to inject the tracer into the groundwater through the well, Thiem's solution for a pumping well in an unconfined aquifer may be used with opposite signs for injections (see equation 6). h(r) is the pressure head very near to the well, H is the pressure head at the distance from the well where it's influence no longer disturbs the groundwater pressure head. T represents the transmissivity of the aquifer, r is the radius of the well, and R is the distance from the well where H is determined. For the TNX area, at an injection rate of 0.5 gpm, transmissivity of 600 ft2/day, r of 1.5 inches, and R of 50 feet (as determined from the pumping tests at the Geosiphon), the pressure head in the well would rise 1.1 feet. This estimate is heavily influenced by the transmissivity of the aquifer; for example, if the transmissivity were actually 15% less than the estimate the pressure head in the well would rise 1.4 feet.

$$h(r) - H = \frac{Q}{2\pi T} ln\left(\frac{r}{R}\right) \tag{12}$$

Based on these calculations, we designed our tracer injection at monitoring well TCM-2 with a projected injection rate of .5 gpm and a change in pressure head in the well of 1.1 feet. The injection rate was increased to 1gpm during the actual test, when it was observed that the injection of the tracer showed less than .5 feet of pressure head increase in injection well TCM-2.

5. Field Test Layout

Four electrode strings were installed in the ground adjacent to the Geosiphon cell as shown in Figure 5.28. Each electrode installation is composed of five discreet electrodes approximately six inches long and spaced vertically along the string every 2.5 feet beginning at 5 feet bgs. Each electrode includes a sampling port and is sheathed in a stainless steel filter media. Figure 5.31 presents a description of the electrode design, each electrode also serves as a sampling port and an individual tube is connected to allow a discrete sample to be withdrawn at depth. The electrodes, when installed in saturated media, are in good electrical contact with the soil as the soil collapses around them when the installation rods are withdrawn.

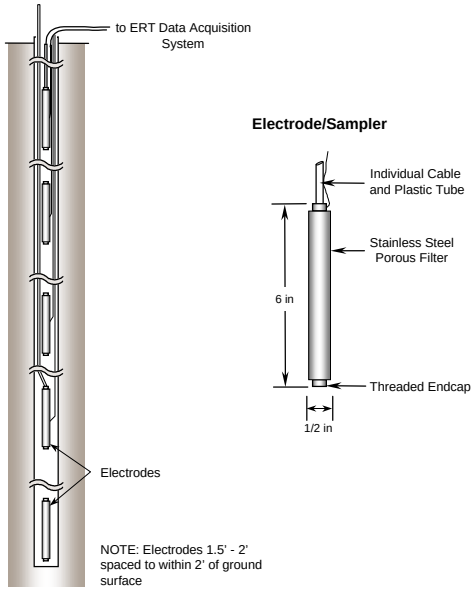

Figure 5.31. Dual electrode and discrete interval sampler used at TNX area.

A bromide tracer solution was injected in the upper part of the water table aquifer at the existing TCM-2 well. TCM-2 is a four-inch diameter PVC well, screened in the water table aquifer from the clay layer at 25-ft bgs, to where the water table begins at 5-ft bgs. The total tracer volume injected was approximately 2,160 gallons (49kg of sodium bromide at 6 grams/liter). The tracer was injected continuously at 1 gpm for 48 hours. The injection rate was raised from 0.5 gpm to 1 gpm when no noticeable raise in the pressure head of the well was observed during the injection at 0.5 gpm.

Groundwater samples were obtained from the TCM-2, and the electrodes before and during the tracer test to monitor the advancement of the salt plume towards the Geosiphon. The samples were analyzed using a conductivity meter to measure the change in resistivity of the groundwater. ERT surveys and GPR surveys were also conducted before and during the tracer test and analyzed on site to image the change in resistivity of the saturated zone due to the injected salt plume.

ERT surveys were taken between each nearby vertical electrode string and then various combinations of electrode strings were used in additional surveys both before and during the tracer test. GPR surveys were gathered between TCM-2 and TCM-4.

6. Integrated CPT, ERT, and GPR Results

The dual purpose of the electrode design physically determined the arrival of the salt tracer at the electrode locations. Salt was significantly observed at 36 hours as is shown by the breakthrough curves in Figure 5.32. The background conductivity of the groundwater is approximately 67 microsiemans/cm, and the tracer injected was approximately 5 millisiemans/cm in the injection tanks and approximately 2 millisiemans/cm when sampled in the injection well TCM-2. The tracer moved much faster than expected, it was originally estimated to arrive between 3 and 5 days after injection began. However, these estimates were based on natural gradient conditions, without the activity of the Geosiphon. During the tracer test, the Geosiphon was actively removing water at a rate of approximately 7 gpm which would increase the flow velocities through the strata in the area surrounding it, causing the tracer to move much more quickly through the aquifer.

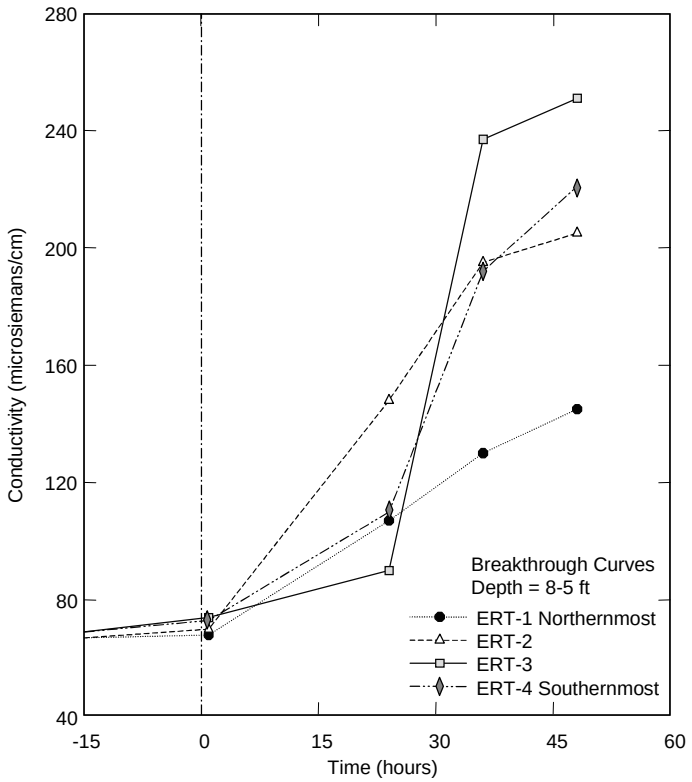

Figure 5.32. Samples from electrodes shown time of arrival of potassium bromide.

The sampling from the electrodes at depth indicated that the majority of salt was moving through the upper strata of the aquifer. Although Potassium Bromide solutions are denser than water, the sampling over the duration of the test revealed that the majority of salt moving through the aquifer and toward the Geosiphon was above a depth of 11 feet. The curves shown in Figure 5.33 are plots of the advancement of the tracer with time over the vertical cross section from samples taken from electrode strings 1, 2 and 3. The highest increases in conductivity were observed in samples taken between 5 and 8 feet in depth.

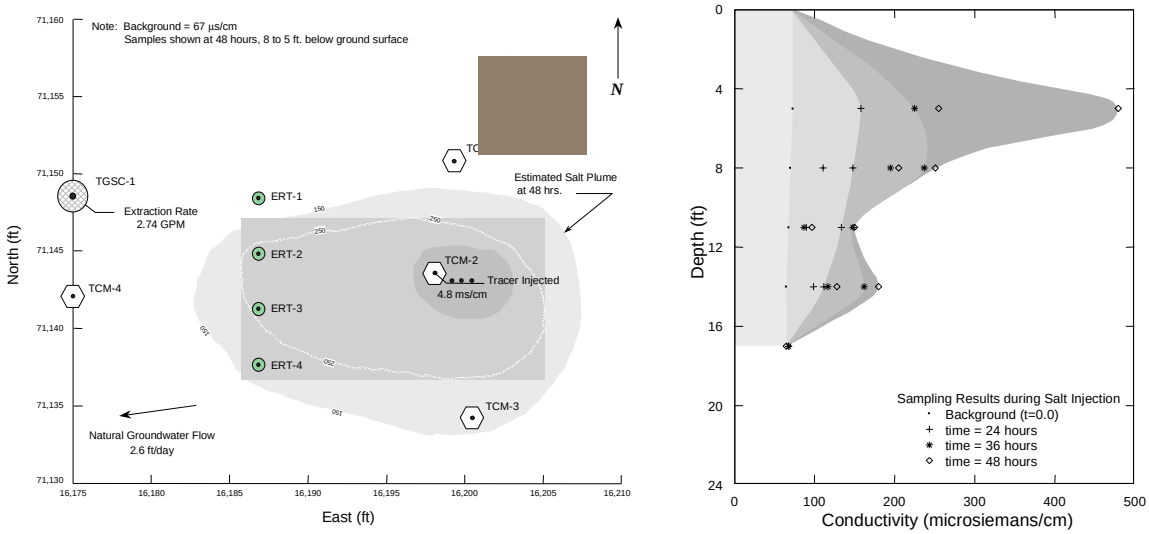

Figure 5.33. Potassium bromide advancement in the upper part of the aquifer caused changes in groundwater conductivity during tracer test.

The ERT surveys and resulting images corroborate the sampling evidence and indicate a significant change in resistivity in the area occurred in the upper layers, specifically above 11 feet bgs. Soil electrical resistivity is a function of the pore water saturation, pore water salinity and soil/rock clay content. Since we are monitoring a saturated system and not changing the constituents of the soil, any changes observed in the resistivity images are due to changes in the pore water salinity and in this case, the movement of the Potassium Bromide toward the Geosiphon. Because these measurements are quantitatively small, and there could be electrical noise in the measurements, electrical surveys were repeated between the same electrodes before the tracer injection began, and the differences between these images are shown in Figure 5.34.

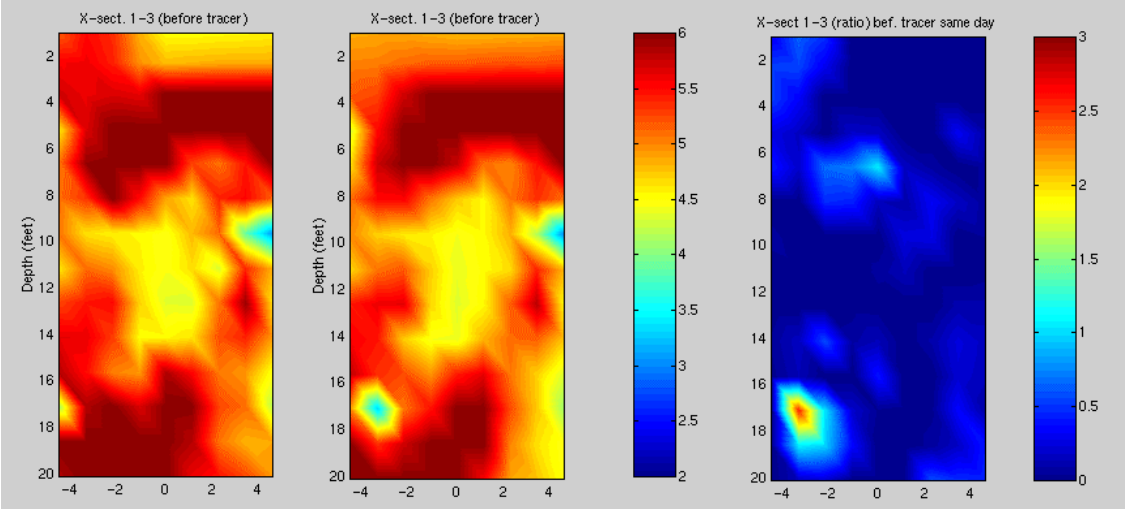

Figure 5.34. ERT images constructed from two surveys taken the same day, four hours apart, before the tracer injection began. Image on the right shows the difference between resistivity profiles.

This indicates the relative noise at the site, or change from one ERT survey to another, when subsurface conditions are relatively stable or constant. The two images on the left were obtained from ERT data taken between electrode strings 1 and 3 and were taken before the tracer injection began and on the same day. The image on the right in Figure 5.34 is the ratio of the two images and shows very little change except for a small change in resistivity in the lower left corner. Because the electrodes were installed 24 hours before these were taken, they may still be equilibrating. The images between electrode strings 1 and 3 after the injection has begun do not show the low resistivity in this location. Figure 5.35 are the ERT images obtained before, at time = 0, 36, and 48 hours after Potassium Bromide injection.

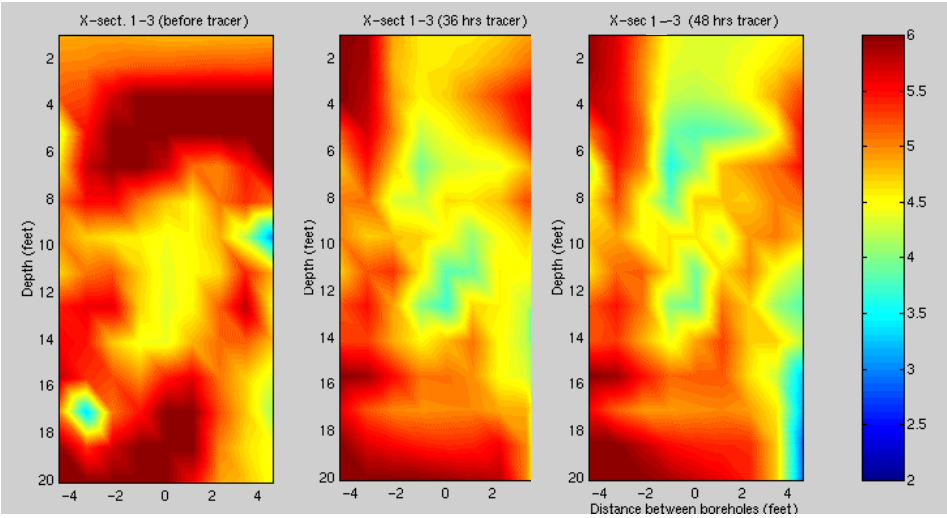

Figure 5.35. ERT image constructed from surveys taken during the tracer test.

The images in Figures 5-36 and 5-37 indicate the advancement of the salt tracer above the 11-ft depth through taking the ratios of the images at two different time lapses. The images on the left in Figures 5-36 and 5-37 are images of log resistivity values calculated through geophysical numerical inversion of the electrical resistivity survey data. The image on the right in Figure 5-36 is the ratio of the image created at 36 hours to the image created before the tracer was injected. Figure 5-37 shows this comparison at 48 hours. In order to compare images with the same level of uncertainty the smoothing parameters were kept the same between images and the same reciprocity criteria was used for the weights in the numerical inversion of each image.

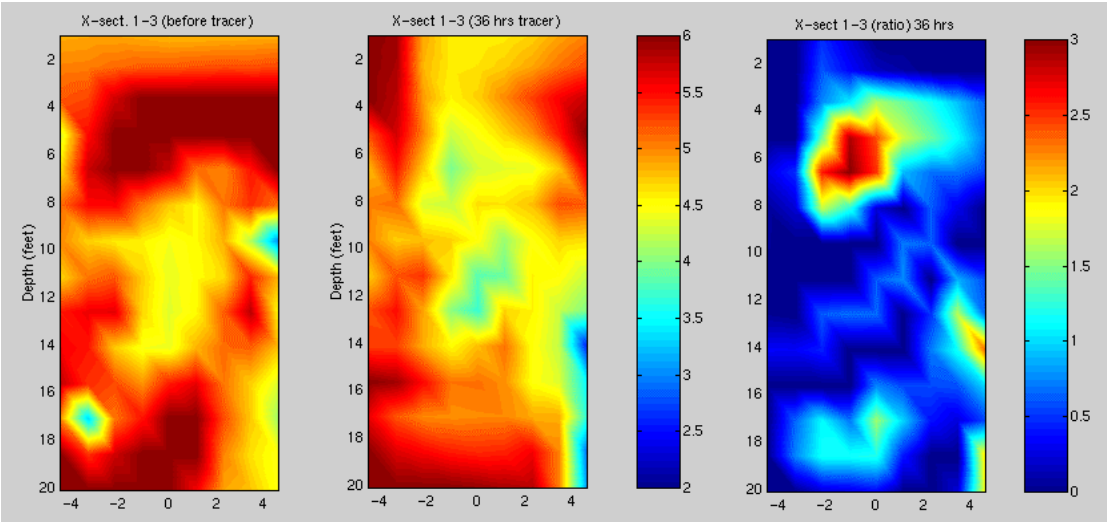

Figure 5.36. Image on right shows difference between image constructed from data gathered at t=0 and t=36 hrs.

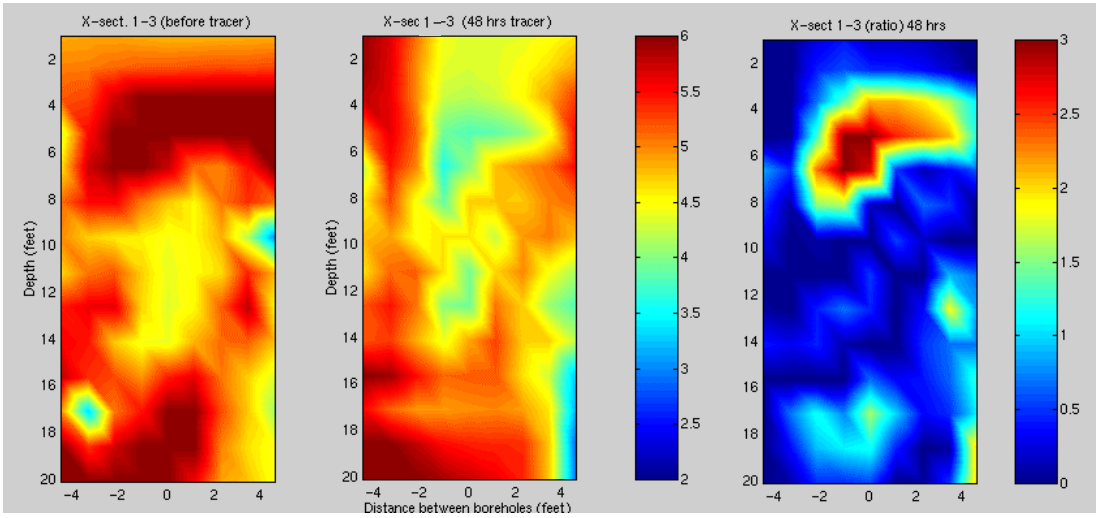

Figure 5.37. Image on right shows difference between image constructed from data gathered at t=0 and t=48 hrs.

Figure 5.38is a time lapse showing the advancement of the potassium bromide tracer through the three ratio images.

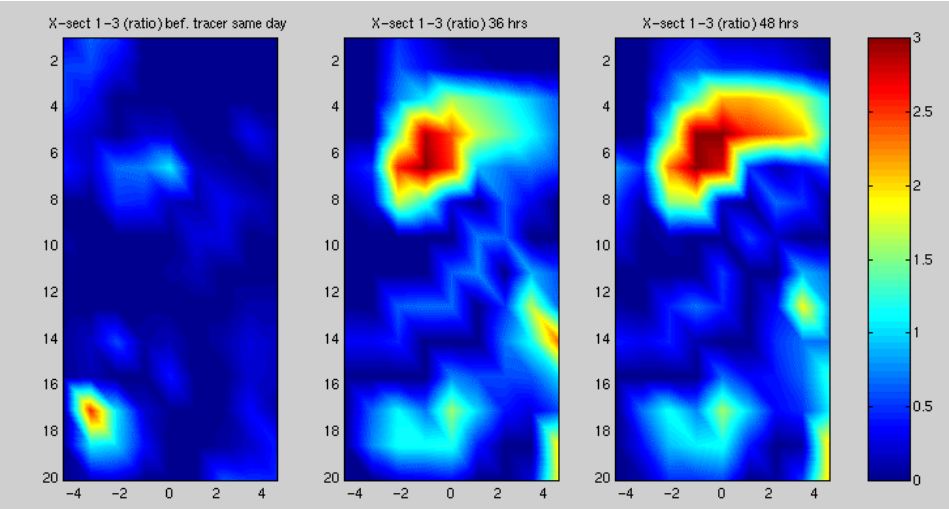

Figure 5.38. Images indicating the changes in resistivity during the tracer test. Significant decrease in resistivity above the 11 feet and depth indicates a preferential pathway toward the Geosiphon.

Unfortunately, analyzing GPR results only yielded limited information. The site was extremely low in resistivity and the radar wave was only able to be picked up between antennas located at the same depth. Although we used a low frequency borehole radar setup (50 MHz) it was insufficient to produce a good quantitative signal through the layers. Therefore, a crosshole tomographic image at the TNX site between monitoring wells TCM-2 and TCM-4 from GPR was unobtainable.

SECTION 6.
CONCLUSIONS

The success of remediation activities such as soil vapor extraction (SVE), steam injection, or groundwater pump and treat methods is highly dependent on accurate information of the soil properties and hydrogeologic conditions of the site. Since many key parameters which can control the rate of cleanup such as soil moisture, porosity, hydraulic conductivity and preferential flow patterns are estimated from sparse remote measurements, and the cost of increasing the cost of measurements is high, new methods for interpreting these sparse measurements is desired. The integrated sensor packages ARA is developing and the results of the testing completed under this contract provide increased information using minimally invasive methods to more accurately and optimally determine hydrogeologic parameters and soil and site conditions.

Electrical Resistivity Tomography and Ground Penetrating Radar have been developed and tested in integrated field efforts under this contract. Surface ERT and GPR have proven to be useful techniques for imaging subsurface structures and processes; however, depth of investigation is limited. Borehole use of ERT and GPR require the installation of system components via drilled boreholes. The results of this program now make it possible to install ERT and GPR units by CPT methods and thereby reduce installation costs and total costs for ERT and GPR surveys. In addition, CPT provides valuable geologic data which will improve the ERT results through providing information on soil resistivity and improve GPR results through information on soil moisture. These two techniques can complement each other in regions of low resistivity where ERT is more effective and regions of high resistivity where GPR is more effective, through the use of CPT to bridge the gap between them.

A breadboard ERT borehole system was built and successfully tested. A breadboard GPR borehole system was also built and successfully tested. CPT GeoWells were installed at ARA's Vermont Test Site and at a DOE site for the field testing of the two cross-hole systems. A salt water infusion test at the VT and TNX sites demonstrated the ability of the ERT and GPR techniques to image time-variant processes. The pre-infusion and post-infusion tomographic images for both systems clearly show sand and clay layers and salt water plumes. The field test

conducted at the TNX area confirmed the ERT monitoring results in the saturated zone through the use of dual electrode samplers. The electrode samplers are designed to be installed using CPT and in the saturated zone the soil collapses around them as the rods are withdrawn, providing the intimate contact with the soil desired by ERT. The sampling corroborated the ERT images of where tracer movement occurred confirming the ERT results. The demonstration at the TNX area was also actively remediating contaminated ground water and ERT did not disturb the remediation activity while it was being used to determine the preferential flow paths toward the remediation well (Geosiphon).

The results at the MWD site show that CPT-installed GeoWells can be used for both ERT and GPR borehole tomographic subsurface imaging. Testing of various GPR and ERT data acquisition systems have determined that sufficiently rugged and powerful systems are required to make good quantitative measurements in different lithologies and field experimental designs. Although "rule of thumb" guides to ERT and GPR array or borehole placement may provide a rough guide, these measurements are very sensitive to site and soil conditions. Field experimental designs using these techniques for monitoring require adequate information such as CPT and numerical modeling techniques for a successful field implementation.

DOE has identified a need for sensors, sensor deployment means, and sensor data processing, including sensor data fusion methodologies for detection and monitoring of contaminants in soils, groundwater, and process effluents, expediting site characterization, and geological and hydrogeological characterization and monitoring of the subsurface environment.

Our results specifically addresses each of these needs:

1. Sensors: ERT and GPR
2. Sensor Deployment: CPT and site specific electrode designs
3. Sensor Data Processing: Tomographic Imaging integrating CPT data
4. Sensor Data Fusion: ERT, GPR, and CPT

Specific results are:

1. Delineating the continuity of soil layers between penetrometer holes;
2. Locating and mapping sand and clay lenses between penetrometer holes;

3. Determining preferential flow paths through *in situ* monitoring of the groundwater flow patterns; and
4. Use of dual electrode samplers installed with CPT for gathering additional information at discreet intervals.

The dual use of the GeoWells and the electrode samplers improves the fusion of data from the two survey approaches by allowing the collection of spatially co-registered data sets. ERT and GPR are complementary approaches in that subsurface resistivity conditions under one technique either excels or falters and will produce the reciprocal effect on the other technique (i.e. reducing resistivity improves the quality of ERT while diminishing that of GPR, and increasing resistivity improves GPR while diminishing ERT).

GPR Conclusions

Commercially available equipment is more mature than ERT, but optimized for surface surveys; not borehole applications. Frequency range and power of commercial systems are adequate for GPR in some sites. Sites which are very low in resistivity are difficult for good quantitative measurements using GPR. A combination of surface to borehole and borehole to borehole techniques and true integration with ERT may improve results.

ERT Conclusions

Several variants of an ERT vertical electrode array (VEA) design were evaluated. All use a CPT-installation of achieving internal electrical contact with the soil. The Geowell design is not yet optimal due to high friction soils may limit installation depth with CPT and saturated zone use may not be feasibly due to leaking providing electrical shorts between steel sections. However, in the unsaturated zone the Geowell design was used successfully when spring loaded electrical contactors proved to have good electrical contact, speed of deployment, and user operability.

Using CPT resistivity data for the initial guess in ERT inversion, provides more efficient convergence and more accurate solutions. This was demonstrated using both synthetic and actual field data sets. ERT results can be improved by the following:

Optimize ERT system for more rapid measurement multiplexing

Increase field portability
Develop flexible relay matrix with high channel count
Increase power to achieve greater *in situ* current density

Development of an ERT system which uses a combination of fixed and roaming VEAs with CPT and near real-time data inversion would greatly improve the performance and reduce the cost of ERT surveys. ARA is currently proposing development of a true three dimensional real time geophysical imaging system for enhanced vadose zone monitoring and characterization using CPT and ERT.

SECTION 7.
REFERENCES

1. Schroeder J.D., Booth S.R., and Trocki L.K. "Cost Effectiveness of the Site Characterization and Analysis Penetrometer System," LA-UR-91-4016, Los Alamos National Laboratory, Los Alamos, NM, 1991.

2. Booth S.R., Durepo C.J., and. Temper D.L. "Cost Effectiveness of the Cone Penetrometer Technique (CPT)," LA-UR-93-3383, Los Alamos National Laboratory, Los Alamos, NM, 1993.

3. Begemann H.K.S. "The Friction Jacket Cone as an Aid in Determining the Soil Profile," Proc. 6th ICSMFE, Montreal, vol. I, pp. 17-20, 1965.

4. de Reister J. "Electric Penetrometer for Site Investigations," Journal of SMFE Division, ASCE, vol. 97, SM-2, Feb. pp 457-472, 1971.

5. Torstensson B.A. "Pore Pressure Sounding Instrument," Proc. ASCE Spec. Conf. on *In Situ* Measurement of Soil Properties, Raleigh, NC, vol. II, pp. 48-54, 1975.

6. Wissa A.E.Z, Martin R.T., and Garlanger J.E. "The Piezometer Probe," Proc. ASCE Spec. Conf. on *In Situ* Measurement of Soil Properties, Raleigh, NC, vol. I, pp. 536-545, 1975.

7. Timian D.A., Fisk B.E., and Cassem B.R. "Demonstration of Heavyweight Penetrometer Technology at the Hanford Site," WHC-SD-TRP-003, Westinghouse Hanford Company, Richland, Washington, Dec 1992.

8. Daily W., Ramirez A., LaBrecque D., and Nitao J. "Electrical Resistivity Tomography of Vadose Water Movement," Water Resources Research, vol. 28, pp. 1429-1442, May 1992.

9. Ramirez A., Daily W., LaBrecque D., Owen E., and Chesnut D. "Monitoring an Underground Steam Injection Process Using Electrical Resistivity Tomography," Water Resources Research, vol. 29, pp. 73-87, Jan. 1993.

10. Peden I.C., Kipp R., and Allestad J. "A Scale-Model Study of Down-Hole VHF Dipole Arrays with Application to Subsurface Exploration", IEEE Trans. Geosci. Remote Sensing, vol. GE-30, pp 885-891, 1992.

11. LaBrecque D.J., Miletto G., Daily W., Ramirez A., and Owen E. "The Effects of Noise on Occam's Inversion of Resistivity Tomography Data", *Geophysics*, vol. 61, no. 2, pp. 538-548, 1996.

12. Daniels, D., Gunton J., and Scott H.F. "Introduction to subsurface radar," IEE Proceedings on Communication, Radar, and Signal Processing, vol. 135, Pt. F, pp. 278-320, Aug. 1988.

13. Sander K.A., Olhoeft G.R., and Lucius J.E. "Surface and Borehole Radar Monitoring of a DNAPL Spill in 3D versus Frequency, Look Angle and Time," in Proc. Symposium on the Application of Geophysics to Engineering and Environmental Problems, pp 455-469, April 26-29, 1992, Chicago, IL.

14. Horton and Morey R.M. "An Evaluation of Ground Penetrating Radar for Assessment of Low Level Nuclear Waste Disposal Sites", Report NUREG/CR-2212, U.S. Nuclear Regulatory Commission, September, 1981.

15. Sato M. and Thierbach R. "Analysis of a Borehole Radar in Cross-Hole Mode," *IEEE Trans. Geosci. Remote Sensing*, vol. GE-29, pp 899-904, 1991.

16. Olsson O., Falk L., Forslund O., Lundmark L., and Sandberg E. "Crosshole investigation: Results from borehole radar investigations", Stripa Project TR 87-11, SKB, Stockholm, Sweden; 1987.

17. Wright D.L, Watts R.D., and Bramsoe E. "A Short-Pulse Electromagnetic Transponder for Hole-to-Hole Use," IEEE Trans. Geosci. Remote Sensing, vol. GE-22, pp 720-725, 1984.

18. Smith G.S. "Directive Properties of Antennas for Transmission into a Material Half-Space," IEEE Trans. on Antennas and Propagation, vol. 32, pp 232-246, 1984.

19. Sihvola A.H. “Self-Consistency Aspects of Dielectric Mixing Theories,” *IEEE Transactions on Geoscience and Remote Sensing*, Vol. 27, July 1989, pp. 403-415.

20. Selig E.T. and Mansukhani S. "Relationship of Soil Moisture to the Dielectric Property," *Journal of the Geotechnical Engineering Division*, ASCE, 1975, Vol. 101, No. GT8, pp. 755-770.

21. Topp G.C., Davis J.L., and Annan A.P., "Electromagnetic Determination of Soil Water Content: Measurements in Coaxial Transmission Lines," *Water Resources Research Journal*, Vol. 16, No. 3, June 1980, pp. 574-582.

22. Topp G.C. and Davis J.L. "Measurement of Soil Water Content Using Time Domain Reflectometry (TDR): a Field Application," *Journal of Soil Science, Society of America,* Vol. 49, 1985, pp. 19-24.

23. Baker T.H.W and Goodrich L.E. "Measurement of Soil Water Content Using the Combined Time-Domain Reflectometry Thermal Conductivity Probe," *Canadian Geotechnical Journal*, Vol. 24, 1987, pp. 160-163.

24. Zegelin S.J. CSIRO, Centre for Environmental Mechanics, personal communication, 1990, 1991.

25. Argonne National Laboratory, Applied Geosciences and Environmental Management Section, “Evaluation Report: Study of Three Soil Moisture Probes with Laboratory Sample Results,” final internal report, ANL, Argonne, IL, August 1997.

26. Miletto G. and LaBrecque D.J. “Robust Scheme for ERT Inversion Modeling”, in *Proc. Symposium on the Application of Geophysics to Engineering and Environmental Problems: EEGS*, Keystone, CO, pp. 629-638, April 28-May 2, 1996.

27. Ramirez A., et al. “Detection of Leaks in Underground Storage Tanks Using Electrical Resistance Methods,” JEEG, December 1996, Volume 1, Issue 3., pp. 189-203.

28. Maloney J.G. and Smith G.S. "Optimization of a Conical Antenna for Pulse Radiation: An Efficient Design Using Resistive Loading," *IEEE Trans. on Antennas and Propagation*, vol. 41, pp 940-947, 1993.

29. King R.W.P. and Smith G.S. *Antennas in Matter*, The MIT Press, Cambridge, MA, 1981.

30. Marsily, G., “Quantitative Hydrogeology,” Groundwater Hydrology for Engineers, Academic Press Inc., New York, 1986.

APPENDIX A

Vermont Test Site Field Logs

RADAN Filenames :

Vermont Site

GPR Surface Survey at 500 MHz
100 foot Square centered about infusion well
Data taken on 10 foot centers
0 trough 10 from Left to Right Facing away from house
A through K, A being further from house, outer LH corner

RADAN Filename	Start	Stop
File52	D10	D0
File53	C0	C10
File54	B10	B0
File55	A0	A10
File56	E10	E0
File57	F0	F10
File58	A6	K6
File59	NONE	
File60	K7	A7
File61	A5	K5
File62	J10	J0
File63	J0	J10
File64	K10	K0
File65	I0	I10
File66	H10	H0
File67	G0	G10
File68	K10	A10
File69	A9	K0
File70	K8	A8
File71	NONE	
File72	A6	K6
File73	K4	A4
File74	A3	K3
File75	K2	A2
File76	A1	K1
File77	K0	A0

Surface topography data points:

Surface Topography		Feet
Datum F5	5.05	0.00
F0	2.70	2.35
A0	1.87	3.18
A5	5.31	-0.26
A10	6.18	-1.13
F10	5.74	-0.69
K10	4.26	0.79
K5	4.13	0.92
K0	2.96	2.09

Data array for surface contour map:

Surface Matrix in Feet

	0	1	2	3	4	5	6	7	8	9	10
A	3.18	2.49	1.80	1.12	0.43	-0.26	-0.43	-0.61	-0.78	-0.96	-1.13
B	3.01	2.37	1.73	1.08	0.44	-0.20	-0.37	-0.54	-0.70	-0.87	-1.04
C	2.45	1.93	1.41	0.89	0.37	-0.15	-0.31	-0.47	-0.63	-0.79	-0.95
D	2.68	2.12	1.57	1.01	0.46	-0.10	-0.25	-0.40	-0.56	-0.71	-0.86
E	2.52	2.01	1.49	0.98	0.46	-0.05	-0.19	-0.34	-0.48	-0.63	-0.77
F	2.35	1.88	1.41	0.94	0.47	0.00	-0.14	-0.28	-0.41	-0.55	-0.69
G	2.30	1.88	1.45	1.03	0.60	0.18	0.06	-0.05	-0.17	-0.28	-0.40
H	2.25	1.87	1.50	1.12	0.75	0.37	0.27	0.18	0.08	-0.01	-0.11
I	2.20	1.87	1.54	1.21	0.88	0.55	0.48	0.40	0.33	0.25	0.18
J	2.15	1.87	1.59	1.32	1.04	0.76	0.70	0.64	0.59	0.53	0.47
K	2.09	1.86	1.62	1.39	1.15	0.92	0.89	0.87	0.84	0.82	0.79

Data array for clayey-sand layer:

Layer 1 adjusted for surface features

	0	1	2	3	4	5	6	7	8	9	10
A	1.8352	1.1472	0.4592	-0.5568	-3.4096	-7.312	-10.4708	-11.9568	-13.1476	-14.0432	-14.2172
B	1.6652	1.0232	0.3812	-1.4744	-4.9372	-8.0392	-10.208	-12.3768	-14.152	-14.32	-16.1608
C	1.1052	0.5852	0.0652	-3.3412	-6.6164	-9.9572	-11.3636	-12.9668	-14.6684	-14.9596	-16.0708
D	1.3352	0.7792	-1.056	-5.1544	-8.2032	-10.7272	-13.5688	-14.8688	-15.5456	-16.4192	-17.3584
E	1.1752	0.6612	-3.3624	-6.4676	-10.6552	-11.4644	-14.3308	-14.6716	-15.4388	-16.6652	-16.8092
F	1.0052	0.5352	-3.2476	-6.8336	-9.9932	-12.2016	-13.2908	-14.6752	-15.5348	-16.1976	-17.09
G	0.9552	0.5312	-2.7792	-7.172	-12.188	-12.0872	-13.2528	-14.2216	-15.5184	-16.9464	-18.0136
H	0.9052	-0.3892	-4.8324	-7.242	-9.422	-11.9956	-11.862	-12.778	-14.3008	-16.3484	-16.9036
I	0.8552	0.1316	-3.5112	-9.0236	-12.5352	-10.8972	-12.9392	-14.6532	-16.3016	-16.8348	-18.1224
J	0.8052	0.5272	-4.6708	-8.36	-12.2788	-10.9496	-12.6148	-14.4112	-14.666	-15.6752	-16.5532
K	0.7452	0.5112	-3.3964	-7.632	-11.9988	-10.4944	-12.2588	-13.6624	-14.5084	-15.0264	-16.1676

Vermont Test Site

ERT Measurement Schedule

Actual: Feb, 1997

Well	Pre Infusion	Post Infusion
1 to 3	2/12	2/17, 2/17, 2/18
2 to 4	2/12	2/17, 2/17, 2/19
1 to 4	2/12	2/17, 2/19
1 to 2	2/13	2/19
2 to 3	2/13	2/19
3 to 4	2/13	2/19

APPENDIX B

IRIS: SYSCAL JUNIOR, a single purpose field portable instrument for measuring resistivity. This is a single channel instrument (combines transmitter and receiver) which can be used in conjunction with an "intelligent electrode nodes system", its usefulness is limited to a small number of electrodes. A limited data set can be downloaded into a laptop PC. Our experience with this instrument, was measuring resistivity with two VEAs at the Vermont Test Site. Four hours was required to take each data set from ten pairs of electrodes. An external battery set is required. An external computer and relay multiplexer system would be required to automate resistivity measurements. Control software would have to be written.

OYO: McOHM-21, a single purpose portable instrument for measuring, processing and displaying resistivity (combines transmitter and receiver). A built in CPU and hard disk make this unit truly self contained though the programming for borehole ERT is limited. Data processing for tomograms still requires an external computer.

The cost noted above includes a 32 channel scanner (multiplexer) such that two VEAs of 16 electrodes can be addressed. A number of scanners can be daisy chained together and it is possible to access a total of 750 electrodes. A 12 volt rechargeable battery is included.

Zonge A: GDP-32 electrical methods receiver, ZT30 Transmitter, and ISO/1 in combination is a multifunctional, multipurpose electrical geophysical instrument with which ERT data can be gathered. A built-in CPU controls the instrumentation. Data must be downloaded into a laptop or PC for storage and analysis. The configuration above is for four channels and assumes a necessary breakout box to access large ERT arrays. This unit is extremely rugged and field ready and represents the state of the art. A 12 volt rechargeable battery is included.

Zonge B: GDP-32 electrical methods receiver, ZT30 Transmitter, and ISO/1 and MX30 multiplexer (scanner) in combination is a multifunctional, multipurpose electrical geophysical instrument with which ERT data can be gathered. An external laptop or PC is required in the field control these units for large ERT arrays. Data must be downloaded into a workstation or PC for storage and analysis. This configuration has 30 channels and allows access to two, 15 electrode VEAs. This unit is extremely rugged and field ready and represents the state of the art. A 12 volt rechargeable battery is included. This configuration has been purchased by Lawrence Livermore National Laboratory for their ERT research.

U of AZ: (University of Arizona, Dr. Douglas LaBrecque) This planned instrument would utilize a Hewlett Packard power source as the transmitter and HP voltmeters as the receiver. Combined with signal conditioning and signal multiplexing of UAZ design, this rather large, rack mounted instrument would be extremely flexible as a research instrument, though not particularly adept in field conditions. A PC or laptop would be required to control this instrument though the data storage and processing could be included for the possibility of real-time tomography. Thirty multiplexed (*) channels were assumed for cost estimating. Increasing the channel count for this system, which is still under development, would be relatively easy and additional cost would be minimal. A 120 volt external power is necessary.

Keithley: This multipurpose source/measure system designed for the semiconductor test industry is extremely cost effective though not proven that it would work in the ERT application. Coupled with a 100 MHz PC, this system would be extremely fast at taking data. External AC power is required.

APPENDIX C

Cost Information for Field Demonstration of CPT, ERT, and GPR

In order to apply the CPT, ERT and GPR technology in a field demonstration, certain components of the system must be assembled and mobilized to the site. To better understand the costs incurred in a demonstration, the following summary will provide a discussion of the process involved for a successful field demonstration. The total cost may be thought of as a sum of the individual components:

Total Cost = Investigation/Design/Permitting + CPT Mobilization/Data Acquisition/Electrode Installation + Manufacturing/Assembly + ERT/GPR Data Acquisition + Analysis/Reporting.

The following is a brief discussion of each of the times making up the total cost. After the discussion the approximate time involved in the task and associated costs are listed in ranges appropriate to the level of work involved.

Investigation/Design/Permitting

To deploy this technology at a DOE site, numerous permits must be submitted, reviewed and approved before work may begin and are dependent on the level of effort and contamination at the site. Some of the requirements may be: a work clearance permit, an excavation/trenching check list, monitoring well approval, program plan approval, injection control permit, a site specific health and safety plan, an environmental evaluation checklist (the National Environmental Policy Act), and site clearance requests. Turnaround time may take anywhere from one day, to months, depending on the level of effort.

Engineering Staff : 40 to 200 hrs.

Permitting Cost: $2,000 to $10,000

Sufficient planning of the field investigation includes modeling the expected outcome to help in experimental design. Uncertainty in behavior of ERT and GPR at sites where variable geology exists makes designing and building an appropriate electrode string difficult. Numerical modeling of the outcome using estimates of field parameters will help design the frequency and total number of electrode strings needed to gather

quantitatively significant data. In this way, an estimate can be made of the minimum number of electrodes to manufacture. Engineering level depends on the complexity of the experiment.

Engineering Staff: 16 to 80 hrs.

Planning Cost: $800 to $5,000

CPT Mobilization/Data Acquisition/Electrode Installation

In addition to installing electrode strings, or monitoring wells, CPT provides valuable information that can be used to improve the GPR and ERT images. CPT high resolution profiles are obtained from pushing cones with resistivity, soil moisture, pore pressure, tip and sleeve sensors from which soil classification information can be gathered at a site, and soil stratigraphy estimated. CPT profiles reduce the uncertainties associated with ERT and GPR by providing a better initial guess and corroborating results of the numerical inversion techniques used by GPR and ERT. The costs associated with mobilizing the CPT to a site are dependent on mileage, and the cost of CPT to install electrodes, monitoring wells, and gather CPT profiling data is dependent on the size of the field effort. CPT rates are based on the ability to push 500 linear ft per day.

Mobilization/Demobilization: $2 to $4/mile

CPT data acquisition/Installation: $2,200 to $3,000 per day

Manufacturing/Assembly

Electrical Resistivity Tomography requires the use of electrodes either inserted into the ground, or on the ground surface, and wired to a geophysical data acquisition system. They are usually manufactured and assembled according to the results of numerical modeling based on the estimated site characterization parameters at the site. They may be simple metal cylinders, or they may be sintered cylindrical filters to be used for both ERT and sampling of the groundwater. Ground Penetrating Radar may also be used in the form of surface penetrating radar, or borehole radar. Once the experiment design has been determined the appropriate radar equipment can be selected and either purchased or rented on a daily or monthly basis.

Manufacturing/Assembly: $45 to $57 per electrode

ERT/GPR Data Acquisition

Both ERT and GPR require geophysical data acquisition equipment to gather their surveys of data. Either they may be rented, or purchased. In the case of a DOE site, certain equipment may already be available, and also be appropriate for the test. The cost of an ERT or GPR survey depends on the size and complexity of the field experiment. A simple test may be to gather ERT and GPR data between two boreholes, each with a small number of electrodes. Numerical inversion of the data may reveal a few simple cross sections. More complicated testing, such as imaging changes that are occurring in the subsurface over time, would require more time in the field gathering data, and inverting for possible time lapse imaging. The ERT and GPR costs (below) do not reflect the cost of a laptop computer which is required to run them, nor a separate power source required for the laptop while taking ERT data, to avoid electrical noise interference that may be caused by a power grid. The rental prices also do not reflect any insurance costs that may be necessary to rent the equipment from the vendor.

Engineering Staff (no equipment use fee): $800 per day

ERT Geophysical Data Acquisition System: $604 per day

Borehole GPR Data Acquisition System: $295 per day

Analysis/Reporting

Results of the experiment may simply be a few cross sectional images, or may require full detailed explanation of field techniques, data acquisition, and extensive data inversion and analysis.

Engineering Staff : 40 to 200 hrs.

Total Reporting Cost: $1000 to $10,000

The total cost involved in site characterization is highly dependent on the level of effort and the state of the site. We based our estimates of the costs involved on our experience using CPT, ERT and GPR to date. Unforeseen costs due to difficult geology, equipment failure, weather, or extensive delays in permitting due to complex field experiments, are not uncommon and can contribute significantly to the total cost of site characterization.